A methodology to assess the combined effect of climate change and groundwater overexploitation over the Upper Guadiana basin, Spain

PhD Thesis

Gonzalo Sapriza Azuri

Advisors:

Dr. Jesús Carrera Ramírez

Dr. Jorge Jódar Bermúdez

December, 2013

Hydrogeology Group (GHS)

Institute of Environmental Assessment and Water Research (IDAEA)

Spanish Research Council (CSIC)

Dept. Geotechnical Engineering and Geosciences, Universitat Politecnica de Catalunya, UPC-Barcelona Tech

I. Abstract

There is a growing concern about the combined effect of climate change and groundwater overexploitation on the availability of water resources in the Upper Guadiana basin (UppGb) in central Spain. General Circulation Models (GCMs) are used to evaluate the possible impact of climate change based on future scenarios of greenhouse gas emissions. However, the output of these models cannot be applied directly to hydrological models because their spatial resolution is coarse and because their simulated precipitation is highly biased. A stochastic downscaling method for generating daily spatial rainfall fields was developed. The model termed Stochastic Rainfall Generating Process (SRGP) incorporates two major non-stationarities – changes in the frequencies of different precipitation generating mechanisms (frontal and convective), and spatial non-stationarities caused by the interactions of meso-scale atmospheric circulation patterns (ACP) with topography (orographic effects). SRGP was developed to incorporate good climate outputs simulated by GCMs (i.e. ACP), and actual observations. These capabilities enabled us to (1) use SRGP as a downscaling method for climate change impact study, and (2) generate stochastic rainfall fields conditioning to the information of rain gauges. The latter capability was used to investigate the effect of rainfall spatial variability (RSV) on the hydrological response in the UppGb. RSV exerted a major influence on the response of the system especially on the groundwater recharge and the aquifer related responses.

GCMs considered in the fifth assessment report of the Intergovernmental Panel on Climate Change were used to evaluate the impact of climate change. The RCP8.5 future emission scenario (GCM-RCP8.5) and the GCM historical control (GCMH) were selected. The climate change was assumed to be the accumulated effects of increases in Temperature, changes in annual and climatological ACP frequency, and changes in probability and volume of rain. Transformations were applied to correct the bias in the temperature, probability and volume of rain, whereas the ACP sequences were used directly. The SRGP method was employed as a rainfall downscaling method for the GCMs. GCMH was used to evaluate the hydrological response obtained with GCMs as driving climate variables, introducing the concept of stochastic equivalence. This evaluation was based on the comparison of the hydrological response obtained with actual observations and transformed (bias correction and SRGP) GCMH. Although an exact stochastic equivalence response was not totally achieved,

the seasonal variations were well captured and some response reported very good agreements.

The combined effect of climate change and groundwater overexploitation in the UppGb was evaluated in two stages: (1) comparing the hydrological response of the system simulated under natural conditions (absence of pumping), using GCMH and GCM-RCP8.5 as climate driving variables. (2) Groundwater pumping was applied using the same GCM climate driving variables and again the responses were compared. Climate change led to reductions of 14% and 25% in the number of rainy days and volume of rain respectively and an increase of 20% in potential evapotranspiration. Under natural conditions because of climate change, soil moisture and the actual evapotranspiration were reduced by 20% and groundwater recharge, runoff generation, groundwater-river exchange and river discharge were reduced by 40%. As a result of the combined effects of pumping and climate change, all variables were reduced; soil moisture and actual evapotranspiration were reduced by 20% and recharge was reduced by 50%. Moreover, the aquifer related responses yielded annual average reductions of approximately 60%. In general, the results showed an increase in the dry season from April to October.

II. Resumen

El efecto conjunto del cambio climático y la sobreexplotación de las aguas subterráneas podría llegar a ser crítico para la disponibilidad de recursos hídricos en la cuenca del Alto Guadiana (CAG) en el centro de España. Los modelos de circulación general del clima (GCM) son utilizados para evaluar el posible impacto del cambio climático en base a futuros escenarios de emisión de gases de efecto invernadero. No obstante, la salida de estos modelos no puede aplicarse directamente en modelos hidrológicos porque: (1) la resolución espacial es demasiado grande, y (2) el gran sesgo con que simulan la precipitación. Por tanto, se desarrolló un modelo para el downscaling diario de campos espaciales de precipitaciones. El modelo denominado *Stochastic Rainfall Generating Process* (SRGP) incorpora dos importantes no-estacionaridades: (1) cambios en la frecuencia de los mecanismos de generación de precipitación (frontal y convectivo), y (2) no estacionaridades espaciales causadas por la interacción de patrones de circulación atmosférica (ACP) con la topografía (efecto orográfico). El SRGP se diseñó para que incorpore variables simuladas por los GCMs con sesgo reducido (ACP), así como también observaciones. Estas prestaciones permiten: (1) utilizar el SRGP como un método de downscaling para el estudio del cambio climático, (2) poder generar múltiples realizaciones de campos de precipitación condicionando a la información de estaciones meteorológicas. Esta última función fue utilizada para investigar el efecto de la variabilidad espacial de la precipitación (RSV) en la respuesta hidrogeológica en la CAG. Se constató que la RSV afecta fuertemente la respuesta hidrológica especialmente para la recarga de agua subterránea y las respuestas asociadas al acuífero.

GCMs utilizados en el quinto informe de evaluación del Panel Intergubernamental del Cambio Climático fueron empleados para evaluar el efecto del cambio climático. En todos los casos se consideraron las simulaciones correspondientes al periodo histórico (GCMH) (escenario de control) y el escenario futuro de emisiones RCP8.5 (GCM-RCP8.5). El cambio climático se evaluó como el efecto acumulado en el incremento de las temperaturas, cambios en la frecuencia climatológica anual de los ACP y cambios en la probabilidad y volumen de precipitación. Se aplicaron transformaciones para corregir el sesgo en la temperatura, probabilidad y volumen de precipitación, mientras que se utilizó de forma directa los ACP. Se aplicó el SRGP como método de downscaling de precipitaciones. El GCMH se utilizó para evaluar la respuesta hidrológica obtenida, introduciendo el concepto de equivalencia

estocástica. Esta evaluación se basó en comparar la respuesta hidrológica obtenida al aplicar como forzantes la salida transformada (corrección del sesgo y SRGP) de los GCMH, en relación a la obtenida con observaciones. Se comprobó que no se alcanza una respuesta estocástica equivalente exacta para todas las respuestas, pero sí, reproducir variaciones estacionales.

El efecto conjunto del cambio climático y la sobreexplotación por bombeo en la CAG se realizó en dos etapas: (1) Se simuló en condiciones naturales (sin bombeo) comparando la respuesta hidrológica obtenida de aplicar como forzantes la salida de GCMH y GCM-RCP8.5. (2) con los mismos forzantes se incorporó los bombeos y nuevamente se compararon las respuestas. Se determinó que el efecto del cambio climático produce una reducción de 14% y 25% en el número de días de lluvia y en el volumen de precipitación respectivamente. Mientras que un incremento del 20% en la evapotranspiración potencial. En condiciones naturales esto se tradujo en una reducción relativa del 20% para la humedad de suelo y la evapotranspiración real. En tanto que, para la recarga de agua subterránea, generación de escurrimiento, intercambio río-acuífero y caudal en el río la reducción fue del 40%. Finalmente, el efecto conjunto de los bombeos y cambio climático, resultó en una reducción para todas las variables, siendo la reducción relativa de un 20% tanto para la humedad del suelo y al evapotranspiración real y del 50% para la recarga. Para las respuestas asociadas al acuífero, la reducción fue del 60 %. Los resultados mostraron un incremento de la estación seca, extendiéndose de Abril a Octubre.

III. Resum

L'efecte conjunt del canvi climàtic i la sobreexplotació de les aigües subterrànies podria arribar a ser crític per a la disponibilitat de recursos hídrics en la conca de l'Alt Guadiana (CAG) en el centre d'Espanya. Els models de circulació general del clima (GCM) són utilitzats per avaluar el possible impacte del canvi climàtic sobre la base de futurs escenaris d'emissió de gasos d'efecte hivernacle. No obstant això, la sortida d'aquests models no pot aplicar-se directament en models hidrològics perquè: (1) la resolució espacial és massa gran, i (2) el gran biaix amb què simulen la precipitació. Per tant, es va desenvolupar un model pel downscaling diari de camps espacials de precipitacions. El model denominat Stochastic Rainfall Generating Process (SRGP) incorpora dos importants no-estacionaritats: (1) canvis en la freqüència dels diferents mecanismes de generació de precipitació (frontal i convectivo), i (2) no estacionaritats espacials causades per la interacció de patrons de circulació atmosfèrica (ACP) amb la topografia (efecte orogràfic). El SRGP es va dissenyar perquè pugui incorporar variables simulades pels GCMs amb biaix reduït (ACP), així com també observacions. Aquestes prestacions permeten: (1) utilitzar el SRGP com un mètode de downscaling per a l'estudi del canvi climàtic, (2) poder generar múltiples realitzacions de camps de precipitació condicionant a la informació d'estacions meteorològiques. Aquesta última funció va ser utilitzada per investigar l'efecte de la variabilitat espacial de la precipitació (RSV) en la resposta hidrogeologic en la CAG. Es va constatar que la RSV afecta fortament la resposta hidrològica especialment para la recarrega d'aigua subterrània i les respostes associades a l'aqüífer.

GCMs utilitzats en el cinquè informe d'avaluació del Panell Intergovernamental del Canvi Climàtic van ser emprats per avaluar l'efecte del canvi climàtic. En tots els casos es van considerar les simulacions corresponents al període històric (GCMH) (escenari de control) i l'escenari futur d'emissions RCP8.5 (GCM-RCP8.5). El canvi climàtic es va avaluar com l'efecte acumulat en l'increment de les temperatures, canvis en la freqüència climatològica anual dels ACP i canvis en la probabilitat i volum de precipitació. Es van aplicar transformacions per corregir el biaix en la temperatura, probabilitat de pluja i volum de precipitació, mentre que es va utilitzar de forma directa els ACP. Es va aplicar el SRGP com a mètode de downscaling de precipitacions. El GCMH es va utilitzar per avaluar la resposta hidrològica obtinguda amb els GCMs, introduint el concepte d'equivalència

estocàstica. Aquesta avaluació es va basar a comparar la resposta hidrològica obtinguda en aplicar com forçants la sortida transformada (correcció del biaix i SRGP) dels GCMH, en relació a l'obtinguda amb observacions. Es va comprovar que no s'aconsegueix una resposta estocàstica equivalent exacta per a totes les respostes, però sí, reproduir variacions estacionals.

L'efecte conjunt del canvi climàtic i la sobreexplotació per bombament en la CAG es va realitzar en dues etapes: (1) Es va simular en condicions naturals (sense bombament) comparant la resposta hidrològica obtinguda d'aplicar com forçants la sortida de GCMH i GCM-RCP8.5. (2) amb els mateixos forçants es va incorporar els bombaments i novament es van comparar les respostes. Es va determinar que l'efecte del canvi climàtic produeix una reducció de 14% i 25% en el nombre de dies de pluja i en el volum de precipitació respectivament. Mentre que un increment del 20% en la evapotranspiració potencial. En condicions naturals això es tradueix en una reducció relativa del 20% per a la humitat de sòl i la evapotranspiració real. Mentre que, per la recarrega d'aigua subterrània, generació de escolament, intercanvio riu-aqüífer i cabal en el riu la reducció va ser del 40%. Finalment, l'efecte conjunt dels bombaments i canvi climàtic, va resultar en una reducció per a totes les variables, sent la reducció relativa d'un 20% tant per a la humitat del sòl i al evapotranspiració real i del 50% para la recarrega. Pel les respostes associades a l'aqüífer, la reducció arriba fins al 60 %. Els resultats van mostrar un increment de l'estació seca estenent-se d'Abril a Octubre.

IV. Acknowledgments

This thesis would have been not possible without the support of many people. I would to thanks to my PhD advisors Dr. Jesus Carrera and Dr. Jorge Jodar, for supporting me all these years and to providing me the opportunity to pursue my PhD in the Hydrogeology Group. I am especially grateful to Dr. Hoshin V. Gupta who in his sabbatical year in Barcelona and subsequence visits, gave me the gift of his time and wisdom to reinforce my PhD at the right time.

I must also acknowledge all of the colleagues of the Hydrogeology Group. I am especially grateful to Estanis P., Enkhbayar D., Anna J., Silvia D., and Quim S. I would also like to thank the administrative staff Tere, Monica and Silvia.

A special thanks to Pablo Gamazo who always have had a wise counsel. Thanks also to Jorge de los Santos, Alejandro Oleaga and Fernando Pacheco who introduce me to the hydrogeology world.

I would like to thank my family and my fried Maty. They were always supporting me and encouraging me with their best wishes.

Este camino que ha sido la tesis, no hubiera sido posible sin el amor, cable a tierra, y soporte incondicional de mi compañera y amor Maine. Sin duda alguna, tienes que ir como coautora de esta tesis. Gracias a mi hija Pilar, por llenarnos la vida de alegría y felicidad.

This thesis was co-funded by the Technical University of Catalonia with a grant "*Programa D'Ajuts per a la realització de la tesis doctoral a la UPC, FPI-UPC*" and by the Hydrogeology Group (GHS) through the *European Union (FP6) funded Integrated Project Water and Climate Change WATCH (contract number 036946).*

A mis dos amores Maine y Pilar

V. Index

VI. List of Figures

VII. List of Tables

1 Introduction

1.1 Motivation and Aims

The last assessment report (***IPCC, 2013***) of the Intergovernmental Panel on Climate Change (IPCC) confirms earlier projections (***IPCC, 2007***). Spain will be drier in the future. Rainfall reduction is especially critical for semi-arid zones whose water resources are sensitive to overexploitation (***Llamas and Martínez-Santos, 2005***). This is the case of the Upper Guadiana basin (UppGb) in central Spain. Special attention should be focused on the management of water resources concerning the combined effect of climate change and overexploitation in a non-stationary framework, and an appropriate assessment of all the uncertainties should be carried out (***Milly et al., 2008, Beven, 2011***).

General Circulation Models (GCMs) simulate the climate dynamics of the earth. Their outputs can be used to study the impact of climate change for different future projected scenarios (***Moss et al. 2010***). In particular, they provide acceptable results of the synoptic atmospheric circulation patterns (***Gupta et al., 2013***). However, their spatial scale resolution is too coarse for hydrological basin scale modeling and their simulated precipitations are clearly biased (***Dai, 2006***). Statistical downscaling methods (SDM) have been developed to overcome this limitation (***Maraun et al., 2010***, ***Fowler et al., 2007***). Such models seek to simulate the most important non-stationarities of rainfall while incorporating relevant information provided by GCMs (***Hay et al., 1991***; ***Bardossy and Plate, 1992***; ***Goodess and Palutikof, 1998***; ***Corte Real et al., 1999***; ***Bellone, 2000***; ***Fowler et al., 2000, 2005***; ***Yang et al., 2010***). Furthermore, there is a need to simulate spatially distributed rainfall fields at any spatiotemporal scale (***Maraun et al. 2010***).

The interest in high resolution rainfall fields is largely motivated by the little known role of rainfall spatial variability (RSV) in the hydrological basin scale and in the propagation of rainfall uncertainty through the hydrological system, especially in overexploited hydrogeological systems. Most authors have focused on river discharge and hydrograph peak properties for event responses (***Wilson et al., 1979***; ***Krajewski et al., 1991***; ***Obled et al., 1994***; ***Nicotina et al., 2008***; ***Younger et al., 2009***). Moreover, they only agree on the role of the total volume of water per event in the river discharge (***Obled et al. 1994***). Few studies have analyzed the impact of RSV on aquifer response. ***Schuurmans and Bierkens, (2007)***

investigated the effect of RSV on the hydrogeological response of a flat shallow groundwater basin with a rapid time of response, demonstrating that RSV affects the internal spatial distribution of hydrological state variables but not the overall system response. Thus, it is not easy to generalize earlier results. Moreover, although it may be assumed that RSV filtered into a hydrogeological system response, spatial intermittence and orographic effects on the rainfall fields (important source of spatial variability) can lead to significant differences in the hydrogeological response. It is therefore essential to account for the two effects in the context of climate change impact studies where a fine space scale detail SDM is necessary (***Maraun et al., 2010***; ***Wilby et al., 2004***).

Apart from the adopted SDM used and regardless of whether the hydrological response is sensitive to RSV, another problem stems from the manner in which the impacts of climate change are evaluated using GCMs. The simulated GCMs projected scenarios are incorporated into SDM to generate future climate driving variables to run hydrological models that were previously calibrated with observation. Both responses (past and future) are then compared to assess the impact of climate change (***Chiew et al., 2009; Fowler et al., 2007***). This approach assumes that SDM based on GCM projection can produce a hydrological response equivalent to those obtained with actual observations. This underlying assumption is however rarely verified (***Wood et al., 2004***) and only very few studies compare the performance of SDM for the historical control period (***Frost et al., 2011; Vrac et al., 2007***).

Accordingly, the aims of this thesis are as follows:

1. To develop a non-stationary stochastic rainfall generator that evaluates the impacts of climate change on water resources and that takes full advantage of the fact that GCMs are able to simulate other hydrometeorological variables (e.g. ACP). This model includes two major non-stationarities – changes in the frequency of different precipitation generating mechanisms (frontal and convective) and spatial non-stationarities caused by interactions of meso-scale atmospheric patterns with topography (orographic effects).
2. To investigate the effect of RSV on the hydrogeological response in the UppGb and the manner in which this variability Tois propagated though the system.
3. To evaluate the combined impact of – future projected climate change and groundwater overexploitation in the UppGb. This includes defining a

consistent evaluation procedure for the interpretation of the information generated by GCMs.

1.2 Thesis Outline

This thesis consists of five chapters including the introduction. The remaining four chapters are organized as follows.

Chapter 2 presents the model for generating daily spatial correlated rainfall fields suitable for evaluating the impacts of climate change on water resources. The model, termed Stochastic Rainfall Generating Process (SRGP), is designed to incorporate temporal non-stationarities – i.e. changes in the frequency of different precipitation generating mechanisms (frontal and convective) – and spatial non-stationarities, caused by interactions of meso-scale atmospheric patterns with topography (orographic effects). These non-stationarities are approximated as discrete sets of time-stationary SRGPs, each of which represents the different spatial patterns of rainfall (including its variation with topography) associated with different Atmospheric Circulation Patterns (ACP) and times of the year (seasons). Each discrete SRGP generates daily correlated rainfall fields as the product of two random fields. First, the amount of rainfall is generated by a transformed Gaussian process applying sequential Gaussian simulation. Secondly, the delimitation of rain and no-rain areas (intermittence process) is defined by a binary random function simulated by sequential indicator simulations. To explore its applicability, the model was tested in the UppGb in Spain. Results suggest that the model provides an accurate reproduction of the major spatio-temporal features of rainfall for hydrological modeling and water resource evaluations. The results were significantly improved by incorporating spatial drift related to orographic precipitation into the model.

Chapter 3 is concerned with the effect of RSV on the hydrogeological response at long term time scales and on an overexploited system. In particular, we show how uncertainty in the spatial distribution of rainfall is propagated through the hydrological system, and how it is affected by local differences in dominant hydrological processes (such as wetlands) and/or by the degree of exploitation (pumping).Further, the amount of information lost (i.e. how the assessed impacts are affected) owing to the use of up-scaled rainfall fields is discussed. To this end, the SRGP was applied to generate stochastic rainfall fields at a daily time scale. The rainfall fields were used to drive a spatially distributed hydrogeological model for the UppGb. The results show that RSV has a considerable impact on the response

of the system especially in the case of groundwater recharge and the aquifer related responses.

Chapter 4 discusses the evaluation procedures for the assessment of the combined effect of climate change and groundwater overexploitation. Traditionally, climate change impact studies rely on scenario projections provided by General Circulation Models (GCMs). Such projections are transformed (e.g., downscaling, bias correction) and used as inputs to hydrological models, which were previously calibrated against historical observations. The impacts of climate change can be assessed by comparing the historical and projected hydrological responses. Therefore, it is assumed that the downscaled GCM simulations can function as surrogates for the corresponding actual values (represented by observations or reanalysis fields), which implies a stochastic equivalence. This chapter formalizes the Stochastic Equivalence concept used to evaluate the validity of the hydrological response driven by downscaled GCM simulations. In addition, an evaluation procedure to assess the combined effect of climate change and groundwater pumping in a basin is presented. The evaluation procedure and the impact assessments were applied to the UppGb in Spain. As a result of the combined effect of pumping and climate change, all the variables were reduced; soil moisture and actual evapotranspiration were reduced by 20% and recharge was reduced by 50%. Similarly, the aquifer related responses show annual average reductions of approximately 60%.

Chapter 5 lists the main conclusions of this thesis.

The contents of chapters 2 to 4 are based on papers that have already been published or submitted to peer-reviewed international journals.

2 Stochastic Simulation of Non-Stationary Rainfall Fields, Accounting for Seasonality and Atmospheric Circulation Pattern Evolution [1]

2.1 Introduction

Climate Change Impact Studies (CCIS) rely upon simulations of past, present, and potential future climate scenarios provided by General Circulation Models (GCMs) (***Randall et al., 2007***; ***CCSP, 2008***). However, these simulations do not provide rainfall fields at the high spatial resolution generally required for hydrological impact assessments (***Maraun et al., 2010***). GCMs currently have a spatial discretization of around 250 km, whereas the resolution of hydrological models typically ranges from 2 km to 50 m. Moreover, simulated rainfall intensities are often significantly biased and fail to reproduce patterns of long-term variability (***Dai, 2006***; ***Gleckler et al., 2008***; ***CCSP, 2008***; ***Ehret et al., 2012***; ***Johnson and Sharma, 2011***).

To overcome these limitations, Stochastic Rainfall Models (SRMs), also known as Statistical Downscaling Models, have been recently developed (***Fowler et al., 2007***; ***Maraun et al., 2010***). Such models seek to simulate the most important non-stationarities of rainfall while incorporating relevant information provided by GCMs (***Hay et al., 1991***; ***Bardossy and Plate, 1992***; ***Goodess and Palutikof, 1998***; ***Corte Real et al., 1999***; ***Bellone, 2000***; ***Fowler et al., 2000, 2005***; ***Yang et al., 2010***). Furthermore, there is a growing interest in being able to simulate spatially distributed rainfall fields at any spatio-temporal scale required (***Maraun et al. 2010***).

[1]This chapter is based on the paper: *Sapriza Azuri, G., Jódar, J., Carrera, J., & Gupta, H. (2013). Stochastic Simulation of Nonstationary Rainfall Fields, Accounting for Seasonality and Atmospheric Circulation Pattern Evolution. Math. Geosci., 45(5), 621-645. doi:10.1007/s11004-013-9467-0*

Four main types of SRM are discussed in the literature: (1) Multivariate Stochastic Rainfall Models (MSRMs), (2) Point Process Models (PPMs), (3) Random Cascade Models (RCMs), and (4) Transformed Gaussian Process Models (TGPMs). Each of these approaches has strengths and weaknesses. MSRMs provide the ability to simulate precipitation at a fixed set of locations by interpolating values across the domain; examples include autoregressive models (***Bardossy and Plate, 1992***), generalized linear models (***Chandler and Wheater, 2002***; ***Yang et al., 2005***), multi-site Markov models (***Wilks, 1998***), nonparametric multi-site models (***Buishand and Brandsma, 2001***), and reshuffling approach models (***Methrotra and Sharma, 2009***). PPMs have the ability to simulate rainfall at a very high temporal resolution (***Waymire et al., 1984***, ***Rodríguez-Iturbe et al., 1986***; ***Cowpertwait, 1995, 2010***; ***Northrop et al., 1998***, ***Wheater et al., 2005***; ***Zhang and Switzer, 2007***; ***Burton et al., 2010***) but need large amounts of high quality data for model calibration.

RCMs arise from the study of scale-invariance of rainfall (***Schertzer and Lovejoy, 1987***; ***Gupta and Waymire, 1993***) and apply multiplicative random cascade models in space and time (***Jothiyangkoon et al. 2000***; ***Kang and Ramírez, 2010***). They can incorporate both climate information and the orographic effects on rainfall (***Perica and Foufoula-Georgiou, 1996***; ***Ebtehaj and Foufoula-Georgiou, 2010***). Although such models are parsimonious and can reproduce characteristics such as spatio-temporal intermittence and clustering, they require long sequences of radar images that may not always be available. Finally, the TGPM approach assumes that rainfall can be represented as a transformed multi-Gaussian stochastic process (***Mejía and Rodríguez-Iturbe, 1974***; ***Bell, 1987***; ***Shah et al., 1996***; ***Guilliot, 1999***; ***Lanza, 2000***; ***De Oliveira, 2004***; ***Kyriakidis et al., 2004***; ***Teo and Grimes, 2007***), conditioned on the knowledge of spatial average rainfall (***Onibon et al., 2004***) within a generalized linear model framework (***Kleiber et al., 2012***). One advantage of this approach is its ability to exploit information from either rain gauges or radar images. Models within this group differ in terms of the transformation used to generate a multi-dimensional stationary Gaussian process, the type of algorithm used to generate spatial realizations of rainfall, and the way in which rainfall intermittence is represented. Nevertheless, none of these models incorporate the major sources of non-stationarity in rainfall processes within a common framework. While consideration of spatial non-stationarity including climate information (only specific humidity) was incorporated by ***Kyriakidis et al. (2004)***, they did not explicitly represent the spatial intermittence of rainfall and focused only on conditional simulations. Meanwhile, ***Bell, (1987)***, ***Guilliot, (1999)***, ***Lanza, (2000)***, ***De Oliveira, (2004)*** and ***Teo and Grimes***

(2007) explicitly included spatial intermittence of rainfall via threshold transformation or Sequential Indicator Simulation, but did not incorporate other sources of non-stationarity (i.e.: orographic effect, climate).

To generate non-stationary stochastic rainfall fields suitable for evaluating the impacts of climate change on water resources, it is necessary to represent two major non-stationarities – changes in the frequencies of different precipitation generating mechanisms (frontal and convective) and spatial non-stationarities caused by interactions of meso-scale atmospheric patterns with topography (orographic effects) (***Barros and Lettenmaier, 1994***). This paper introduces a new TGP termed Stochastic Rainfall Generating Process (SRGP) designed to simulate such non-stationarity in daily rainfall fields in the context of downscaling relevant climate information from GCMs. Instead of being based on GCM simulations of rainfall which are typically poor, SRGP takes advantage of the fact that GCMs are able to generate good simulations of other hydrometeorological variables (***Gleckler et al., 2008***) and, in particular, of atmospheric circulation patterns (ACP) at the synoptic scale (***Randall et al., 2007***). The methodology was developed using data from the Upper Guadiana basin in central Spain.

2.2 Methodology

In general, SRGP is a two-part model (***Stern and Coe, 1984***). The first part decides whether a day is rainy or not, over the entire area of interest, while the second part deals with the manner in which the spatio-temporal pattern of rainfall is generated. The rain/no-rain decision can be made in the context of climate impact studies, on the basis of information GCM outputs or stochastic simulation using, for example, a first or second order Markov Chain Model or any of its variants (see ***Sharma and Mehrotra, 2010***). The spatio-temporal rainfall pattern can be generated using a stochastic model designed to reproduce the observed spatial correlation structure of rainfall.

However, it is well known that the spatio-temporal patterns of rainfall intensity vary with changes in temperature, and with changes in the velocity and direction of winds (and their interactions with local topography and landscape), all of which vary throughout the year with changes in the regional atmospheric circulation patterns over the area. Our approach, therefore, is to assume that the overall non-stationary SRGP can be approximated by a time sequence of draws from a discrete set of time-stationary SRGPs, each of which represents the spatial patterns of rainfall (including its variation with topography) associated with different

ACPs and seasons of the year. More specifically, the discrete set is constructed by classifying days according to a) the ACP type for that day, and b) the time of year (either month or season).

This results in a three-part SRGP model: (1) select the prevalent ACP, (2) decide whether the day is rainy or not and (3) simulate the spatial rainfall field. Again, each of these decisions can be made via stochastic simulation, provided that the probability of rain in the second stage depends on the selected ACP and time of year. Although conditional probability Markov Chain models of this type can be easily constructed from observed data, including long term variability in their construction (***Mehrotra and Sharma 2007, 2010***), our attention here is focused on climate impact studies, in which case both the regional ACP type and rain/no-rain information for a day can be provided by a GCM with proper post processing to handle the rain no-rain transition (***Johnson and Sharma 2011, 2012***). Therefore, in this paper to further explore the rainfall field generation processes, we assume that the daily sequence of ACP types and whether a day is rainy or not are given. Based on this information, an appropriate SRGP model for the particular time of year (month or season) is selected from the discrete set.

Consequently, the overall SRGP model is based on climatological information from three spatial scales – the synoptic scale (embodied through atmospheric circulation patterns), the basin scale (embodied through orographic effects and the spatial correlation structure of observed rainfall), and the point scale (embodied through rain-gauge measurements). Meanwhile, the model assumes that the temporal day-to-day persistence and the correlation structure of (catchment-scale) mean areal rainfall are largely determined by the (externally determined) ACP and rain-no-rain sequence with the result that daily persistence effects within and across ACP types can be ignored. While such effects could certainly also be modeled and reproduced, we leave such investigation for future studies.

2.2.1 The problem of simulating stochastic rainfall fields

Our main aim here is to simulate daily precipitation fields that reproduce the observed rainfall **m**ultidimensional **c**umulative **d**istribution **f**unction (*mcdf*) at any desired spatial resolution. Of course, characterization of this *mcdf* is not trivial since it is (in general) non-stationary in space and time, has an unknown covariance structure, and depends on an unknown number of parameters.

Let *z(u,t)* denote a random value indicating the intensity of rain at a specific location in space (*u*) and time (*t*). This variable can be interpreted as a realization of a random variable *Z(u,t)* which is characterized by the **c**umulative **d**istribution **f**unction (*cdf*):

$$F(u,t;z) = \Pr\{Z(u,t) \le z\} \tag{1}$$

The set of all the dependent random variables define a spatio-temporal random function *Z*(*u*,*t*) that is totally characterized by its *mcdf* (***Goovaerts, 1997***) given by:

$$\begin{aligned} F_A(Z(u,t)) &= F_A(u_1,t_1,\ldots,u_N,t_N;z_{11},\ldots,z_{NT}) \\ &= \Pr\{Z(u_1,t_1) \le z_{11},\ldots,Z(u_N,t_T) \le z_{NT}\} \end{aligned} \tag{2}$$

where N and T are the total number of points in the spatial and temporal domain respectively. This function has an arbitrary mathematical form (***Kyriakidis and Journel, 1999***). For rainfall, the random function (RF) can be regarded as composed of two terms (1) a continuous random function *R*(*u*,*t*) representing its intensity and (2) a categorical random function *I*(*u*,*t*) representing its space-time intermittence.

$$F_A(Z(u,t)) = F_A(R(u,t),I(u,t)) \tag{3}$$

To model this random function it is necessary to make assumptions about (a) the main causes of temporal non-stationarity in the rainfall generating process, (b) the spatial rainfall mean and variance, (c) the probability distribution function of rainfall intensity, (d) the causes of spatial non-stationarity in rainfall intensity, and (e) the structure of spatial intermittence.

2.2.1.1 Main causes of temporal non-stationarity

As stated above, we assume here that the major causes of temporal non-stationarity in the rainfall generating process are its dependence on (1) seasonal variations in the climatological variables, (2) synoptic scale atmospheric factors (circulation patterns; see ***Bardossy and Plate, 1992***; ***Hay et. al., 1991***; ***Corte Real et al., 1998***; ***Bellone, 2000***; ***Fowler et al.,2000, 2005***; ***Yang et al., 2010***), and (3) interactions between atmospheric conditions and local factors such as topographic slope and aspect (***Barros and Lettenmaier, 1994***). Accordingly, we assume that $F_A(Z(u,t))$ can be approximated by a discrete set of *N* SRGPs $\{F_{A_1}(Z(u,t)),...,F_{A_N}(Z(u,t))\}$ in such a way that each day corresponds only to one SGPR and

where each member $F_{A_j}(Z(u,t))$ is assumed to be stationary in time but may be non-stationary in space.

Consequently, temporal changes in the rainfall regime (the spatial distribution of rainfall intensities) are due primarily to changes in the sequence of SRGPs with the result that the functional form of each SRGP is conditionally independent. This means that the temporal correlation in the rainfall regime arises primarily from the correlation in the daily sequence of SRGP occurrences, and the daily spatial distributions are assumed (for simplicity) to be temporally independent. Hence, the rainfall field on any day is assumed to be conditionally independent of the rainfall field on any previous day. This does not mean, however, that the daily sequence of rainfall fields has no temporal dependence since a temporal relationship exists in the sequence of the different SRGPs because of the temporal evolution in synoptic scale atmospheric circulation patterns.

2.2.1.2 Spatial rainfall mean and variance

For a given SRGP, the strength of the link between the synoptic and the basin scales can be quantified by characterizing the daily spatial rainfall mean (Eq.4) and variance (Eq.(5)) with respect to the predominant atmospheric synoptic scenario:

$$\hat{\mu}_{Z_j}(t) = \frac{1}{N_j}\sum_{i=1}^{N_j} z_i(t) \quad , j = 1,\ldots,N \tag{4}$$

$$\hat{\sigma}^2_{Z_j}(t) = \frac{1}{N_j}\sum_{i=1}^{N_j} (z_i(t) - \hat{\mu}_{Z_j})^2 \quad , j = 1,\ldots,N \tag{5}$$

where N_j is the number of rain gauge stations for a day belonging to the j^{th} SRGP. Here, we assume temporal disaggregation of rainfall intensities (the sequence of rainy days is time independent and controlled by the daily transition of ACPs), which allows us to estimate the spatial daily average and variance of rainfall by obtaining their respective Probability Distribution Functions (*pdfs*) for each SRGP. However, as might be expected $\hat{\sigma}^2_{Z_j}(t)$ and $\hat{\mu}_{Z_j}(t)$ are not independent. In our case study (see section 6) we observed a strong linear dependence between the log transformed values (Figure 2-1) and so that we can express $\hat{\sigma}^2_{Z_j}(t)$ as a function of $\hat{\mu}_{Z_j}(t)$ by fitting a linear regression model:

$$\log \hat{\sigma}^2_{Z_j}(t) = m_{Z_j} \log \hat{\mu}_{Z_j}(t) + c_{Z_j} \tag{6}$$

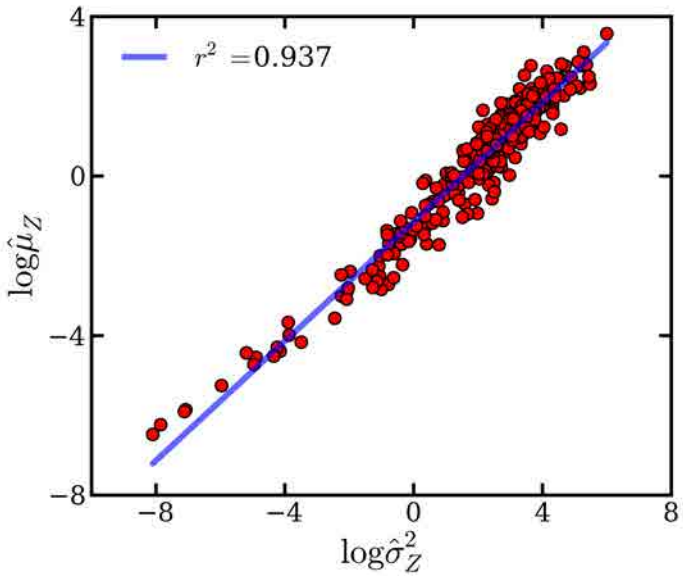

Figure 2-1 Example of empirical relationship between spatial average and variance of rainfall for rainy days of April and May that belong to the HYC ACP type. Red dots denote observations.

Several possibilities for the *pdf* of $\hat{\mu}_{Z_j}(t)$ have been proposed in the literature including the lognormal distribution (***Kedem and Chiu, 1987***), gamma distribution (***Cho et al., 2004***), GLM (***Stern and Coe, 1984***), and more recently a class termed the infinitely divisible distribution (***Kundu and Siddani, 2007***). Here, we assume a gamma distribution (Eq. (7)) because of its parsimony in the number of parameters:

$$\Gamma_{\hat{\mu}_{Z_j}}(\alpha_j, \beta_j) = \frac{\left(\frac{\hat{\mu}_{Z_j}}{\beta_j}\right)^{\alpha-1} e^{-\frac{\hat{\mu}_{Z_j}}{\beta_j}}}{\beta_j \Gamma(\alpha_j)} \tag{7}$$

where α and β are the shape and the scale parameters, respectively. To estimate them a maximum likelihood approach was applied, obtaining the relatively good fit shown in Figure 2-2.

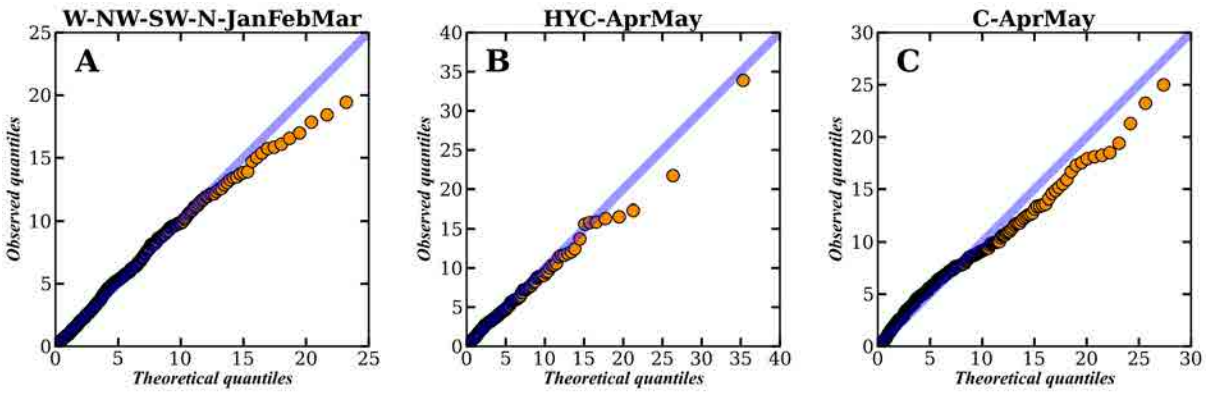

Figure 2-2 Quantile-Quantile plots illustrating Gamma distribution fits to spatial average rainfall. There are for days associated with the rainiest season–ACP combination in the Upper Guadiana Basin. A) Directional W-NW-SW-N in January February and March B) Hybrid Cyclonic in April and May and C) Cyclonic in April and May

2.2.1.3 Probability distribution function of rainfall intensity

The rainfall intensity $\{R_j(u,t)\}$ random function for each SRGP has an unknown multidimensional distribution shape F_{R_j}, which is clearly not multi-Gaussian. To take advantage of the theory of Gaussian random processes, we therefore transform each rainfall intensity *mcdf* into a multi-Gaussian distribution by applying a normal score transformation (also known as quantile-quantile mapping or anamorphosis transformation) (***Goovaerts, 1997***).

In practice, we first compute the standardized daily rainfall amount $Y_j(u,t)$ as follows:

$$Y_j(u,t) = \frac{R_j(u,t) - \hat{\mu}_{Z_j}(t)}{\hat{\sigma}_{Z_j}(t)} \tag{8}$$

and then perform the normal score transformation by establishing a quantile-quantile mapping between the *cdf* of all the standardized rainfall intensity measurements $Y_j(u,t)$ for the SRGP and the *cdf* of a standardized Gaussian distribution to obtain:

$$\psi_j(u,t) = G^{-1}_{\psi_j}(F_{Y_j}(Y_j(u,t))) \tag{9}$$

where $\psi_j(u,t)$ is the new normal scored variable, $G^{-1}_{\psi_j}$ is the inverse Gaussian *cdf* of $\psi_j(u,t)$, and F_{Y_j} is the *cdf* of $Y_j(u,t)$.

2.2.1.4 Spatial non-stationarity in rainfall intensity

Rainfall intensity can be spatially non-stationary due to local factors such as topography, agricultural irrigation, and urbanization, etc. To represent such spatial non-stationarities, we consider $\psi_j(u,t)$ to be an intrinsic stationary function composed of a trend and a residual:

$$\psi_j(u,t) = \overline{\psi}_j(u) + \xi_j(u,t) \tag{10}$$

where $\overline{\psi}_j(u)$ represents the deterministic dependence of rainfall intensity on external factors (known as the trend term), and a residual $\xi_j(u,t)$, which is a zero-mean Gaussian random function whose spatial correlation structure is described by a semi-variogram $\gamma_{\xi_j}(u)$ (termed variogram hereafter). In this study, we assume that rainfall intensity varies only with topographic elevation and estimate the trend term by linear regression. After removing the trend from $\psi_j(u,t)$, the variogram was experimentally inferred for each SRGP (Figure 2-3). Given this model, spatial random fields at any desired resolution can be generated using **S**equential **G**aussian **S**imulation (SGS) (***Gómez-Hernández and Cassiraga, 1994***; ***Deutsch and Journel, 1998***).

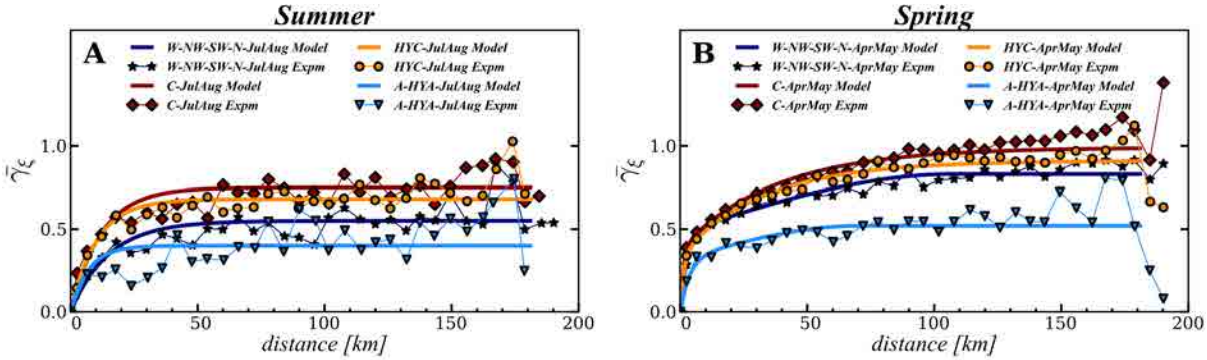

Figure 2-3 Experimental and model semivariograms for Summer (A) and Spring (B) for the rainiest and most frequent ACPs (W-NW-SW-N, C, HYC and A-HYA). The model semivariograms are isotropic and in most cases have two structural components, exponential and spherical.

2.2.1.5 Structure of spatial intermittence

The rainfall intensity model described above will generate non-zero rainfall intensity values at all spatial locations where values are desired. However, the observed rainfall tends to be spatially intermittent (contiguous regions of zero and non-zero rainfall). To be realistic, the rainfall generation process must emulate the patterns of spatial intermittence, and in

particular should reproduce the daily variation in the fraction of rain-covered area (***Doneaud et al., 1984***; ***Kedem and Pavlopoulos, 1991***; ***Eltahir and Bras, 1993***; ***Kursinski and Zeng 2006***). Figure 2-4 shows an example of the dependence between spatial mean rainfall $\hat{\mu}_{Z_j}(t)$ and the fraction of rain-covered area $\theta_j(t)$ in our study area, to which an exponential curve of the following form can be fitted:

$$\theta_j(t) = a(1-\exp(-b\hat{\mu}_{Z_j}(t)) \tag{11}$$

where *a* and *b* are the fitted parameters.

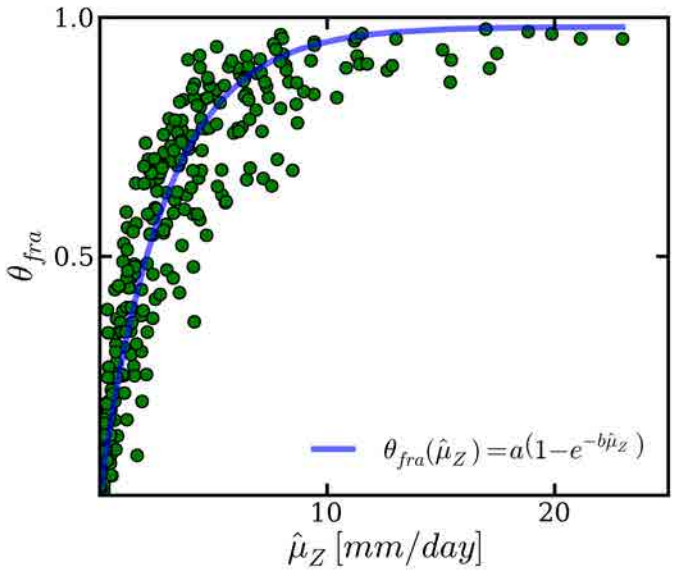

Figure 2-4 Example of empirical relationship between spatial average rainfall and fraction of rain-covered area for the rainy days of January February and March that belong to the HYC ACP type. Green dots denote observations.

To delimit the spatial extension of non-zero rainfall intensity, we assume that the simulated rainfall field $P_j(u,t)$ (Eq. 12) is the combination of two independent random variables (***Barancourt et al., 1992***): (1) the intensity of rainfall $R_j(u,t)$ and (2) a binary RF $I_j(u,t)$ representing spatial intermittence (Eq. 13).

The binary random field $I_j(u,t)$ is assumed to be stationary with a marginal probability equal to the fractional area covered by rain (Eq.14) and with a spatial correlation structure that is different for every *j={1,…,N}*. To simulate rainfall intermittence, a **S**equential **I**ndicator **S**imulation (SIS) approach with simple kriging is applied (***Gómez-Hernández and Srivastava, 1990***; ***Deutsch and Journel, 1998***) in such a way that

$$P_j(u,t) = K_j(t) R_j(u,t) I_j(u,t) \tag{12}$$

$$I_j(u,t) = \begin{cases} 0 \rightarrow Z(u,t) = 0 \text{ for } t \in \text{SRGP}_j \\ 1 \rightarrow Z(u,t) > 0 \text{ for } t \in \text{SRGP}_j \end{cases} \tag{13}$$

$$\theta_j(t) = E[I_j(u,t)] \tag{14}$$

The multiplying factor $K_j(t)$ in equation 12 is necessary to preserve the spatial mean intensity of rainfall $\hat{\mu}_{Z_j}(t)$, which is altered by the removal of areas assumed to have zero rain ($I_j(u,t)$).

2.2.2 Definition of the Atmospheric Circulation Patterns

One major characteristic of our method is its decomposition of the *mcdf* into *N* conditionally independent and temporally stationary SRGPs. This decomposition seeks to account for the dependence of the rainfall generating process on climatological and other (earth system process) factors.

There are several ways to construct the mapping from $t \rightarrow j$ depending on the hypothesis made in regard to the dominant causes of temporal non-stationarity in $F_A(Z(u,t))$. In general, the dominant causes of this non-stationarity are: (1) mesoscale and regional climatological processes such as ACPs and moisture convergence (***Trenberth et al., 2003***) and (2) earth system processes such as the interactions of the local atmospheric conditions with the topography and the direction of the prevailing winds (***Jódar et al., 2010***), etc.

One relatively simple way to incorporate climate information is to relate synoptic general circulation patterns to local scale precipitation ($F_A(Z(u,t))$).Such assumptions have been postulated and tested by (***Hay et. al., 1991***; ***Bardossy and Plate, 1992***; ***Perica and Foufoula 1996***; ***Goodess and Palutikof, 1998***; ***Corte Real et al., 1999***; ***Bellone, 2000***; ***Fowler et al., 2000, 2005***; ***Yang et al., 2010***) with some success. In our study, we implement a decomposition approach where the frequency of rainy days, the daily mean intensity of rain and the patterns of spatial rainfall are controlled by the frequency and seasonality of the ACPs over the study area.

This requires a method for classifying atmospheric circulation patterns into a discrete set of consistent ACP types. For this study we use an automated version of the Lamb Weather Type classification scheme (***Jenkinson and Collinson, 1977***; ***Jones et al., 1993***) in accordance with ***Goodess and Palutikof (1998)***, which is based on the direction of surface wind and on its vorticity in geostrophic units. For our study area, we use gridded values of mean sea level pressure at 16 points distributed over Spain, obtained from the gridded NCEP-NCAR re-analysis data set (***Kalnay et al., 1996***); the result is 8 ACP types (Table 2-1).

ACP Type	Description
C	Cyclonic
HYC	Hybrid cyclonic
UC	Unclassified/light flow cyclonic
A/HYA	Anticyclonic/ hybrid-anticyclonic
UA	Unclassified/light flow-anticyclonic
W/NW/SW/N	Westerly/ northwesterly /southwesterly/northerly directional types
E/NE	Easterly/northeasterly directional types
S/SE	Southerly/southeasterly directional types

Table 2-1 Atmospheric Circulation Pattern classification.

2.3 Model Identification Procedure

The steps used to calibrate the stochastic rainfall generation model are as follows.

1) Define the SRGP classification scheme. For example, classify ACPs using the modified Lamb Weather Type classification and group days by ACP and time of year (season or month).

Then, for each SRGP type:

2) Compute the daily spatial mean $\hat{\mu}_{Z_j}(t)$ and variance $\hat{\sigma}^2_{Z_j}(t)$ (Eq. 4 and 5) of rainfall intensity by using all available weather stations (including the locations with zero values) for each rainy day (a day is considered to be rainy if there is at least one meteorological station in the study area with non-zero precipitation).
3) Estimate the parameters of equation (6) relating $\hat{\mu}_{Z_j}(t)$ and $\hat{\sigma}^2_{Z_j}(t)$.
4) Estimate $\hat{\mu}_{Z_j}(t)$ by fitting the gamma distribution function $\Gamma_{\mu_{Z_j}}(\alpha_j, \beta_j)$ (Eq.7).

5) Estimate the exponential regression parameters *a* and *b* of the functional relationship between the daily spatial mean intensity $\hat{\mu}_{Z_j}(t)$ and the daily fraction of rain-covered area $\theta_j(t)$ (Eq.11).
6) Standardize the daily rainfall intensities (Eq.8).
7) Apply the normal score transformation to the standardized rainfall (Eq.9).
8) Estimate the trend between the standardized variable $\psi_j(u,t)$ and the elevation topography.
9) Obtain the residuals $\xi_j(u,t)$ (Eq.10).
10) Estimate the experimental daily variogram of the residuals $\gamma_{\xi_j}(u)$ for each day, compute the average and then fit the model variogram.
11) Estimate the daily experimental variogram of the binary rainfall occurrence variable $\gamma_{I_j}(u)$ for each day, compute the average and then fit the model variogram.

2.4 Stochastic Simulation Procedure

The daily sequence of rainfall fields is simulated by applying the following steps:

1) Obtain the daily sequence of SRGPs according to the classifying scheme chosen.
2) Determine whether a day is rainy or not.
3) For each rainy day t_n belonging to each SRGP$_j$, use SGS to generate $\xi_j(u,t_n)$ fields with the appropriate variogram $\overline{\gamma}_{\xi_j}(u)$.
4) Add the trend component $\overline{\psi}_j(u)$ (Eq.(10)) to obtain $\psi_j(u,t_n)$.
5) Obtain the $Y_j(u,t_n)$ fields by applying the inverse normal score function (Eq.(9)) to $\psi_j(u,t_n)$.
6) Sample $\hat{\mu}_{Z_j}(t_n)$ from the gamma distribution and obtain the corresponding variance $\hat{\sigma}^2_{Z_j}(t_n)$ by applying equation (6).
7) Obtain the rainfall intensity field $R_j(u,t_n)$ by adding $\hat{\mu}_{Z_j}(t_n)$ and multiplying by $\hat{\sigma}^2_{Z_j}(t_n)$ (Eq. 8).

8) Obtain the fraction of rain-covered area $\theta_j(t_n)$ for the given $\hat{\mu}_{Z_j}(t_n)$ by using equation (11).
9) Simulate the spatial intermittence binary field $I_j(u,t_n)$ applying SIS and using the appropriate variogram $\gamma_{I_j}(u)$ and the corresponding fraction of rain-covered area $\theta_j(t_n)$.
10) Use (Eq. 12) to compute the final rainfall field $P_j(u,t_n)$, where the multiplying factor $K_j(t_n)$ is computed so as to preserve the spatial mean of rainfall intensity selected in step 6.

2.5 Test Case Application

In the following section, the rainfall field simulation method is applied to the Upper Guadiana basin (UppGb) in Spain for the period 1959 to 2007. The SRGP$_j$ parameters were estimated using daily rainfall data from meteorological stations located in the study area. The ACP classification was obtained by applying the Lamb Weather Type classification scheme to the NCEP-NCAR re-analysis data set (***Kalnay et al., 1996***).

2.5.1 Study Area

The UppGb forms part of the central Spanish Plateau, and covers an area of approximately 16000 km^2 (Figure 2-5). The basin is located between latitudes 38º37'N and 40º08'N, and longitudes between 2º25'W and 3º51'W. Morphologically, the main part of the basin is characterized by a smooth topography with altitudes ranging from 550 to 700 m a.s.l. (above sea level). Nevertheless, the northern and southern boundaries (Sierra Altomira and Campos de Montiel, respectively) show a mountainous landscape with an altitude exceeding 1000 m a.s.l.

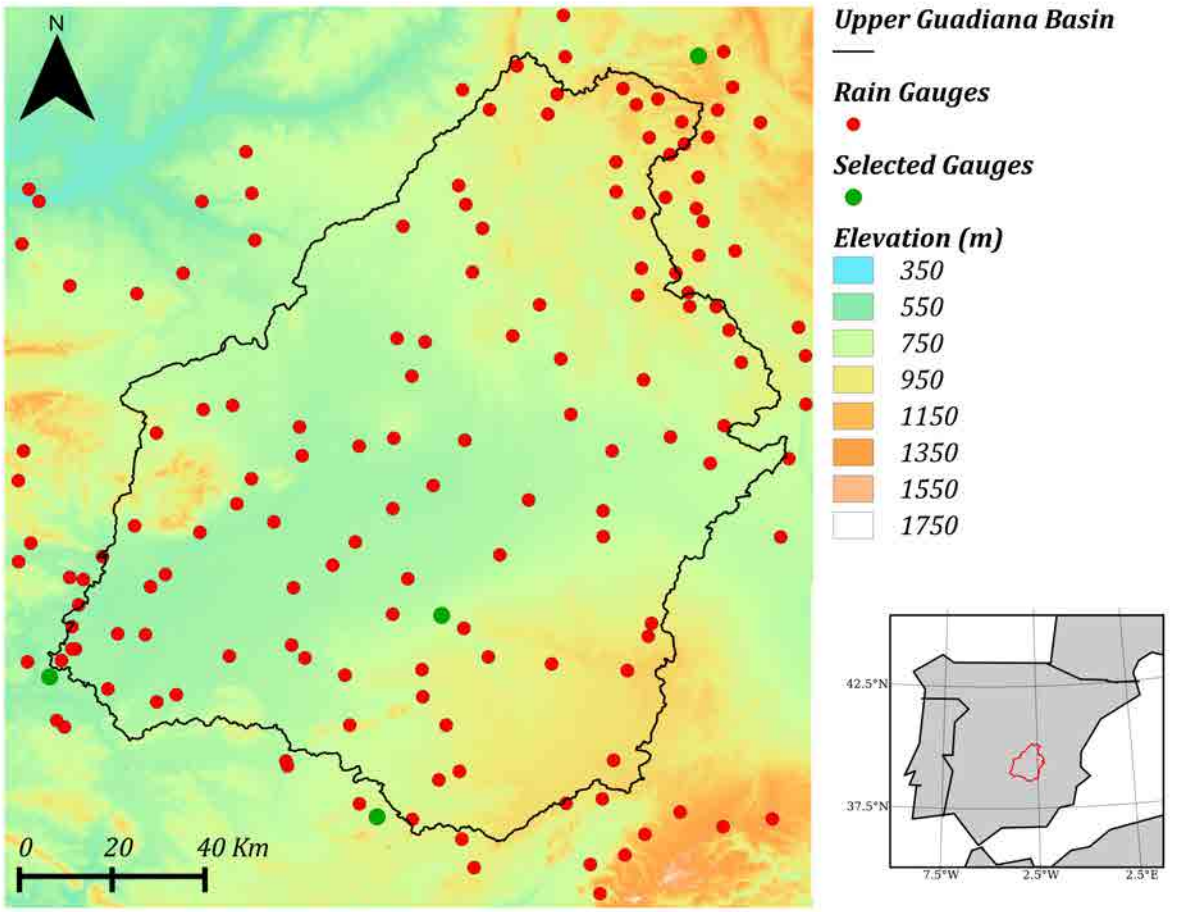

Figure 2-5 Location of study area. The black line is the administrative limit of the Upper Guadiana Basin, and the red dots indicate locations of the meteorological stations.

The UppGb has a mixed continental, semi-arid, Mediterranean climate. Precipitation has notable space-time variability because of Atlantic and Mediterranean influences and because of orographic effects. The mean areal annual precipitation in the basin is approximately 450 mm/y, but varies both spatially (recorded minimum and maximum gauges display means of 173 and 824 mm/, at the valley and mountains, respectively) and temporally (the standard deviation of the total yearly rainfall at the same stations are 121 and 233 mm/y respectively).

Its main characteristics are seasonal variability (Figure 2-6) with a dry season in summer (especially in July and August accounting for 5 % of the annual precipitation). This precipitation is dominated by small convective rain cells of short duration. The wettest seasons, autumn and spring, are characterized by stratiform frontal rain with large spatial continuity and duration. At point (rain gauge) scale, the number of dry days can be as high as 80% on average (varying with the seasons), but this percentage drops to 50 % if we consider areal average rainfall, which suggests a high degree of spatial variability in the occurrence of

precipitation. Orographic effects also contribute to spatial variability in rainfall intensities, with an average increase in precipitation with an elevation of around 0.0075 mm/ m.

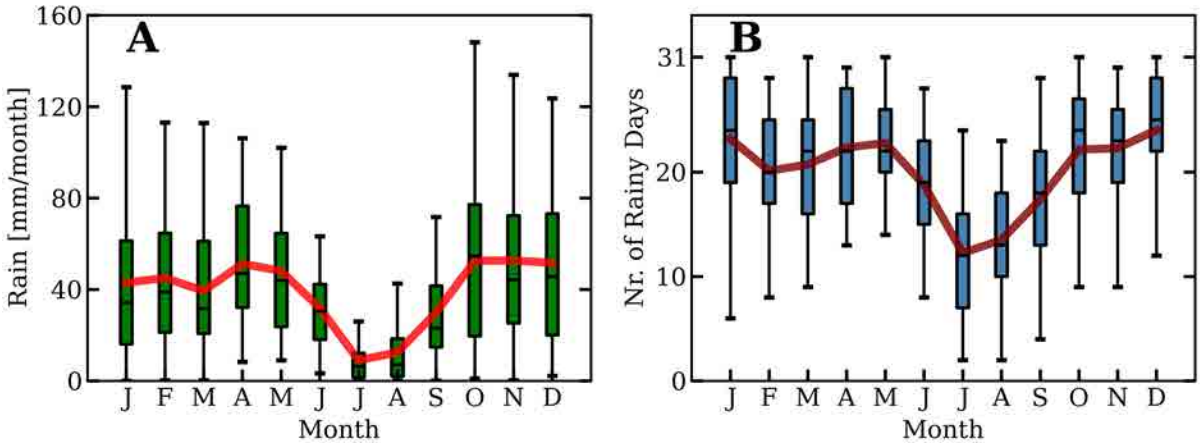

Figure 2-6 Climatology plots for the Upper Guadiana Basin. A) Spatial average rainfall, B) Number of rainy days per month. A day is defined as rainy if at least one meteorological station reports daily measured rainfall exceeding zero.

Application of the ACP scheme indicates that higher rainfall amounts are associated with (1) the directional type ACP (W/NW/SW/N), which brings moisture from the Atlantic ocean, (2) the cyclonic C and hybrid-cyclonic types HYC, which are associated with low pressure systems, and (3) the anti-cyclonic A and hybrid-anticyclonic types A-HYA, which are associated with high pressure systems (Figure 2-7). Figure 2-7b shows the mean annual volume of rainfall associated with the study area for each ACP type. One very important feature is the climatological pattern of rainfall for each ACP. This pattern must be properly reproduced by the selected hypothesis regarding the classification of the non-stationary rainfall process.

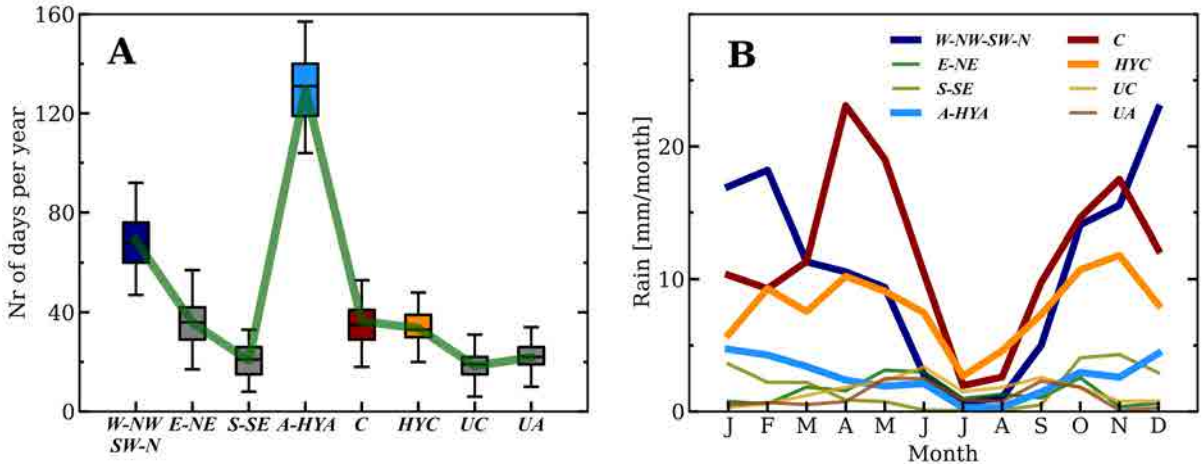

Figure 2-7 Rainfall characteristics in the Upper Guadiana Basin for the different Atmospheric Circulation Patterns: A) Average annual frequency of occurrence for each ACP type. B) Climatology of spatial average rainfall for each ACP type (wetter ACPs are highlighted using thicker lines).

2.6 Results

Our evaluation of the performance of the proposed method is made from two perspectives: (1) Reproduction of Climatology and (2) Reproduction of the spatial distribution of rainfall. In addition, we present an example of how well the intermittence process is reproduced.

Eleven conceptual models regarding the non-stationary structure of the SGRP with different levels of clustering were explored (see Table 2-2) to evaluate the hypothesis of rainfall (non)stationarity in time (Figure 2-7b) and to explore the dominant factors controlling the rainfall process in our test case. These include **NoCluster** and **NoCluster-Rand** (no classification), **ACP** (classification into 8 ACP types), **Season** (classification into 4 seasons), **Season6** and **Season6-Rand** (classification into 6 seasons), **Monthly** (classification into 12 months), **Season-ACP** (classification into 8x4=32 classes), **Season6-ACP** (classification into 8x6 classes), **Season6-ACP-ND** (same as **Season6-ACP** but without inclusion of topographic drift), and **Season6-ACP-GC** (same as **Season6-ACP** but conditioned on the gauge data). Here the dominant control processes of interest are (1) ACPs, (2) seasonality, and (3) sequencing of rainy days. Accordingly, the **season**, **season6** and **monthly** models incorporate only seasonality, the **ACP**, **season-ACP**, **season6-ACP** models incorporate ACPs (with and without seasonality) and the **NoCluster-Rand** and **season6-Rand** models use randomization of the rainy day sequences.

The model parameters were calibrated using the available data (without a validation period) so as to minimize the possibility of biasing the model towards a specific climate persistence condition (long wet or dry cycles).

For each conceptual SRGP model structure, we generated one hundred rainfall field simulations (replicates) with a spatial resolution of 2.5 km for each of the rainy days from 1959-2007 (11735 days x 100 realizations). These simulations were “unconditioned” (not conditioned on the rain gauge data), with the exception of those for the **season6-ACP-GC** case, for which the simulations *were* conditioned on the rainfall measurements. This model case should be very close to reality and was used as a benchmark case to compare the spatial distributions of rainfall obtained with all other models.

Model Name	ACP Clustering	Conditioned Simulation	Topography External Drift	Rainy days Sequence	Description
NoCluster	No	No	Yes	Observed	No classification
NoCluster-Rand	No	No	Yes	Synthetic	No classification
ACP	Yes	No	Yes	Observed	W/NW/SW/N, E-NE, S-SE, A-HYA, C, HYC, UC, UA
Season	No	No	Yes	Observed	JanFebMar, AprMayJun, JulAguSep, OctNovDec
Season6	No	No	Yes	Observed	JanFebMar, AprMay, Jun, JulAug, Sep, OctNovDec
Season6-Rand	No	No	Yes	Synthetic	JanFebMar, AprMay, Jun, JulAug, Sep, OctNovDec
Monthly	No	No	Yes	Observed	Jan, Feb, Mar, Apr, May, Jun, Jul, Aug, Sep, Oct, Nov, Dec
Season-ACP	Yes	No	Yes	Observed	Each ACP is classification by seasons
Season6-ACP	Yes	No	Yes	Observed	Each ACP is classification by season6
Season6-ACP-ND	Yes	No	No	Observed	Each ACP is classification by season6
Season6-ACP-GC	Yes	Yes	Yes	Synthetic	Each ACP is classification by season6

Table 2-2 Description of the several SRGP model classification levels implemented.

2.6.1 Reproduction of Climatology

2.6.1.1 Climatological Pattern of Mean Areal Rainfall

Here we compare the **a**real-average **c**limatological **r**ainfall (ACR) plot for the different SGRP models (Table 2-2) with the observed ACR data (Figure 2-8).

Figure 8a compares the ACR plots for the **season-ACP** and **season6-ACP** cases. Both cases involve ACP clustering of the rainy days, but each uses a different time-resolution for seasonal classification: **season-ACP** cluster into four seasons, and **season6-ACP** into six periods of different time lengths (Table 2-2). Note that **Season6** better represents the seasonal transitions from spring to summer and from autumn to winter and the driest months (July and August) in the UppGb. Clearly, **season6-ACP** provides a better fit to the observed ACR data.

To further explore the hypothesis regarding role of the ACPs, we examine the ACR plots obtained using the **season**, **season6** and **monthly classification** models. None of these models include classification by ACP, but differ in the seasonal classification of rainy days (Table 2-2). Figure 2-8b shows that the higher the number of classification levels, the better the fit to the climatological pattern. Moreover, the fit for **season6** is very similar to that obtained for **season6-ACP** (Figure 2-8**a**). Given that the only difference between **season6** and **season6-ACP** is the ACP clustering of rainy days, this seems to suggest that ACPs

provide only a weak control in the reproduction of average climatological rainfall. This is an expected result due to the seasonality of the rainfall by ACP as shown in Figure 2-7b. To shed more light on this, we remove the seasonal classification of the rainy days (Figure 2-8**c**) and show the computed ACR series for **NoCluster** and **ACP** (only clustering by ACPs) models (both of which used the same sequence of rainy days). The result shows that the last two models are biased, even though they partly reproduce the climatological pattern. This tends to support the finding regarding the role played by the ACP information in climatology of areal average rainfall, and illustrates the importance of (1) using the correct sequence of rainy days, and (2) the clustering by seasons in the simulation procedure.

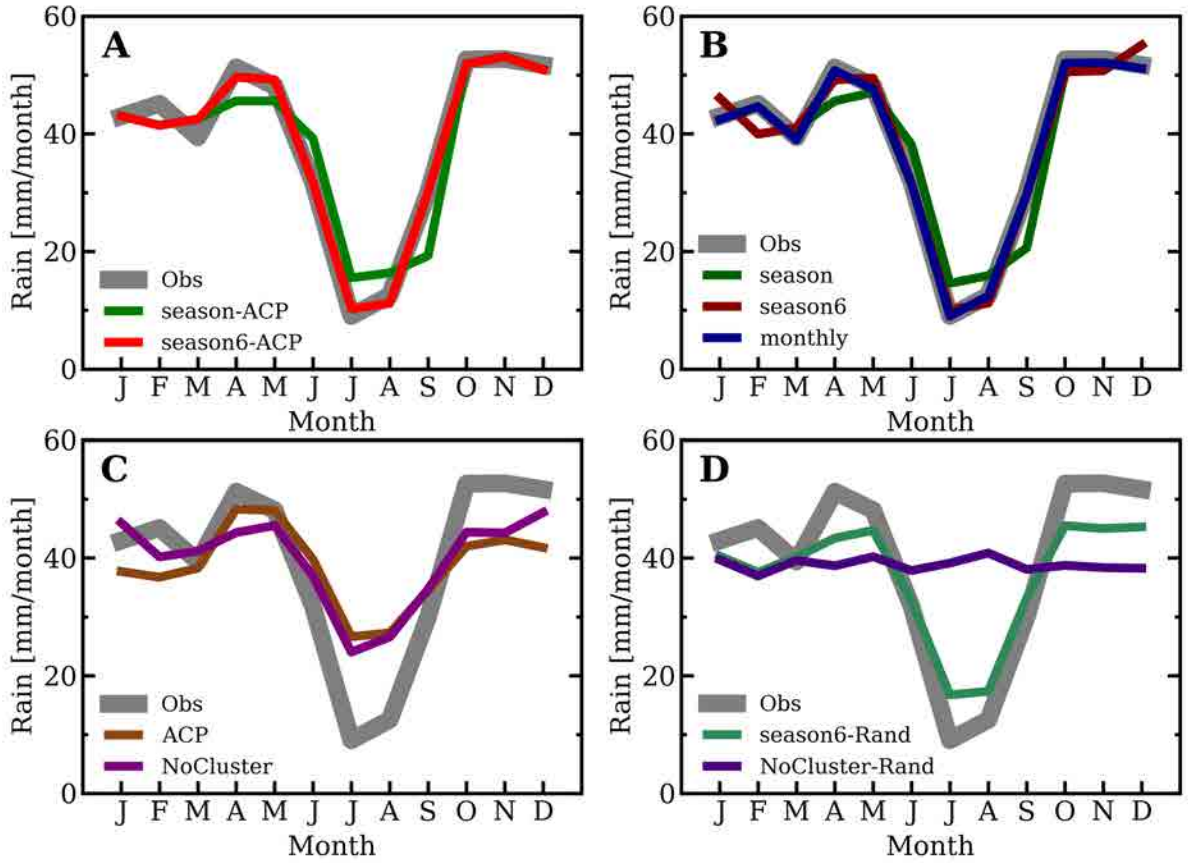

Figure 2-8 Climatology plots of spatial average precipitation for different conceptual SRGPs classification models. Observed climatology is shown using a bold grey line. A) Comparison between **season-ACP** and **season6-ACP**; both models have the same ACP aggregation model but **season6-ACP** has a higher number of seasonal divisions for classifying the rainy days. B) Model response when the ACP classification is removed to leave only classification by **season**, **season6** and **monthly**. C) Effect of removing the seasonality (leaving only **ACP**) and no classification (**NoCluster**). D) Comparison between **season6-Rand** and **NoCluster-Rand** to demonstrate the effect of randomizing the sequence of rainy days for a given ACP sequence.

To gain a better understanding of this point, we develop two new SRGP models termed **NoCluster-Rand** and **season6-Rand**, each of which uses a *synthetic sequence* of rainy days for parameter calibration, obtained by *randomly ordering* the rainy days for the whole time period. Neither of these models includes ACP clustering, and only in **season6-rand** is a seasonal classification of the rainy days considered. Figure 2-8**d** shows that only **season6-Rand**, which accounts for seasonal clustering, displays some seasonal behavior, whereas the ACR plot for the **NoCluster-Rand** case only reproduces the mean precipitation value with no climatological pattern. Clearly, seasonal classification of the number of rainy days plays a key role in the climatology of rainfall.

2.6.1.2 Inter-annual Variability in the Climatological Pattern

Although the results above indicate that ACPs play a weak role in controlling mean annual climatology, it is also important to reproduce the *inter-annual variability* in the climatological pattern. The observed climatological rainfall variability (Figure 2-9) is shown as a modified box plot (instead of inter-quartile range we show the 5th, 10th, 90th, 95th quantiles) for every month. The plot also shows the simulated climatological rainfall variability for the **season6** and **season6-ACP** models. It is clear that the ACP-based model reproduces the inter-annual variability much better, revealing the importance of ACP-based clustering of rainy days.

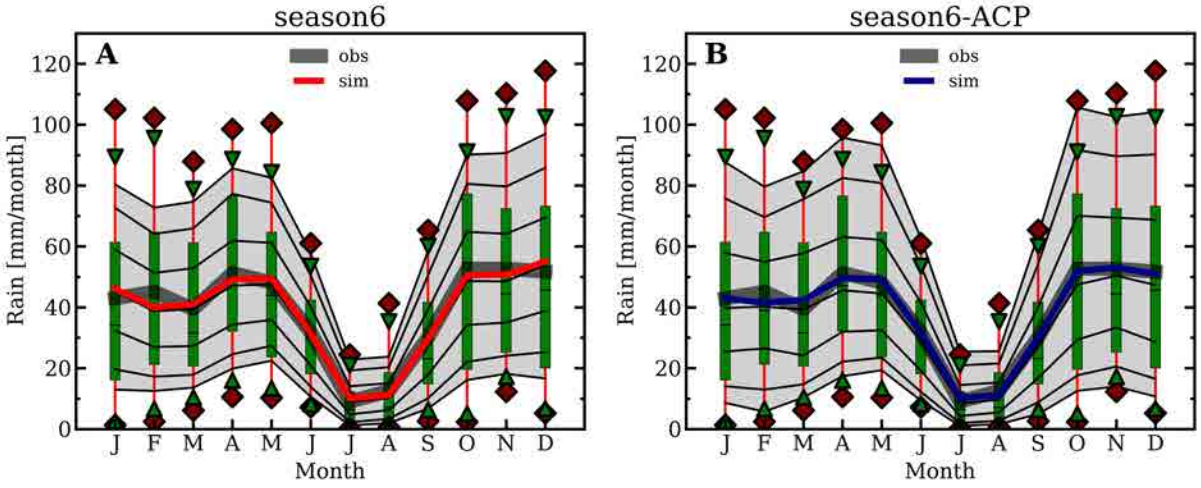

Figure 2-9 Plots showing extent of inter-annual variability of the climatology of spatial average precipitation. Observed variability is represented by modified box plots showing has two upper percentile limits (95th and 90th represented by the upper diamond and triangle, respectively) and two lower percentile limits (5th and 10th represented by the lower diamond and triangle, respectively). The observed mean climatology is represented by the bold grey line. Simulated variability (averaged over 100 realizations) is shown by different quantile intervals (5, 10, 25, 50, 75, 90, 95). The two plots represent different conceptual SRGP models: A) **season6**, and B) **season6-ACP**. Red and blue lines represent the respective simulated ensemble mean climatologies.

2.6.1.3 Climatological Pattern of Rainfall at the Gauges

The results presented in Section 2.6.1.1 allow us to determine whether basin average rainfall value is reproduced, and to investigate dominant processes at the catchment scale. To evaluate the ability to simulate spatial non-stationarity of rainfall, we select, from the simulated field, the pixels coinciding with the locations of meteorological stations in the basin. We examine the performance of the season6-ACP and season6-ACP-ND models, both of which include ACP clustering and seasonal classification (Table 3), but which differ in that the topographic external drift is only included in season6-ACP.

Figure 10 displays the observed average annual climatology of rainfall for meteorological stations located at different points in the UppGb, with elevations of 625, 740, 810 and 984 m a.s.l., respectively. The plot also shows the results for the 100 simulation ensembles, along with their confidence intervals (5% to 95%). The inclusion of the orographic effect on rainfall improves the results in areas with high and low elevations. In average elevation zones, both models (i.e., Drift and No Drift) yield the same results. The confidence intervals for the No Drift (pink shaded areas in Figure 2-10) are similar regardless of the rain gauge elevation. The observed rainfall that increases with elevation is captured by the Drift model.

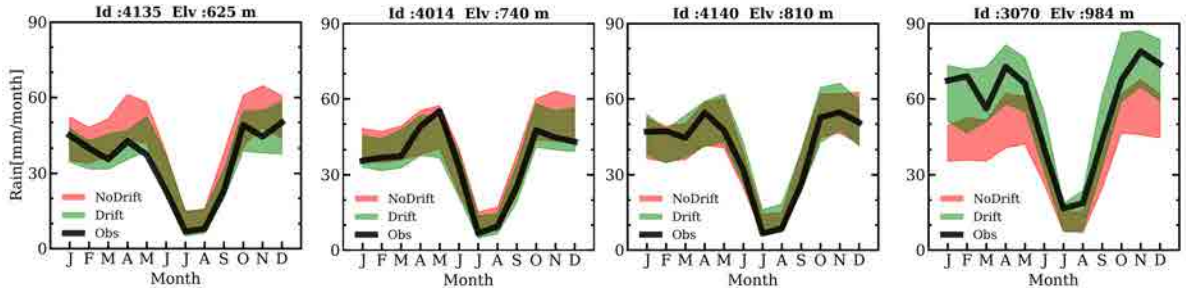

Figure 2-10 Climatology of rainfall at three different locations for a model that includes the spatial drift (**season6-ACP**) and for one that does not (**season6-ACP-ND**). Elevation increases from left to right. Shaded areas represent variability over the100 simulation ensembles, along with their confident intervals (5% to 95%). The dark green shaded area corresponds to the intersection zone between the two models.

2.6.1.4 Climatology of Spatial Rainfall Distribution

Here, we compare the climatological spatial patterns of rainfall for the **season6-ACP** and **season6-ACP-ND** models with the results obtained using the **season6-ACP-GC** model, in which the simulations are conditioned on the observed rain gauge data (and hence provide the best possible estimate of the spatial distribution of rain at the desired resolution).

Figure 2-11 compares the normalized error fields for the wettest (May) and driest (August) months (Figure 2-11 middle and lower panels), along with the digital terrain model (DTM) for the UppGb. In the wettest case, the mean rainfall field for **season6-ACP** bears a greater resemblance to the DTM than do the models that do not include the rainfall orographic effect. In contrast, the driest case shows no significant difference between **season6-ACP** and **season6-ACP-ND**. This contrasting behavior may be explained in terms of the spatial correlation structure of rain during May and August; rainfall in May is characterized by large-scale stratiform precipitation fronts slowly crossing the whole UppGb, whereas rainfall in August is mainly due to small/local convective cells of short duration.

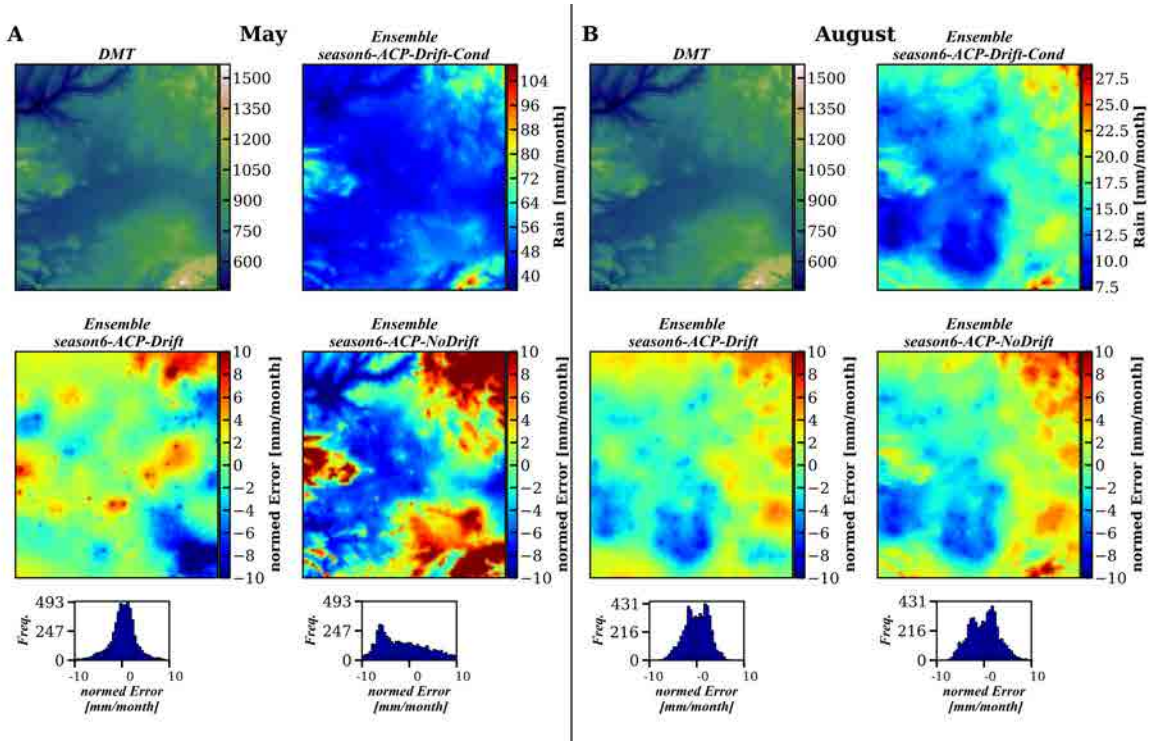

Figure 2-11 Plots of the mean ensemble spatial rainfall fields for A) May, the wettest month, and B) August, the driest month. Each panel presents the digital terrain model (upper left panel) of the Upper Guadiana Basin and the comparison between three different conceptual SGRP models with the same classification level (**season6-ACP**) but with different conditional information. The **season6-ACP-Drift-Cond** results (upper right panel) are conditioned to the historical time series observations and incorporates topographic spatial drift. The **season6-ACP-Drift** results are unconditional simulations and include spatial topographic drift. The **season6-ACP-NoDrift** results are unconditional simulations and do not include spatial drift. In the middle and bottom panels are the normed error difference field and histograms between **season6-ACP-Drif-Cond** and **season6-ACP-Drif**t (left middle and bottom panel) and **season6-ACP-NoDrift** (right middle and bottom panel).

2.6.2 Spatial Distribution of Rainfall

Next, we determine whether the simulated spatial distribution of rainfall matches the observations. To this end, we use the quantile-quantile (Q-Q) plot to compare the observed

and the simulated rainfall for (1) the selected rain gauge sites, and (2) the basin averaged rainfall. Here, we only use the **season6-ACP model**.

2.6.2.1 Rainfall distributions at the gauges

Figure 2-12 shows the Q-Q plots corresponding to several meteorological stations distributed throughout the UppGb. In general, the rainfall distributions appear to be well reproduced regardless of the elevation of the rain gauge. This is especially true for values of precipitation below 30 mm. Higher values show increased dispersion (the shaded area ranges from 5% to 95% of the confident interval) and a tendency to overestimate large rainfall values. Since the model uses empirical rainfall distributions with a finite sample size, the above problems could be resolved (1) by increasing the sample size using any interpolation technique or (2) by modifying the limits of the normal score distribution. In other words, the amount of (observed) data used to define the normal score transformation, and the amount of simulated data values must be large enough to correspond to the recurrence time of the extreme values that we wish to simulate.

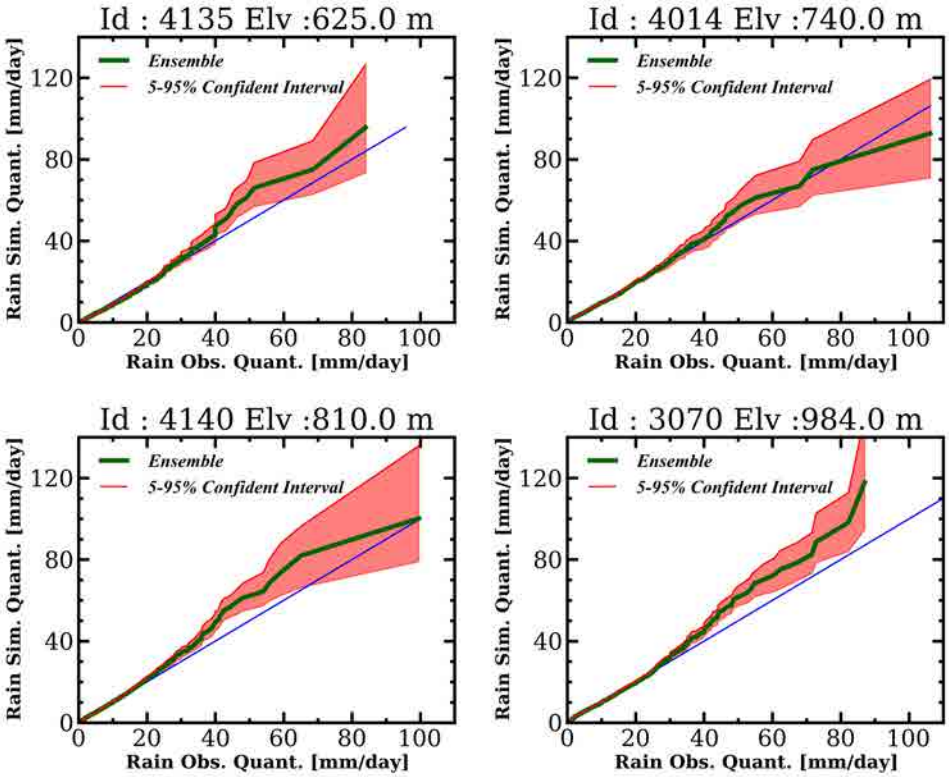

Figure 2-12 Quantile-Quantile plots comparing distributions of observed and simulated daily rainfall intensities at four different rain gauge locations.

2.6.2.2 Distribution of areal-average rainfall

We evaluate the Q-Q plots for areal-average rainfall for three different time scales: (1) daily, (2) monthly accumulated (3) yearly accumulated. The results (Figure 2-13) are fairly good for daily rainfall, but not so good for the two other cases. Nevertheless, the yearly Q-Q plot shows that the model overestimates the minimum values (driest years) and underestimates the maximum values (wettest years). This is mainly due to the choice of the gamma function $\Gamma_{\hat{\mu}_{z_j}}$ (Eq. (7)) to represent the pdf of the spatial average rainfall. The gamma function fits the mean and the mode values fairly well but is not so good for the tails of the distribution (Figure 2-2). This effect could be resolved by other distributions that better represent the extreme values (e.g. ***Vrac and Naveau, 2007***; ***Furrer and Katz, 2008***; ***Solari and Losada, 2012***), an issue we intend to explore further in an on-going work.

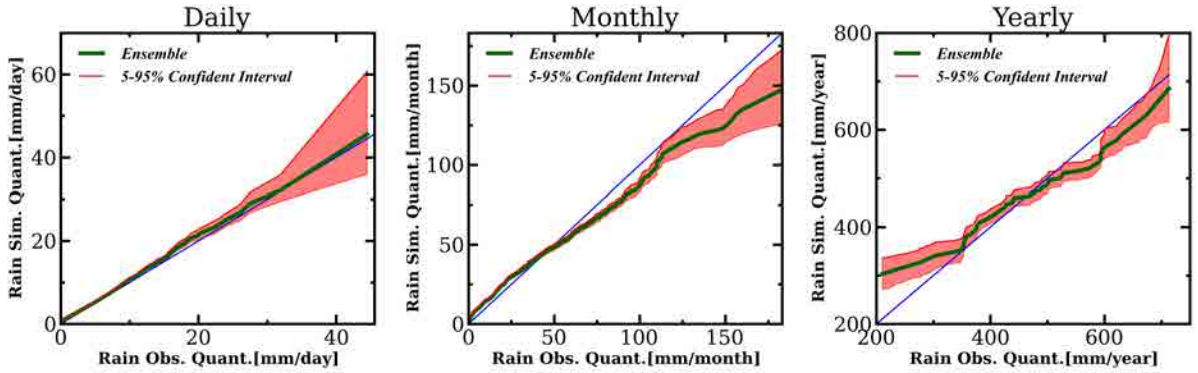

Figure 2-13 Quantile–Quantile plots comparing distributions of observed and the simulated daily (left), monthly accumulated (center) and yearly accumulated (right) spatially averaged precipitation.

2.6.3 Intermittence of Rainfall

Figure 2-14, shows an example of the final rainfall fields obtained by applying the methodology for different percentage of fractional area covered by rain: 5, 25, 50 and 80. Results are shown for the **season6-ACP** model including the representation of external drift with elevation. The plots show that the SIS method realistically reproduces the intermittence process in terms of the clustering of regions with rainfall. However, the fields tend to show sharp transitions between rain and no rain areas because of the assumption of independence between the intensity and intermittence processes.

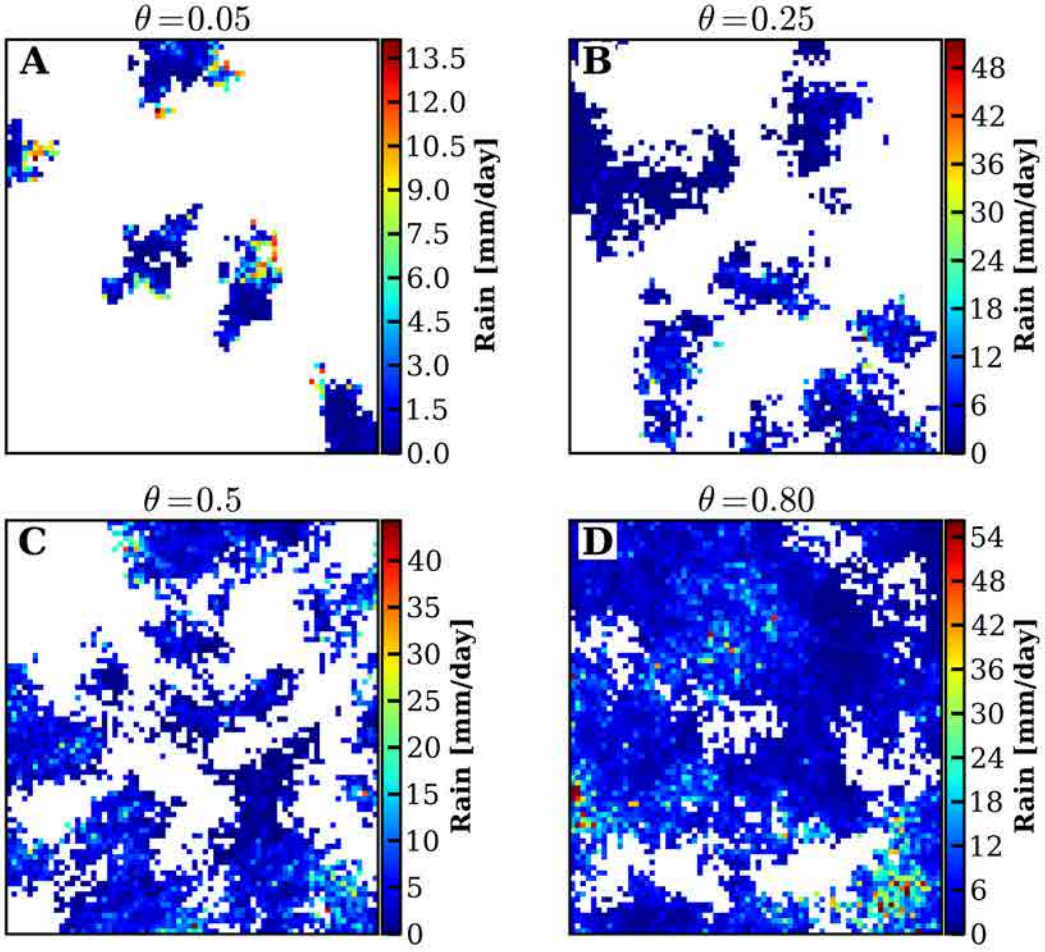

Figure 2-14 Examples of daily rainfall fields generated for different days with variable fraction of rain-covered area: A) 0.05, B) 0.25, C) 0.5 and D) 0.8.

2.7 Discussion and Conclusions

We present a method to simulate daily rainfall fields with sufficient spatial resolution to be used in spatially distributed hydrological modeling. The approach incorporates several sources of information, and simulates major non-stationarity features of the rainfall fields.

By exploiting information regarding the sequence of ACPs we are able to obtain time stationary sequences of SRGPs. This allows the model to exploit invaluable information regarding climate variability/change provided by GCMs. Consequently, the approach can be used for developing multiple stochastic ensembles of downscaled rainfall fields for use in CCIS assessments (including uncertainty analysis).

Further, the approach has the ability to generate both conditional and unconditional rainfall field simulations. As a result, the model can be used to fill observation data gaps in the historical rainfall data sets.

We tested the model for the Upper Guadiana Basin in Spain and found that it provides an accurate reproduction of the major spatio-temporal features of rainfall needed for hydrological modeling and water resource evaluations. The incorporation of spatial drift related to orographic precipitation significantly improved the results. The incorporation of seasons enabled the reproduction of the observed climatology of spatial averaged rainfall. ACP clustering improved the reproduction of the inter-annual climatological variability.

Nevertheless, certain aspects of the model need to be improved. First of all, the assumption of independence between rainfall amount and the rainfall intermittence fields produces sharp transitions between the areas of rain and no rain in the daily rainfall fields obtained. This is an important issue that should be addressed in the future. Some authors (***Bell 1987***; ***Guilliot, 1999***; ***Kleiber et al., 2012***) use a threshold-based method to simulate rainfall occurrence, which employs the same latent Gaussian process that simulates rainfall amounts. Comparing both methods, ***De Oliveira (2004)*** suggests that the application of one of the two models depends mainly on the precipitation patterns of the specific region under study. From the hydrological point of view, the correlation between rainfall intensity and intermittence should be better represented. Second, the Q-Q plot analysis indicates that extreme rainfall values and their frequency of occurrence are overestimated.

In an on-going work, we are evaluating the usefulness of the approach for downscaling rainfall fields in the context of climate change. Such analysis is supported by the expectation that climate change will affect the frequency of the ACPs and hence the precipitation regimes (***Trenberth, 2011***). To establish the robustness of such applications, it is necessary to ascertain whether the SRGP model parameters can be assumed as stationary for the future. Naturally, for climate impact analysis *some* assumptions should be made. However, it is important to evaluate the degree to which the results could be affected by these assumptions. Moreover, when the approach is used in the context of distributed catchment modeling, we can expect the spatio-temporal variability of the precipitation to affect the response of the hydrological processes in different ways. It is therefore necessary to determine the degree of sensitivity of these responses to uncertainties in the SRGP model parameters.

3 Impacts of Rainfall Spatial Variability on Hydrogeological Response [2]

3.1 Introduction

3.1.1 Background

Rainfall Spatial Variability (RSV) exerts a considerable influence on the space-time distribution of state variables of a hydrological system. Its impact depends on factors, such as basin scale related to rainfall variability (***Wood et al., 1988; Gabellani et al., 2007***), precipitation type (convective or stratiform) (***Bell and Moore, 2000***) and predominant hydrological partitioning processes (***Shah et al., 1996; Brath and Montanari, 2003; Gabellani et al., 2007***). These factors in addition to the influence of the model structure and measurement errors in input fluxes (***Younger et al., 2009***), etc. have prevented a consensus of the effects of RSV on the hydrological response (***Nicotina et al., 2008***) from being reached.

Furthermore, studies have tended to focus on the characteristics of river discharge (such as peaks), during an event response (***Wilson et al., 1979***; ***Krajewski et al., 1991; Obled et al., 1994; Nicotina et. al. 2008***). Moreover, these studies generally agree on the effect of the total volume of water during an event with respect to the river discharge (***Obled et al. 1994***) and on which runoff generation processes that are most sensitive to RSV (infiltration saturation processes)(***Nicotina et al., 2008***). In general, these studies have paid little attention to the spatial distributions or the long term effects on other important hydrological responses (e.g.: soil moisture, recharge, groundwater levels, groundwater storage variations etc.). One exception is the work of ***Schuurmans and Bierkens (2007)***, who studied the effect of the RSV on soil moisture, groundwater level and river discharge at daily time scale in a flat shallow groundwater basin with a rapid response. These authors found that the RSV has an effect on the internal spatial distribution of the state variable analyzed and that the general behavior was largely determined by the areal average rainfall (uniform case).

---

[2] This chapter is based on paper: *Sapriza Azuri, G., Jodar, J., Carrera, J., and Gupta, H. (2013). Impacts of rainfall spatial variability on hydrogeological response . Submited*

Earlier studies are not easily generalized. Moreover, although RSV may be assumed to have be strongly damped in the hydrogeological response of the system, spatial intermittence and orographic effects on the rainfall fields (important source of spatial variability), can lead to significance differences in the hydrogeological response. At short time scales (less than a year), these differences may be difficult to assess, particularly when looking at an integrated response such as river discharge. However, at long time scales, such differences can give rise to completely different hydrogeological responses. Moreover, the majority of studies have focused on the system response only under "nearly natural" conditions - with some exceptions involving small basins in urban areas (***Smith et al. 2005***). Thus, what the effects of RSV might be on the dynamics of systems that are overexploited, e.g. by groundwater pumping are not yet fully understood.

3.1.2 Objectives and Scope

The primary objective of this work is to investigate the impact of the RSV on the hydrogeological response at "long term time scales" and on an "overexploited system". In particular, we investigate how uncertainty in the spatial distribution of rainfall is propagated through the hydrological system, and how it is affected by local differences in dominant hydrological processes (such as wetlands) and/or by the degree of exploitation (pumping). Further, we discuss the amount of information that is lost (i.e. how the assessed impacts are affected) owing to the use of up-scaled rainfall fields (e.g. information provided by coarse spatial resolution of remotely sensed estimates or regional model simulations, or simply by the use of spatially uniform fields given the lack of spatial variability information – e.g. very few available rain gauges).

With that purpose, we generate stochastic rainfall fields at daily time scale using a Stochastic Rainfall Generation Process (SRGP) that is conditioned to (a) preserve the rainfall values observed at the gauges, (b) reproduce the spatial intermittence of rainfall, (c) account for orographic effects, and (d) reproduce the different local rainfall generation properties associated with different regional-scale atmospheric circulation patterns (for details see ***Sapriza et al. 2013a***).

The stochastically generated rainfall fields are used to drive a spatially distributed hydro-geological model of 16,000 km^2 in the Upper Guadiana basin (**UppG**) in the center of Spain. Since the 1970s, several areas of the basin have been subjected to significant amounts of groundwater pumping, which have affected the dynamics of the system. The model was

calibrated to match the historical input-state-output spatio-temporal response (including pumping and groundwater level history) of the system for the 43 year period between 1959 and 2001. The spatio-temporal hydrogeological response of the system (including Soil Moisture, Actual Evapotranspiration, wetland occurrence, Groundwater Recharge, Runoff Generation, Groundwater Heads levels, Groundwater Storage variations, and River Discharge) was then analyzed.

3.2 Methods

3.2.1 Study Area

The Upper Guadiana basin forms part of the central Spanish Meseta, and covers an area of approximately 16000 km^2 (Figure 3-1). The basin is located between latitudes 38º37'N and 40º08'N, and between longitudes 2º25'W and 3º51'W. Morphologically, the main part of the basin is characterized by a smooth topography with altitudes ranging from 550 to700 m.a.s.l. Nevertheless, the northern and southern boundary (Sierra Altomira and Campos de Montiel, respectively) displays a mountainous landscape with an altitude exceeding 1,000m.a.s.l. The combination of a smooth topography with a lack of a well-defined drainage network and an abundance of large karstic aquifer formations give rise to complex relationships between surface and subsurface waters. These interconnections enable wetlands to flourish (around 250 km2), which is ecologically significant.

The UppGb has a mixed continental, semi-arid Mediterranean climate. The spatial-time variability of precipitation is very wide because of the orography and the influence of the Atlantic and the Mediterranean. The annual precipitation is approximately 450 mm/year. Its main characteristics are seasonal variability with a dry season in summer (especially in July and August accounting for 5 % of the annual precipitation). This precipitation is dominated by small convective rain cells of short duration. The wettest seasons, autumn and spring are characterized by stratiform frontal rain with large spatial continuity and duration.

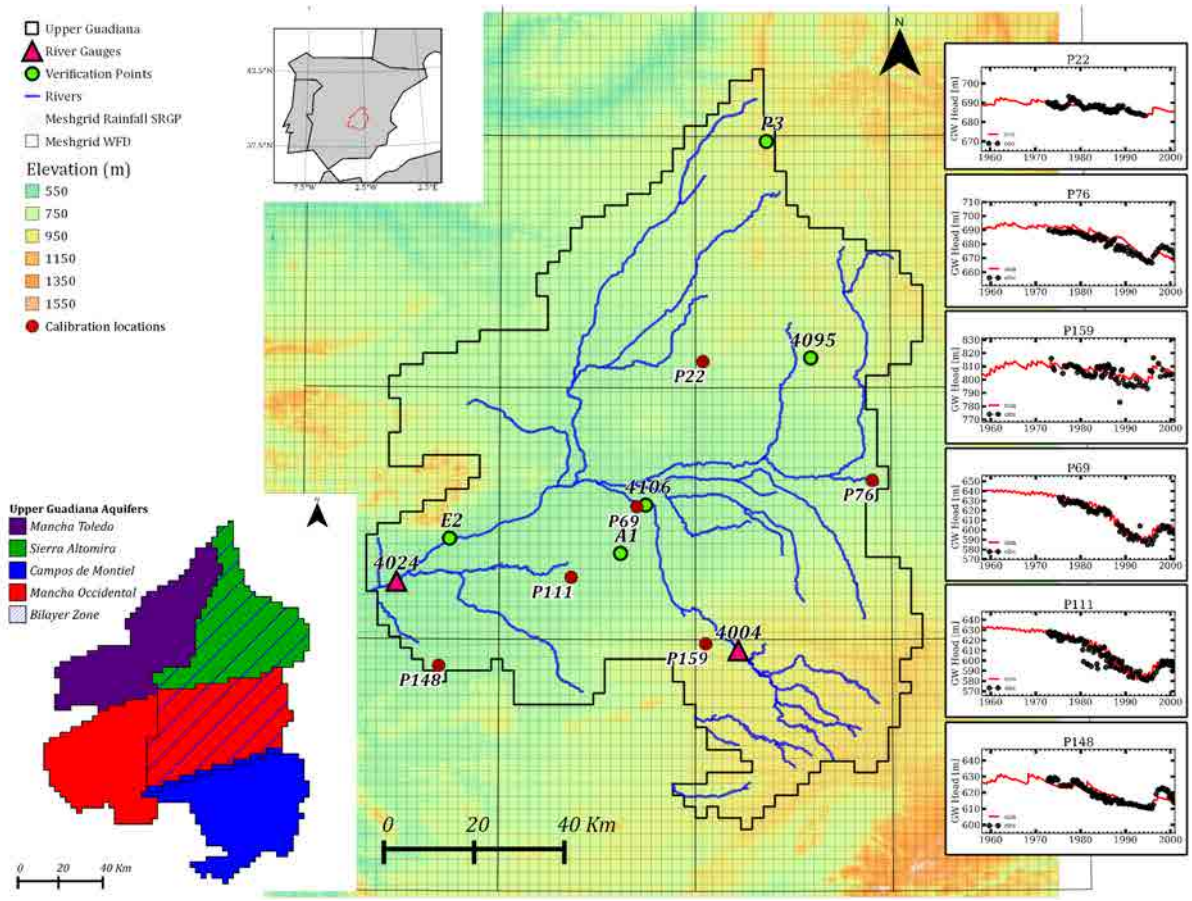

Figure 3-1 Area of study. Principal features are represented: Aquifer delimitations, principal rivers, piezometric and river gauges location with their calibration, rainfall grids (SRGP, WCH), and locations used to evaluate the effect of RSV.

3.2.1.1 Aquifers

The Upper Guadiana aquifer system is divided into four sub-units: "Sierra de Altomira", "Mancha de Toledo", "Campos de Montiel" and "Mancha Occidental", Figure 3-1. The last two units enjoy the dubious reputation of being the first two aquifers in Spain to have been declared overexploited because of pumping drawdown (more than 50 meters of decline in the groundwater levels at some locations).

Figure 3-2 shows the time series evolution for the groundwater extractions integrated over the domain, showing a clear seasonal pattern with a maximum in 1990. The spatial pumping distribution (Figure 3-2c**)** shows that the larger extractions are concentrated in the central zones of the Mancha Occidental aquifer.

Based on the works of ***Martínez-Cortina (2000)*** and the references therein, the main hydrogeological characteristics for every sub-unit can be briefly summarized as follow:

- Sierra de Altomira aquifer is composed of aquifer units. The deepest is a Jurassic semi-confined aquifer formed by sandy and dolomitized limestone,

25-90 m thick, with the transmissivity of 1000-5000 m2/day and a storage coefficient of around 10-4. The upper unit is a Cretaceous free aquifer formed by dolomite and limestone, 60-80m thick with a transmissivity of 100-250 m2/day.

- Mancha Toledo is a Triassic-Miocene-Plioquaternary aquifer formed by detrital sediments. It functions as a free aquifer with a mean thickness between 500 and 600 m.
- Campos de Montiel is a Jurassic limestone karst free aquifer with an average thickness of 160 m and a transmissivity of 50-2500 m2/day.
- Mancha Occidental is a two layer aquifer with a detrital semi-confined layer that functions as an aquitard. The deepest unit is a Jurassic-Cretaceous aquifer that is confined and made up of limestone. It has an average thickness of 160 m, a transmissivity of 200-6000m2/day and a storage coefficient of 10-3- 10-4. The upper unit is a Tertiary-Quaternary free aquifer. The Tertiary materials are composed of Miocene limestone with a thickness of 200 m and a transmissivity close to 20000 m2/day. The Plioquaternary is made up of detrital sediments with a thickness of 60 m and a transmissivity of 500 m2/day.

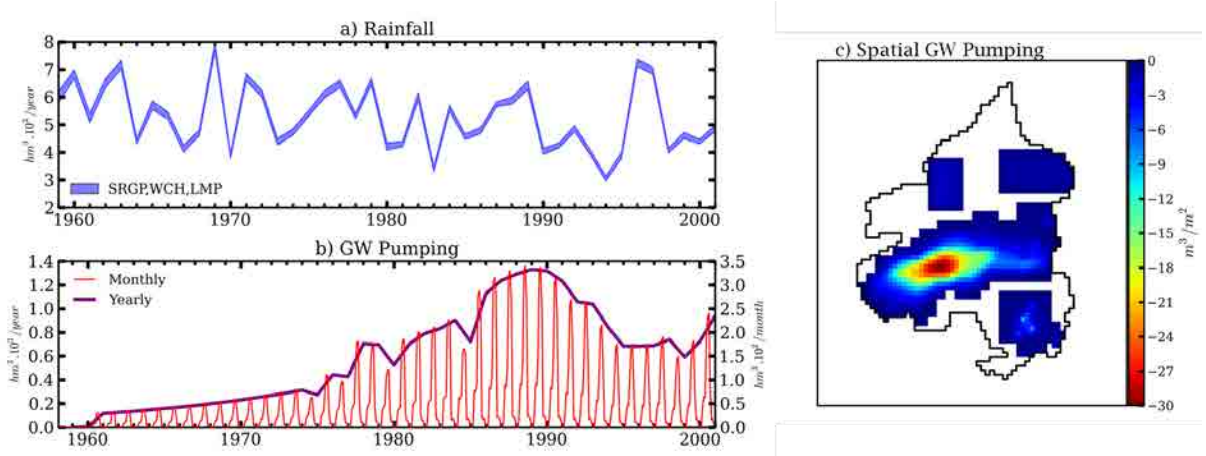

Figure 3-2 Time series of the yearly spatial accumulated of rainfall (panel a) and gw pumping (panel b). Panel c shows the total period spatial distributions of pumping

3.2.2 Hydrogeological Model

The basic conceptualization of the Upper Guadiana aquifer system is represented by one large reservoir where the limit boundary conditions are prescribed as no flow. The system is simulated by using a two layer finite element model: (1) an upper layer that covers the entire domain for simulating the free and semi-confined parts of the aquifer system, and

(2) a lower layer that simulates the confined part of the sub-unit Mancha Occidental and Sierra de Altomira. The two layers are hydraulically connected by 1D element.

This conceptual model follows the work of ***Martínez-Cortina (2000)***, who implemented the numerical model in MODFLOW. This model was used as a pre-calibrated base model to build a new one, migrating from finite differences to a finite element scheme, and from a monthly time scale to a daily one. The migration included an atmospheric boundary condition (soil balance component) and the development of a groundwater-surface water (GW-SW) interaction module. The aim of these changes is threefold: (1) to enhance the GW-SW interaction associated with the marked change in the dynamics of the system (e.g. as a result of the inversion of the GW-SW interaction, the river becomes a source of localized recharge to the aquifer) owing to anthropogenic pressure; (2) providing a better representation of the spatial variability of the recharge process because of spatial variability of the rainfall fields; and (3) to improve the wetlands simulation.

These new boundary conditions define a coupled distributed hydrogeological model that combines a physically based groundwater component (GW) with a conceptual soil-water balance component and water routing component for the runoff propagation.

From the soil-water balance we estimated the soil moisture, AET, runoff generation and the GW recharge. The model estimates two types of GW recharge: (1) the GW recharge that is generated by the soil-water balance, which is considered to be instantaneous and (2) the GW that reaches the GW level. For the latter, we incorporated a transit through the non-saturated zone (composed of a series of linear storage) by the application of a gamma transfer function *(**Besbes and de Marsily, 1984**)*. We only refer to the former in the present analysis.

Routing of the surface and subsurface runoff generation accomplished using the CEQUEAU model (***Girad et al., 1972***, ***Korkmaz et al., 2009***).

The model was implemented into the PROOST (Process Oriented Optimization and Simulation Tool), which is a hydrogeological modeling platform, developed using an object-oriented architecture (***Slooten, 2009***). The code includes the simulation of solute, reactive, multicomponent, multiphase flow and transport process in aquifers, and enables the automatic estimation of parameters via optimization. PROOST is open source and under development by the Hydrogeology Group IDAEA (CSIC) and the technical University of Catalonia.A finite difference scheme was applied to temporal discretization while a finite element scheme is adopted for spatial discretization. The latter uses triangle elements that are

combined to generate regular square zones that occupy an area of 2.5x2.5 km^2. The model has two hydraulically connected layers with a total of 861 one-dimensional elements. The lower layer contains 864 nodes and 1556 elements whereas the upper layer contains 2035 nodes and 3764 elements.

The starting point of for calibration of the model is the the pre-calibrated model of ***Martínez-Cortina (2000)***. Nevertheless, the model architecture has been somewhat changed as described above, and the new model was therefore re-calibrated via a manual process to improve reproduction of the observed piezometric and river discharge data. The model is used to simulate the hydrogeological response of the system between 1959 and 2001.

3.2.3 Data: Rainfall Inputs

To evaluate the impact of RSV on the hydrogeological response simulated by the model we used rainfall gridded data at three different levels of spatial support (Figure 3-1); in each case we obtain a set of 100 daily rainfall field time series for every RSV scheme (i.e. SRGP, WCH and LMP) which are used to drive the UppGb hydrological model.

Fine scale: The SRGP model is used to simulate a total of 100 stochastic time series realizations of daily rainfall fields at the same spatial resolution as the UppGd hydrogeological model (cells with an area of 2.5x2.5 km^2). This model accounts for two major rainfall non-stationary process that affect rainfall generation: temporal non-stationarities caused by changes in the frequencies of different precipitation generating mechanisms (i.e. frontal and convective rainfall regimes), and spatial non-stationarities caused by interactions of meso-scale atmospheric patterns with topography (i.e. orographic effects). The overall non-stationary process is approximated as a discrete set of time-stationary stochastic rainfall generating processes, each of which represents the a characteristics spatial patterns of rainfall (including its variation with topography) associated with a different atmospheric circulation patterns (ACP) and seasons. The SRGP model uses the daily rainfall data available from meteorological weather stations and the mean sea level pressure from the NCEP-NCAR re-analysis data set (***Kalnay et al., 1996***) to generate the rainfall field time series that can be conditioned or unconditioned upon rainfall data observations. For further details of the setup of the SRGP model see ***Sapriza et al. (2013a)***.

Medium Scale: The fine scale rainfall fields generated by the SRGP are aggregated up a cell area of 0.5º x 0.5º (called WCH), having, which is the typical support size used by Regional Climate Models (RCM). This scale also matches the spatial resolution of

meteorological forcing data generated in the context of the WATCH Project (***Weedon et al., 2011***) which this work is a part of.

Large Scale: Finally, the fields are then aggregated up to a large scale grid (called LMP), having only one irregular cell of the same size and shape of the whole basin/model domain. In both the medium and large scale cases, upscaling is by arithmetic averaging.

The daily rainfall fields of the coarser grids were obtained by upscaling (arithmetic averaging) the SGRP rainfall fields onto the WCH and LMP grids. As a result, we obtained a set of 100 daily rainfall field time series for every RSV scheme (i.e. SRGP, WCH and LPM) to drive the Upper Guadiana hydrogeological model.

3.2.4 Investigative Approach

The methodology implemented to explore the effect of **RSV** upon the hydrogeological response is as follows:

a. Calibration of the UppG model using one realization of the rainfall fields generated in (1) above. This is a simplified approach – instead of using all the 100 fields to generate the hydrogeological response and then calibrating to the mean response. We are not interested here in a "perfect" calibration -- an approximate one is sufficient.
b. Simulation of the hydrological model response by driving the calibrated UppG model with the 100 SRGP, WCH and LMP time series ensembles. This generates three ensembles of hydrological model responses, which we will refer to as the SRGP, WCH and LMP ensemble responses.

The analysis of the hydrological response of the model was performed for the whole simulated period (i.e. 1959-2001). This allowed us to evaluate the long term effects of using different forcing rainfall time series with different spatial resolutions. Moreover, the uncertainty propagation through the hydrological system was investigated, elucidating the effect of observation, wetlands, pumping and location on the uncertainty.

The hydrological responses studied are as follow: soil moisture (SM), actual evapotranspiration (AET), fractional area cover by wetlands (WFA), spatial runoff generation (QESC), groundwater recharge (RCH), groundwater surface water exchange (eGSW), river runoff discharge (QRV), net groundwater storage aquifer (STG) and groundwater heads (GWH).

The WFA was estimated as the number of soil cells that are at saturated state (SM=1) divided by the total number of cell of the upper layer in the UppGd model. The STG was computed as the sum of all the input and output fluxes to the aquifers.

Uncertainty was expressed in all cases as the 5-95 % confident interval limit from the ensembles over 100 realizations. For the spatial distribution we expressed the uncertainty as the difference between the 95% and 5% percentiles.

3.3 Results

3.3.1 Overall response: Spatial Cumulative Sum Time Series

Figure 3-3 presents the overall hydrogeological response to different RSV's in terms of (1) the cumulative time series of Rainfall and Withdrawals, AET, QESC, RCH, eGWS and STG, and (2) the spatial averaged time series of SM and WFA.

The cumulative sum allowed us to visualize the overall evolution response integrated for the whole area. The variations in the slope also provided information about changes in the behavior of the system, helping to identify, drier and wetter periods and initiation of exploitation.

Figure 3-3a shows the time evolution of the cumulative volume of precipitation and withdrawals registered in the Upper Guadiana Basin. As can be seen, the slope of cumulative rainfall does not change over the entire period. However, withdrawals are very small before 1980 and subsequently increase at a constant rate. Meanwhile, AET (Figure 3-3b) shows their cumulative time variation. There is no significant difference between the three cases (i.e. SRGP, WCH and LMP). For the total response during the whole period, we obtained only a slightly higher AET for LMP, followed by WCH and then by SRGP. The uncertainty remained narrow in the three cases.

For the QESC response (Runoff Generation; Figure 3-3c), SRGP produces a larger amount of runoff, highlighted by the steep slope. All the models show a marked reduction in the 1980s owing to changes in the regional groundwater pumping scheme, shifting from small to large withdrawals throughout the basin. The slopes of the cumulated evolution are closer to zero for SRGP, WCH and LMP, which reflects the scarcity of runoff generation. Note that the width of the uncertainty intervals increase with increased SRV.

Figure 3-3d shows the evolution of the cumulative groundwater recharge (RCH). This variable is clearly very sensitive to the degree of spatial rainfall variability, with the SRGP

case resulting in almost twice the cumulative recharge than in the cases of WCH and LMP. The mean slope of the evolution for SRGP is larger than those of the two other cases, especially in the driest periods during which the slopes of LMP and WCH attain zero. In all three cases the uncertainty is similar.

The cumulative evolution of of GW-SW exchange (Figure 3-3e) shows similar pattern to that of QESC (Figure 3-3c) but with value of the opposite sign (negative) indicating fluxes out of the aquifer. The three cases show the same evolution pattern despite the fact that SRGP produces a higher discharge from the aquifer. Meanwhile, the cumulative time evolution of groundwater storage (STG, Figure 3-3f) shows that the system is clearly less affected by pumping when the detailed spatial variability of rainfall (SRGP) rainfall is properly represented. It is interesting to note that (1) the starting time at which the system can be considered to be overexploited (i.e. when STG becomes negative) is 1965 for LMP, 1973 for WCH and 1980 for SRGP, and (2) the system response at the end of the simulation period is approximately 91% less affected for the case of SRGP in comparison with LMP.

Interestingly, the trajectory of annual average soil moisture volume (SM; Figure 3-3g**)** is quite similar for all three cases, being slightly larger for LMP followed in decreasing order by WCH and SRGP. However, the monthly average wetland fractional area (WFA; Figure 3-3h) clearly shows the impacts of long term withdrawals caused by pumping. As the groundwater heads started to decline the wetlands began to dry up, and almost completely disappeared by the beginning of the 1980s. Note that the simulation of wetlands dynamics is sensitive to the degree of spatial rainfall variability represented in the model; the greater the spatial variability of rainfall the larger the surface area of wetlands. In terms of re-flourishing an already dried wetland, the greater the degree of spatial rainfall variability the larger frequency/probability of re-flourishing. Regardless of the RSV scheme, the width of the uncertainty interval grows during the wet period (i.e. before 1979) owing the increase in the area covered by wetlands

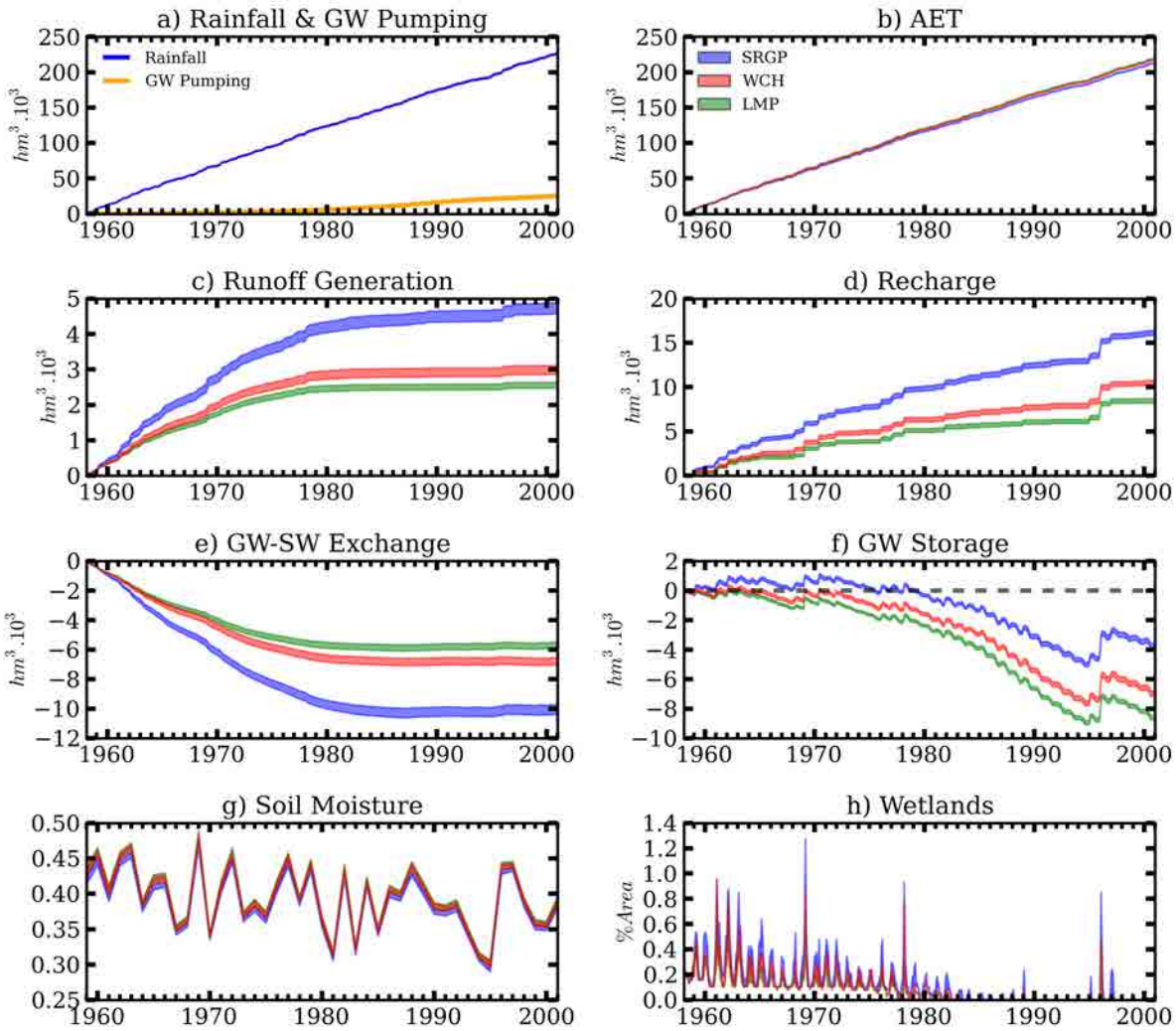

Figure 3-3 Overall responses obtained with the three spatial rainfall resolutions (blue SRGP, red WCH and green LMP). They are presented the spatial cumulative sum time series for : rainfall (a), groundwater pumping (a), AET (b), runoff generation (c), recharge (d), groundwater-surface water exchange (e) and groundwater net storage (f). The spatial average of the soil moisture (g) and fractional area cover by wetlands (h) are also presented.

3.3.2 River Runoff and Groundwater-Surface water exchange

The RSV scheme exerts a significant influence on the evolution of simulated river runoff. Figure 3-4a and b show the yearly-cumulative river runoff computed at two points in the basin: the Guadiana and the Penyarola river gauges (see purple triangles in Figure 3-1). In both cases, the smaller the spatial resolution of rainfall the higher the runoff and the larger the associated uncertainty bound.

Nevertheless, these river gauges differ (1) in the degree of the response between the RSV schemes and (2) to what extent the impact of pumping affected the system. At the Penyarola river gauge (Figure 3-4a), there is a larger difference between WCH and LMP. The response is less affected by pumping and the river never dries up. WCH and LMP show little

difference at the Guadiana river gauge (Figure 3-4b). The uncertainty bound is narrower in the three cases, SRGP being a little larger. The rivers almost dry up in response to the groundwater extractions in 1985 for LMP and WCH and in 1988 for SRGP. In both cases, the greater the degree of spatial rainfall variability the higher the runoff and larger the associated uncertainty bound

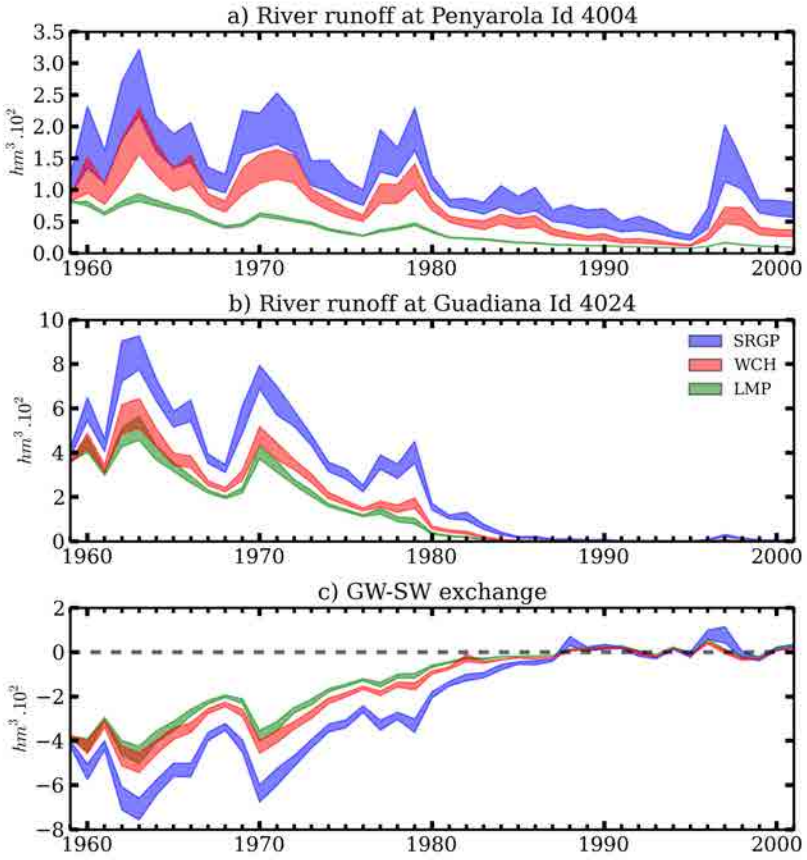

Figure 3-4 River runoff at two locations and the gw-sw exchange for the whole Upper Guadiana Basin.

The degree of RSV also clearly affects the hydrological response in terms of the groundwater and surface water exchange dynamics. Figure 3-4c shows the evolution of the yearly-cumulative GW-SW exchange time series. This figure is complementary to Figure 3-3e but shows more clearly the change in the hydrological dynamics of the system. Massive withdrawals generate a widespread decline in the phreatic level of the aquifer. As a result of the groundwater level drawdown, the exchange of water between the surface and the aquifer is reduced, the rivers being disconnected from the groundwater system. At this point (see in Figure 3-4c the exchange dynamics after 1989) the water flowing in the river infiltrates the river bed towards the aquifer. The values greater and lower than zero represent aquifer

recharge and discharge, respectively. Rivers vary from receiving a base flow from the aquifer to directly recharging the aquifer.

3.3.3 Spatial Distribution of Total

The foregoing findings refer to the spatially aggregated responses of the basin. Here we examine the structure of the spatial distribution and its uncertainty. Figure 3-5 illustrates the differences in spatial distribution due to differences in representation of spatial rainfall variability. Figure 3-6 shows the differences in spatial structure of the associated uncertainty and how that uncertainty is propagated through the hydrological system. From the previous analysis, we can identify recharge (RCH) as being the main driver of the hydrogeological response. Further, the storage (STG) provides a good overall summary of system response. Therefore, we discuss here only these two responses.

3.3.3.1 Magnitudes

The cumulative spatial patterns of rainfall imposed on the system are illustrated in Figure 3-5a-c. SRGP clearly displays the orographic effects caused by topography, the patch pattern in WCH and the uniform distribution shape for LMP.

As should be expected, the three RSV schemes show clearly different response for RCH (Figure 3-5d-f). SRGP clearly shows a wide range with a higher recharge in zones of high altitude, reflecting the orographic signal in the precipitation. For WCH and LMP**,** however, the spatial distribution displays is more indicative of the pattern of the soil type, superimposed on the patchy pattern imposed by data grid.

STG (Figure 3-5g-i) shows large zones with negative values, indicating the extent an severity of overexploitation as a result of pumping in the basin. Nevertheless, the affected area depends on the RSV scheme. For SRGP, the overexploited zone is mainly confined to the central part of the basin i.e. in the “la Mancha Occidental” sub-unit aquifer, which is the zone most affected by the large withdrawals (Figure 3-2c).The two other RSV schemes the area of overexploitation appears to be more extensive, especially toward the south-eastern and north-eastern parts of the basin.

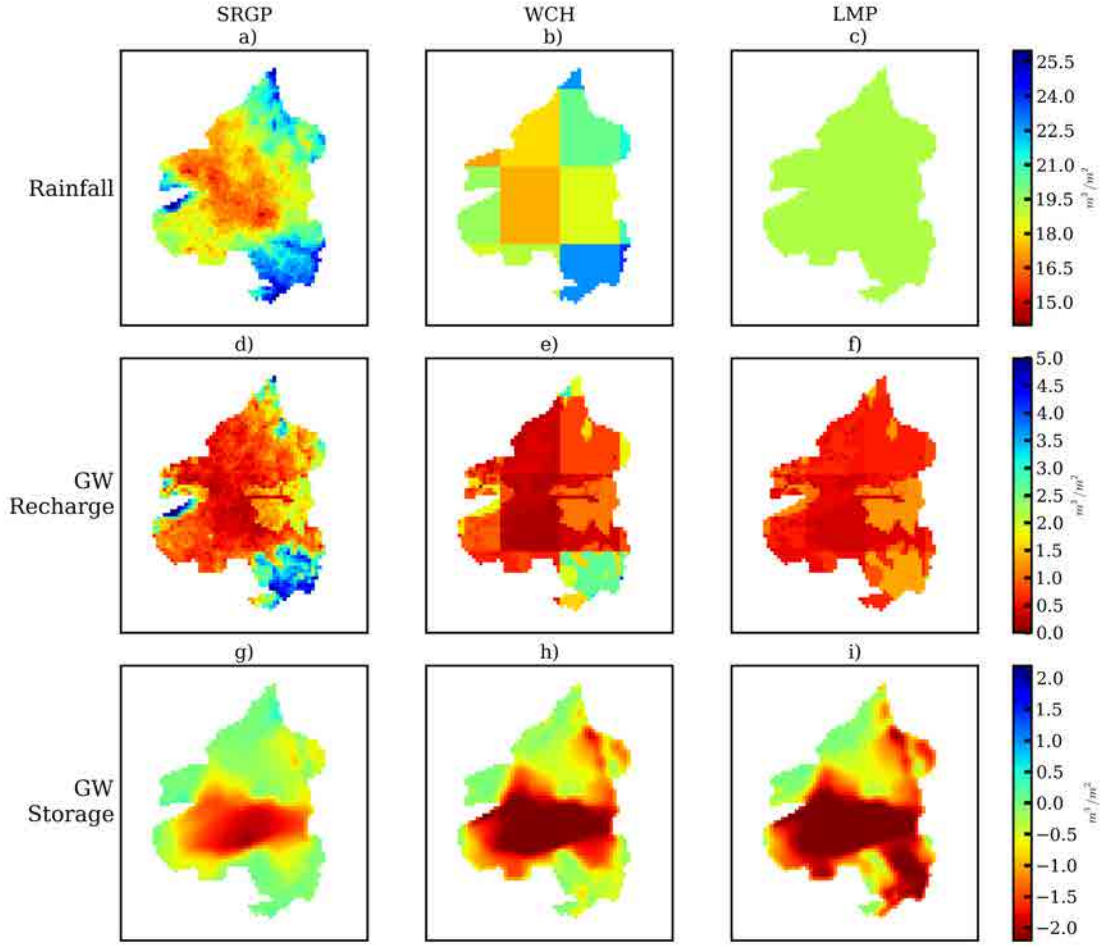

Figure 3-5 Spatial distribution of the total period accumulation for the three RSV schemes.

3.3.3.2 Uncertainty

Figure 3-6 shows the uncertainty as the difference between the 95th and 5th percentiles over the 100 realizations for the rainfall, RCH and STG. The spatial pattern of the uncertainty displays much less information when we upscale the rainfall resolution from SRGP to WCH and then to LMP. Therefore, in the upscaling process we reduce the uncertainty width at the expense of losing information of the real spatial uncertainty.

In SRGP, the uncertainty maps for the rainfall and RCH display dots of low uncertainty (red colors). These dots indicate that rain gauges are available at these locations and are used as information to condition the rainfall stochastic model.

RCH (Figure 3-6d-f**)** shows that the uncertainty for SRGP and WCH is greater in the zones where the amount of RCH is larger (associated with higher elevations) and that reduced uncertainty is associated with lower amounts of RCH and with a greater density of rain gauges in the central zone.

The uncertainty maps for STG (Figure 3-6g-i) show (1) that SRGP presents the widest range and the greatest spatial variation of the uncertainty, (2) the zones where the inputs and outputs are most and least variable (red zones fewest variations, blue zones most variations) and (3) that the reduction of the uncertainty observed in other responses due to the measurements in the rain gauges is filtered

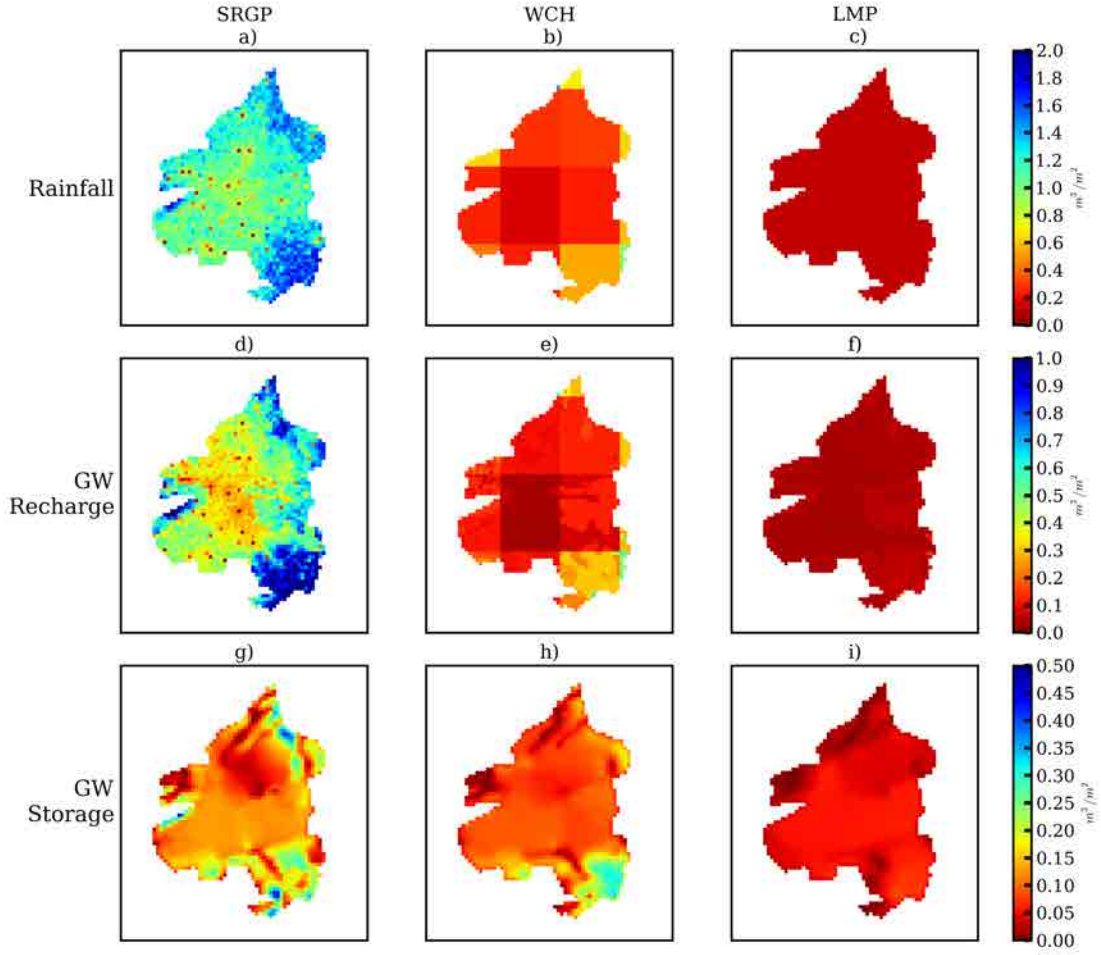

Figure 3-6 Uncertainty spatial distribution of the total period accumulation for the three RSV schemes, expressed as the difference between the 95th and 5th percentiles.

3.3.4 Climatological and Probability Distribution of GW Recharge

To understand why recharge RCH is the hydrologic variable most sensitive to RSV scheme, we compute the basin spatial integrated monthly cumulated RCH, and then examine pattern of climatologic variation (Figure 3-7). The results are shown using a modified boxplot, where the interquartile range is substituted by 10-90 and 5-95 percentiles levels computed from the ensemble of 100 realizations. This allows comparison of the shape distributions and mean seasonal values obtained with the three RSV schemes.

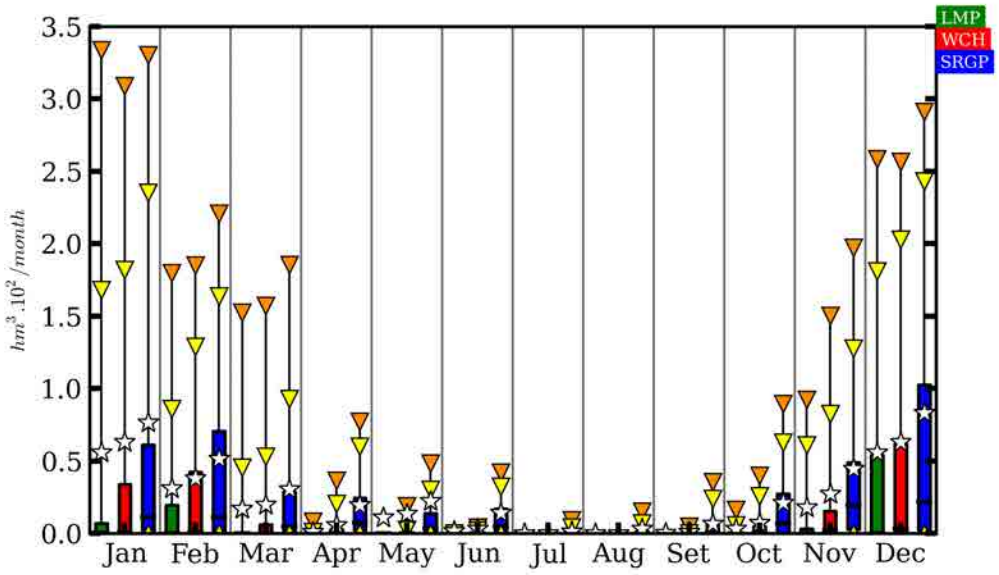

Figure 3-7 Climatologic variability for the GW Recharge spatial accumulation for the three RSV schemes.

Figure 3-7 indicates first that the recharge is mainly produced between November and March and secondly that SRGP produces RCH for about five months (May to October) unlike WCH and LMP. The distributions are positively skewed for all cases. Further, the empirical cumulative distribution function (*cdf)* shows the most significant differences in rainfall regarding RCH (we only show January, August and December in Figure 3-8).For example, in January (the wettest month), SRGP has a probability of occurrence of 90%, whereas this is 64% for WCH and 50% for LMP. In the driest month, August, the probability of occurrence drops to 52.5% for SRGP, 3.5% for WCH and 1.1% for LMP. From the tails of the distributions for the wet months (Figure 3-8a and c) we see there is some probability of occurrence of high RCH events, and these are similar for the three rainfall cases as might be expected due to less dissimilarity in representation of spatial distribution for larger events.

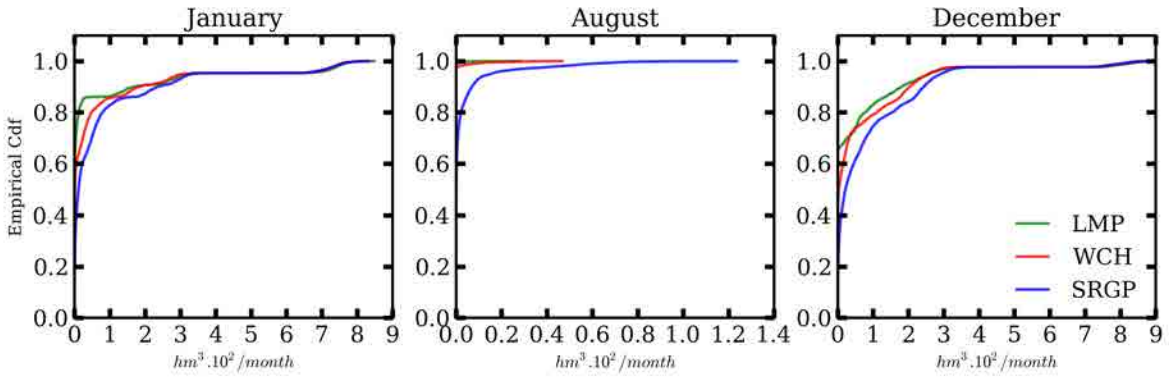

Figure 3-8 Empirical cumulative distribution functions for the GW Recharge Spatial accumulation. a)January, b) August and c) December

3.3.5 Spatial Distribution of Yearly Cumulative Recharge

The spatial distribution of the yearly cumulative RCH also highlights the role played by RSV in the hydrological response, especially for RCH. Figure 3-9 shows a four year transition period (1993-1996) from dry to wet conditions. The spatial RCH pattern for the last year (i.e. 1996) resembles the spatial distribution of cumulative RCH for the whole simulation period 1950-2001 (Fig.5c). The largest differences obtained in the RCH arise in the driest years (1993 and 1994), during which SRGP produced a patchy and discontinuous RCH field with small annual recharge values, whereas the recharge obtained is practically zero for LMP and WCH. These differences in the annual RCH fields are observed in all the dry years analyzed.

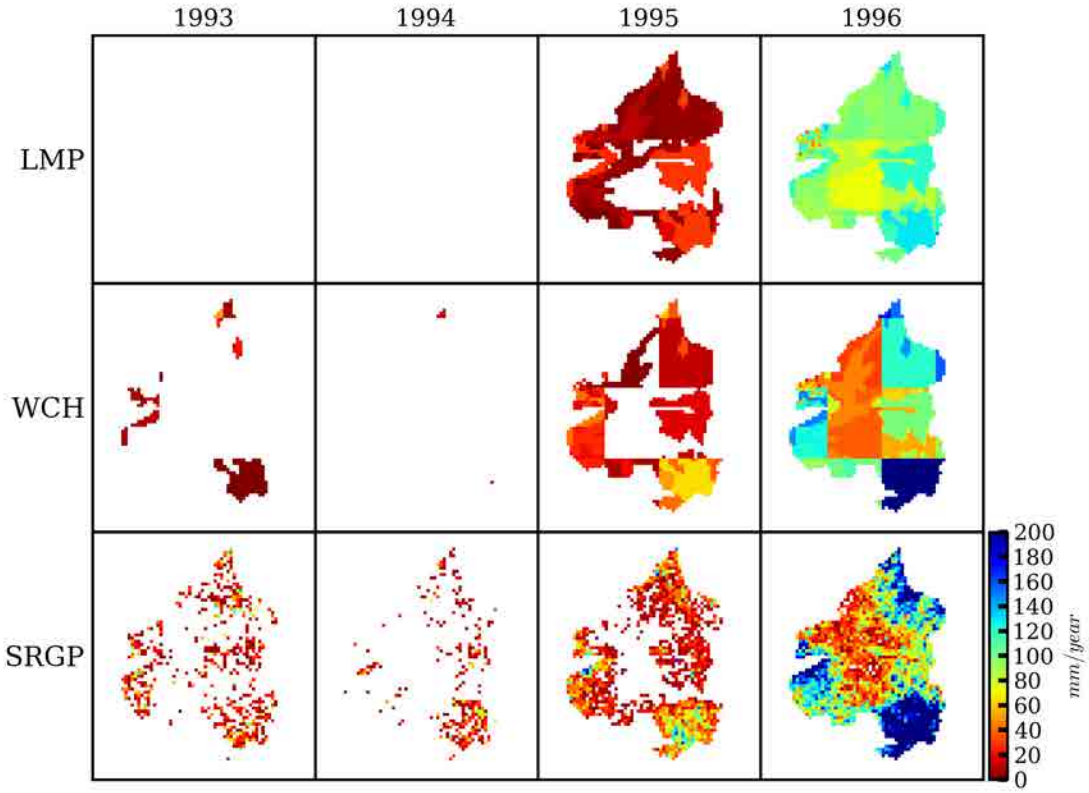

Figure 3-9 The yearly accumulation of the spatial distribution for the of GW Recharge for the three RSV schemes. The years selected are a transition between a dry period (1993-1994) to a wet period (1995-1996).

3.3.6 Time Series at Selected Locations

To explore the dynamic of the system in more detail, we selected five locations distributed over the domain (indicated by green dots Figure 3-1) to illustrate the time series

response and uncertainty regarding (1) the effect of the pumping wells, (2) the occurrence of wetlands, (3) the effect of elevation, and (4) gaps in the data set in rain gauge records (Figure 3-10 and Figure 3-11).

The combined effect of pumping and RSV (using a complete measurement record of rainfall time series) is shown in Figure 3-10a. The uncertainty in rainfall, SM and RCH drop to zero when using the SRGP scheme in which rainfall data conditioned on the data, whereas the uncertainty is not zero for the WCH and LMP schemes because of the averaging that includes variability of the surrounding points. Groundwater level and STG both clearly show the impact of RSV on pumping. Even though the hydrological variables show a similar trend, the effect of pumping varies depending on the RSV scheme. This was especially true in the dynamics of the groundwater level. The higher the spatial resolution of the driving rainfall fields the larger the simulated decline in groundwater levels.

As regards the groundwater levels, the fact that the groundwater pumping filters the uncertainty is noteworthy; the larger the pumping rate the lower the uncertainty, regardless of the RSV scheme. Now, it might be argued that the small uncertainty in the groundwater level is mainly due to the propagation of the small rainfall uncertainty signal. However, Figure 3-10b shows similar results for a place affected by pumping where rainfall estimate are not conditioned on nearby observations (showing a larger rainfall uncertainty bound). While, rainfall, SM and RCH now show wider uncertainty bounds wider uncertainty bounds, the uncertainty in groundwater level and STG remains relatively small. This is, of course, because the dynamics of the system at these locations is dominated by the dynamics of pumping rather than those of rainfall.

The effects of wetlands on the uncertainty are similarly illustrated in Figure 3-10c. When the state of the system is close to “natural” conditions the wetlands remain active and the uncertainty is zero. This is because under natural conditions, the RSV scheme has no effect on (1) local SM because the soil is always saturated, (2) on local AET which is occurring at the potential rate, and (3) on RCH which is nonexistent. These effects are propagated into GWH and STG. However, as the effects of pumping grow and the wetlands disappear, RCH begins to increase with a non-negligible uncertainty bound, especially for the SRGP scheme. As shown in the figure, the RCH uncertainty is not propagated to the groundwater level or to STG. Again, the effect of pumping damped the propagation of uncertainty propagation.

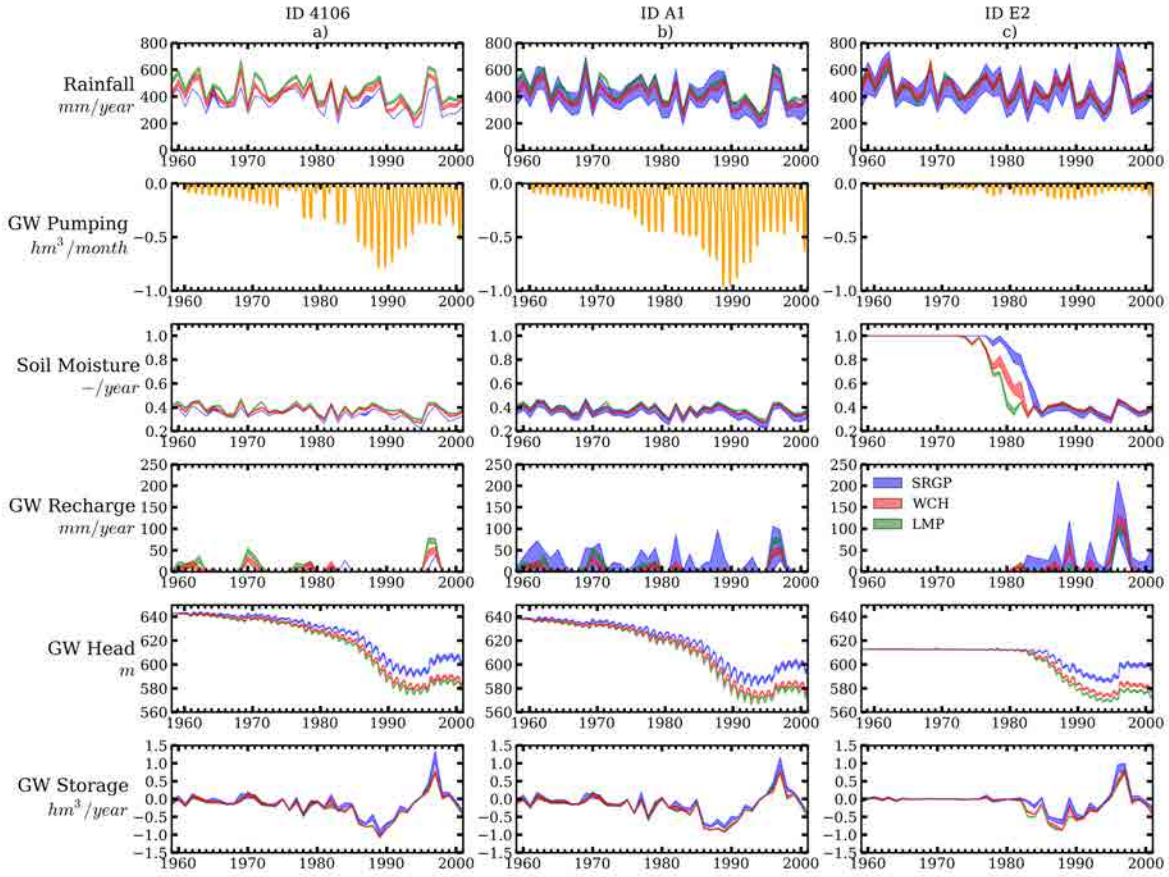

Figure 3-10 Time series at selected locations. Effect of pumping and wetlands on the uncertainty

To contrast with the above, we show the hydrological variable response at two points without groundwater extraction (Figure 3-11**)**. The first is in an elevated zone but has not rain gauge station nearby. The second is located in a mid-elevation zone, where a rain gauge is situated. However, there are some gaps in the rainfall record. This exerts a considerable influence on the simulated rainfall time series (and hence on the corresponding rainfall uncertainty bound) since the SRGP model performs unconditioned rainfall simulation when conditioning data is not available (Figure 3-11b). As shown in Figure 3-11, the smaller the spatial resolution of rainfall the larger the uncertainty of rainfall, RCH, GWH and STG. Moreover, if we compare the uncertainty bounds of GWH and STG with those obtained using high pumping rates (Figure 3-10) we can see that uncertainty is smaller when pumping rates are higher.

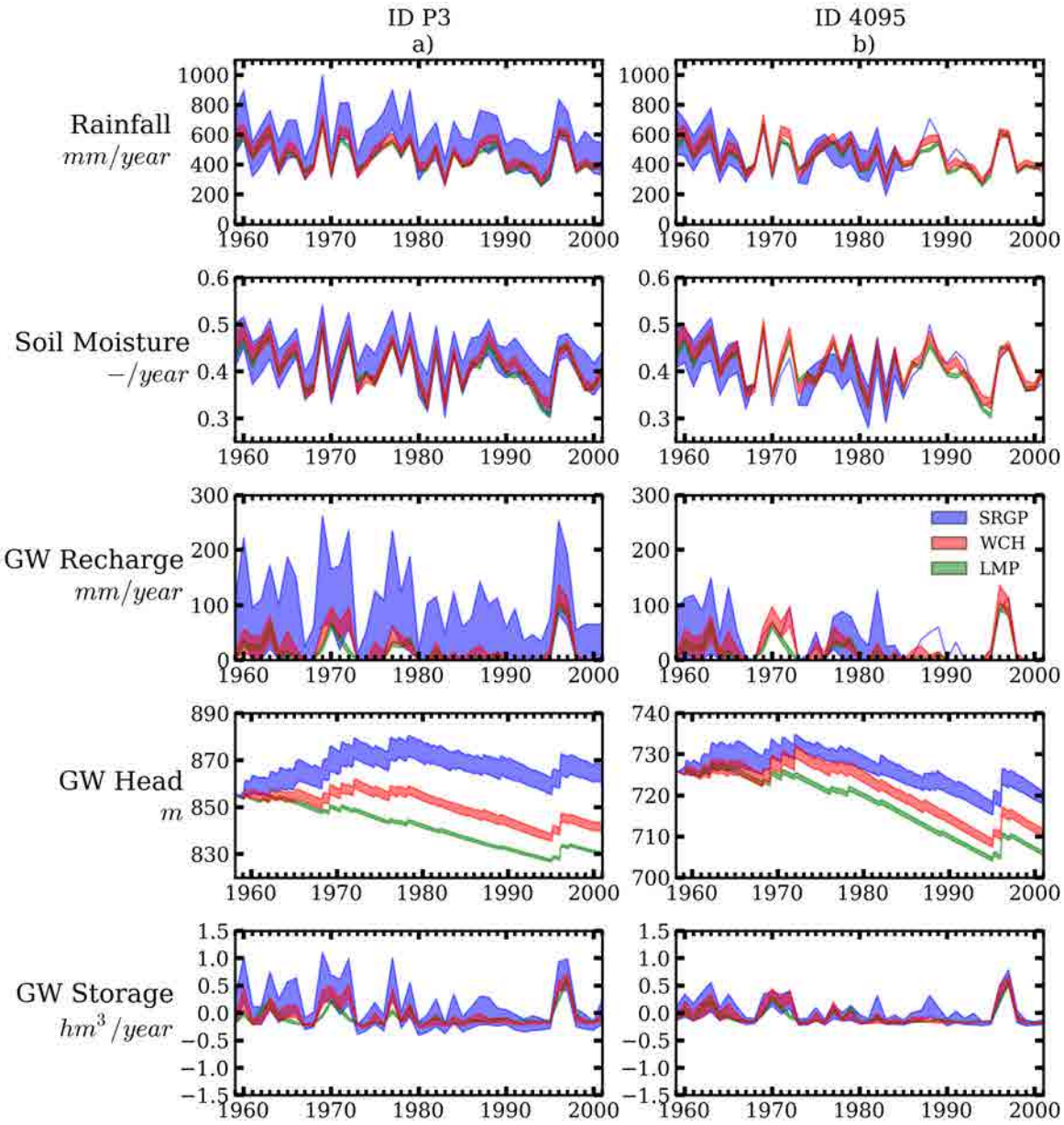

Figure 3-11 Time series at location without groundwater extractions

Due to gaps in the rainfall data, the widths of the simulated uncertainty bounds for the hydrological variables vary depending on whether the conditioning data are available or not. The resulting rainfall uncertainty pattern is propagated into the hydrological system through SM and RCH. However, the abrupt changes in uncertainty of rainfall are damped out and so not observed in GWH and STG. This suggests that the propagation of rainfall uncertainty into the groundwater system is damped in the RCH signal and thereby into the rest of system.

3.3.7 Natural conditions – absence of pumping –

While the UppGb is an overexploited aquifer system, it is instructive to examine the behavior of the system under natural conditions, by turning off groundwater extraction.

Figure 3-12 compares result under the pumped and not-pumped scenarios. Under natural conditions, the fractional area covered by wetlands WFA never attains zero value, indicating that a portion of wetlands will always remain active (Figure 3-12a) Moreover, the groundwater and surface water exchange eGWS is always negative; indicating that aquifer always contributes to surface water supplies.

Figure 3-12b shows that during 1997 (an exceptionally wet year) and in a context of massive exploitation conditions, the increase in the availability of water is directly transferred into aquifer recharge, whereas for natural conditions the increase in the availability of water is transmitted into increased groundwater discharge to the rivers.

Figure 3-12c (STG) illustrates the effect of overexploitation on the aquifer. Under natural conditions, the aquifer largely maintains a positive balance and the system is only affected during periods of hydrological droughts; see also WFA and eGWS (Figure 3-12a and b).

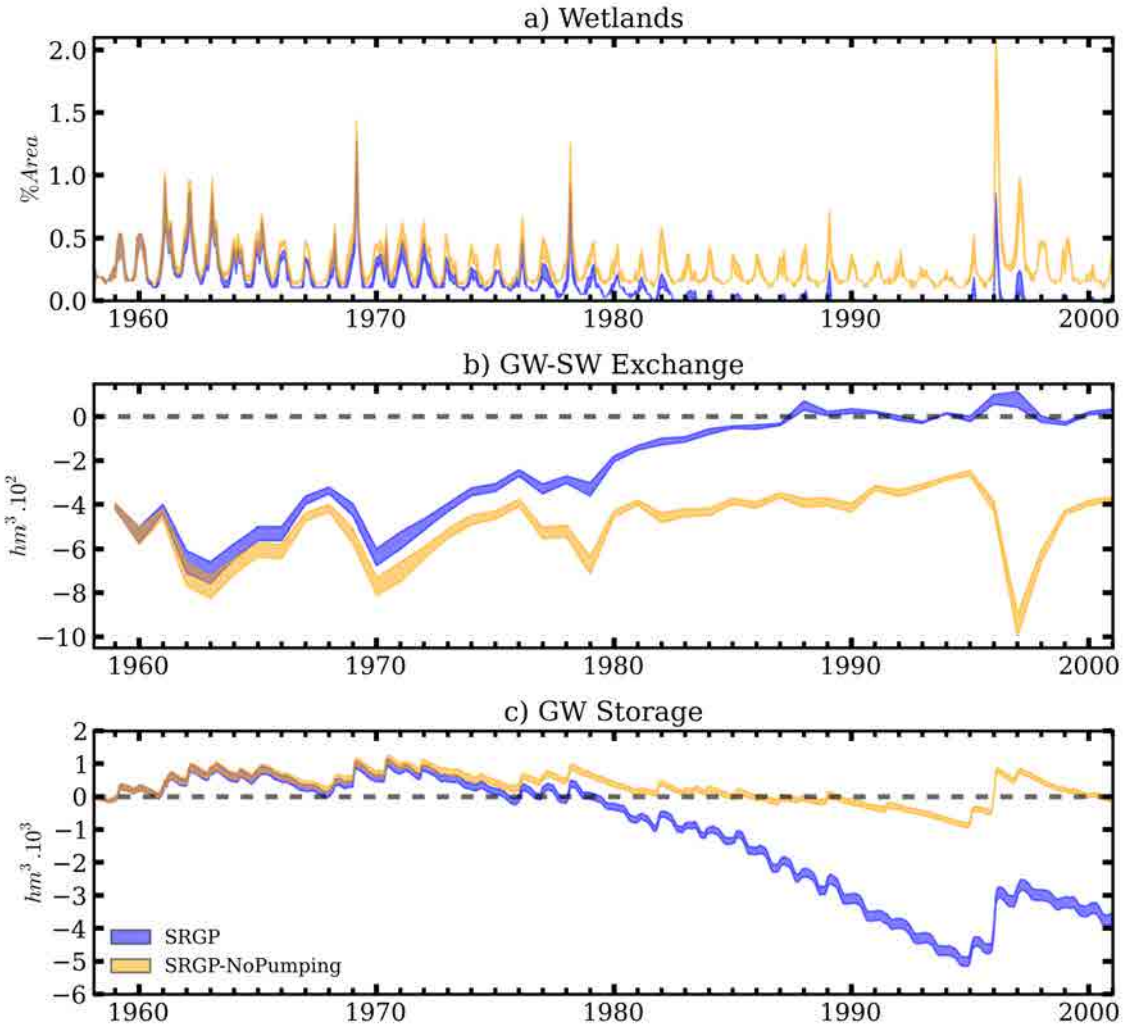

Figure 3-12 Comparison of responses (wetlands, gw-sw exchange, gw storage) under natural conditions and with groundwater extractions for the SRGP rainfall case.

3.4 Discussion

3.4.1 Cause and effect of Hydrogeological Response

Our results indicate that RSV exerts a considerable influence on overall response of the hydrogeological system in the UppGb. The primary variables driving the hydrologic response are RCH and groundwater extraction. Because, the pumping well rates and the total rainfall volume applied were the same, variations in the behavior of the system are mainly the resulted of different amounts and patterns of recharge associated with different degree of RSV.

These differences are explained by the fact that SRGP produces rainfall fields containing considerably larger local scale rainfall values than in the lumped products. These differences affected the spatial pattern distribution of the RCH, resulting in high frequency of spatially intermittence RCH fields (Figure 3-8a), especially, during the driest period and the months with low recharge (July and August) (climatological, Figure 3-7 and empirical *cdf*, Figure 3-8). These patterns in the spatial response show up in the cumulative spatial RCH fields, shown in Figure 3-3c. So while LMP and WCH are characterized by periods of no recharge, whereas the SRGP scheme tends to always result in recharge somewhere in the basin.

These variations in RCH translate into differences in the simulated response of the hydrogeological system (GWH levels). Variations in the recharge imply different ground water level spatial distributions and therefore different groundwater fluxes. This affects the response of all of the other hydrological variables (i.e. runoff generation, gw-sw exchange, river runoff, gw Storage). Since QESC is principally dominated by subsurface runoff, its dynamics are similar to RCH and depend on how shallow the GWH levels are. As SRGP produces a combination of higher GWH levels and RCH, the runoff generated is higher in this case. This response also shows how strongly the drawdown in GWH levels is affected by pumping. Similarly, eGWS depends mainly on GWH levels and QRV, especially when the dynamic of the system are inverted because of groundwater extraction. When that happens, the rivers begin to recharge the aquifer causing a loss of almost all of the river runoff. As the GW heads levels are higher for the case of SRGP, they produce higher levels of discharge from the aquifer, and also higher Qrv (since it is the combination of eGWS with spatial QESC).

Finally, the overall response of the hydrogeological system is reflected inSTG. This amount expresses the total net fluxes and ascertains whether the aquifer is overexploited (negative and positive values, respectively). The use of high resolution rainfall fields strongly suggests that the system response is less affected by pumping (Figure 3-3f and Figure 3-5g-i).

The absolute cumulative values are as follows: (1) recharge for the SRGP scheme is **92.3%** and **55.2%** larger than those obtained for the LMP and WCH schemes, respectively, and (2) storage for the SRGP scheme is **136%** and **91%** less affected than the LMP and WCH schemes, respectively. The "*naturalized-system*" experiment shows that the groundwater extractions do have a significant impact on the hydrogeological response of the system.

3.4.2 Uncertainty

The analysis of uncertainty demonstrated the advantage of using Stochastic Rainfall Generation (***Sapriza et al., 2013a***) when examining the response of a hydrological system. A major source of uncertainty in the estimation of rainfall uncertainty stem from the lack of rainfall information at every location within the basin. The SRGP method enables us to create plausible rainfall fields that retain important characteristics features of the rainfall fields observed (spatial correlation structure, time rainfall intermittence, and variations due to different rainfall generating process), while incorporating rainfall observations from available meteorological stations. In each of the stochastically generated ensembles of rainfall field time series the simulated rainfall uncertainty is set to zero where rainfall data is available (red dot in Figure 3-6 a and b and narrow width uncertainty Figure 3-10b); note that the scheme also allows us to assign a finite uncertainty at each gage location to reflect gauge error, but this error was assumed to be negligible for purposes of this study.

Propagation of the uncertainty in knowledge of spatial rainfall uncertainty through the hydrogeological response showed that:

a. In term of totals (Figure 3-3), uncertainty remains low for soil moisture and AET, increases for the RCH, QESC and eGWS, and becomes low again for STG.
b. At point locations, rainfall uncertainty is transmitted into SM, RCH but not so strongly into the GWH levels and STG. This shows the effects of the filtering of the RCH signal.

c. Simulations in the pumped regions and wetland areas are largely not affected by rainfall uncertainty.
d. The spatial distribution of uncertainty is reduced (SRGP case) in places where raingage data is available (rainfall and RCH).

3.5 Conclusions

We have investigated the impacts of rainfall spatial variability (RSV) on the simulated hydrogeological response of the Upper Guadiana Basin, using representations of rainfall having different spatial resolution but identical volumes. Overall, we find that spatial variability in rainfall affects the response of the hydrogeological system in two different ways: (1) The fast responding soil moisture and actual evapotranspiration fields are largely insensitive to degree of rainfall spatial variability, while (2) the more slowly responding groundwater recharge and the spatial runoff generation processes are significantly affected. These differences directly affect the evolution of groundwater head levels and thereby the groundwater surface water exchanges, river runoff discharge, and sensitivity of the system to groundwater pumping. Further, the spatio-temporal intermittence in the aquifer recharge associated with higher spatial variability of rainfall plays a key role in the dynamics of the system.

To further generalize the findings of this work, it will be necessary to study other test basins, with different parameterization and boundary conditions. However, our results clearly demonstrate the importance of using adequate representation of spatial rainfall distributions when assessing the response of a hydrogeological system. This can be of paramount importance when conducting climate change impact studies, as the results can have dramatically different implications on the evaluation of water resource management strategies.

4 A Circulation Pattern-Based Approach to Evaluate the Combined Impacts of Climate Change and Groundwater Pumping on Catchment Dynamics[3]

4.1 Introduction

The most recent *Intergovernmental Panel on Climate Change* (IPCC) assessment report (***IPCC, 2013***) confirms once again their previous projections (***IPCC, 2007***) .Many parts of the world can be expected to be drier in the future. Such changes in hydroclimatology will likely have severe impacts on the water budgets of highly connected (groundwater-surface water interactions, wetlands, etc.). Many of these are already under considerable pressure, and even overexploited, due to anthropogenic demands (agriculture, energy, industry, cities, ecologic flows, and more) (***Custodio 2002)***. To better manage the water resources in such basins will require evaluations of the combined effects of both climate change and human activity, conducted within a non-stationary framework if possible, and including adequate assessment of all of the uncertainties involved (***Milly et al., 2008; Beven 2011***).

Traditionally, climate change impacts studies rely on scenario projections provided by General Circulation Models (GCMs). The hydrometeorological consequences of such projections are transformed (e.g., downscaled) and used as inputs to hydrological models, which were previously calibrated against historical observations. By comparing the historical and projected hydrological responses, the impacts of climate change can be assessed (***Chiew et al., 2009; Fowler et al., 2007***). Transformation of the GCM projections is necessary, because GCMs are (as of yet) unable to simulate the amount and spatial resolution of precipitation (a key input climate variable) sufficiently well. The most commonly used such transformations are known as statistical downscaling methods (SDMs) (***Maraun et al., 2011;***

[3]This chapter is based on the paper: *Sapriza Azuri, G., Jodar, J., Carrera, J., and Gupta, H. (2013).A Circulation Pattern-Based Approach to Evaluate the Combined Impacts of Climate Change and Groundwater Pumping on Catchment Dynamics .To be Submited*

Fowler et al., 2007). SDMs can be defined by developing relationships between the observed and GCM simulated values (typically of precipitation and temperature) for some historical period, and then using such relationships to develop relatively simple bias correction (BC) strategies (***Johnson and Sharma 2011; Piani et al., 2010;Wood et al., 2004)***. More sophisticated stochastic approaches have also been proposed, based on the use of gridded reanalysis climate data (***Kalnay et al., 1996***) to calibrate the parameters of the SDM (***Sapriza et al., 2013a; Fowler et al., 2005; Hundecha and Bardossy 2008***).

Impact assessment studies of this kind typically treat both the hydrological system and the SDM as remaining stationary with time. While such assumptions are difficult to relax, it is increasingly clear that ways to evaluate the validity of such results need to be developed. Further, such studies also typically assume that the downscaled GCM simulations (e.g., of precipitation and temperature) can function as surrogates for the corresponding actual values (represented by observations or reanalysis fields), which implies an assumption of stochastic equivalence; i.e., that even though the downscaled GCM simulations do not match the actual values exactly, the relevant *stochastic properties* of the actual variables are well enough represented that the impacts of such differences on the estimated hydrological impacts are insignificant. However, this critical assumption is very rarely verified (***Wood et al., 2004***) and only a few studies have rigorously evaluated the SDM assumptions for the control historical period (***Frost et al., 2011; Vrac et al., 2007***).

In this paper we formalize the Stochastic Equivalence concept used to evaluate the validity of hydrological response obtained with the hydrological model driven by downscaled GCM simulations. With that purpose, for the historical period, we evaluate whether the GCM-based simulation produces catchment hydrological responses stochastically equivalent to those actually observed, or to those generated by the Catchment Model by using actually observed forcing data.

In addition, we present an evaluation procedure to assess the combined effect of climate change and groundwater pumping in a basin. To that end, the evaluation was performed in three stages, based on comparing the catchment responses. First, the projected climate change and historical control GCM under naturalized conditions (no groundwater extraction) were evaluated. In a second instance both periods were evaluated separately, comparing the hydrological response with and without pumping, each case by itself. Finally, the combined effect of pumping and climate change was evaluated, comparing the catchment

responses for the historical GCM with the future projection. The proposed analysis took place in the Upper Guadiana Basin (UppGb), located in central Spain.

4.2 Methods

4.2.1 Study Area

The 16000 km2 Upper Guadiana basin (UppGb) is situated in the central Spanish Plateau, and is located between latitudes 38º37'N and 40º08'N, and longitudes between 2º25'W and 3º51'W. Morphologically, the main part of the basin is characterized by a smooth topography, with altitudes ranging from 550 to700 m.a.s.l. Nevertheless, the northern and southern boundaries (Sierra Altomira and Campos de Montiel, respectively) are mountainous with altitudes exceeding 1000 m.a.s.l. The combination of smooth topography explains the lack of a well-defined drainage network and the abundance of large karstic aquifer formations gives rise to complex relationships between surface and subsurface water. These interconnections enable wetlands to flourish (around 250 km2), which is of considerable ecological significance.

The UppGb has a mixed continental, semi-arid, Mediterranean climate. Precipitation has considerable space-time variability because of Atlantic and Mediterranean influences and orographic effects. Average annual precipitation is ~450 mm/year and characterized by strong seasonal variability, with dry summers during which precipitation is dominated by small convective rain cells of short duration. Conversely, the wet Autumn and Spring seasons are characterized by stratiform frontal rain with large spatial continuity and duration.

The groundwater system of the UppGb consists of four aquifer systems, known as the *Sierra Altomira, Mancha Toledo, Campos de Montiel* and *Mancha Occidental* (Figure 4-1). In 1989, the latter two of these units were the first Spanish aquifers to be declared overexploited due to the combined effects of groundwater pumping (with drawdowns exceeding 50 meter at some locations) and the occurrence of several droughts. Briefly, the main hydrogeological characteristics of these aquifer system can be summarized as: (1) the *Sierra Altomira* aquifer consists of two layers, the deeper being a Jurassic semi-confined unit made up of sandy and dolomitized limestone and the upper being a Cretaceous free aquifer formed by dolomite and limestone; (2) the *Mancha Toledo* is a Triassic-Miocene-Plioquaternary free aquifer made up of detrital sediments; (3) the *Campos de Montiel* is a Jurassic limestone karst free aquifer; and (4) the *Mancha Occidental* is a two-layer aquifer

with a detrital semi-confining layer that works as an aquitard between the deeper Jurassic-Cretaceous confined aquifer composed by limestone, and the upper tertiary-quaternary free aquifer composed of Miocene limestone.

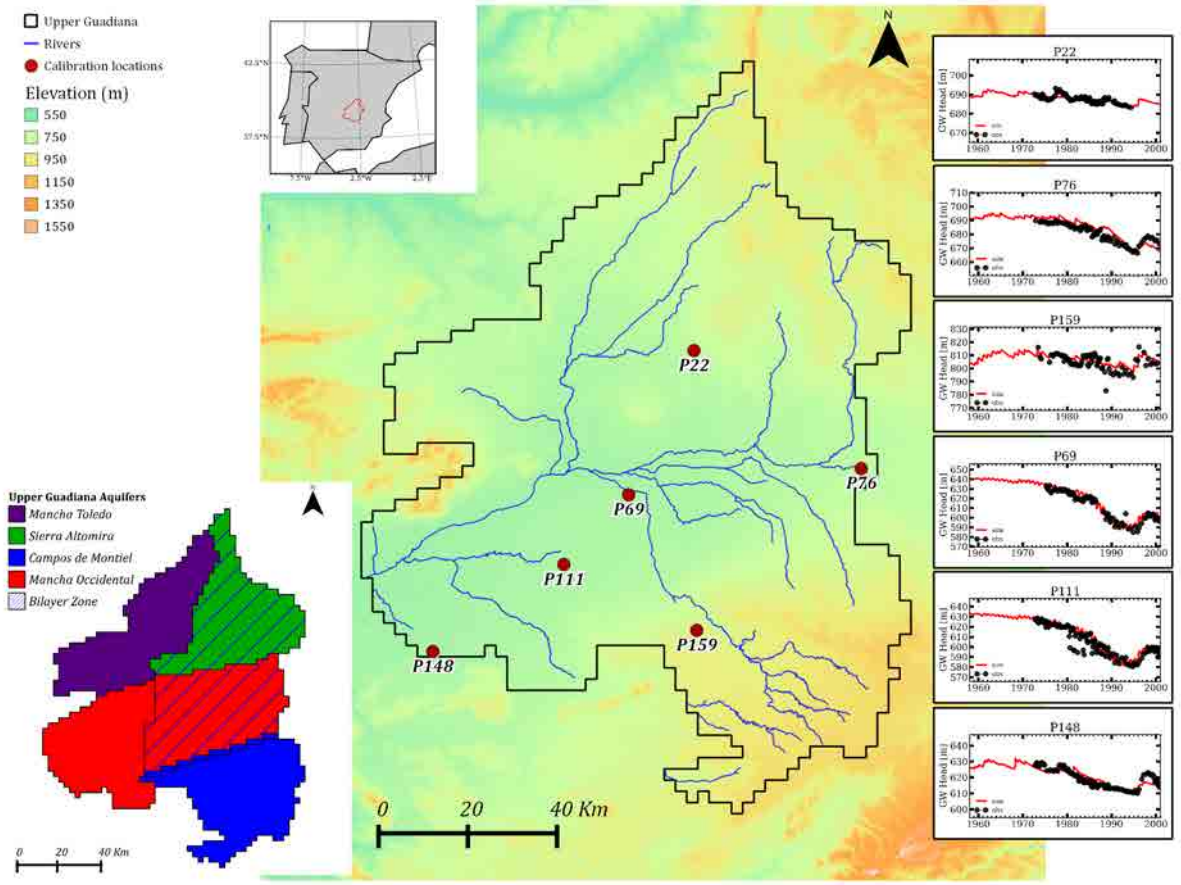

Figure 4-1 Area of study. Principal features are represented: Aquifer delimitations, principal rivers, piezometric location with their calibration.

4.2.2 Hydrogeological Model

In this work, the hydrogeological response of the UppGb was simulated using a distributed hydrogeological model that simulate the soil water balance, groundwater flow, the propagation of runoff into the rivers, and the coupling of surface and groundwater components. Details of the model and its calibration are discussed by ***Sapriza et al., (2013b)***; here we use the same set of model parameters. Note that we used the Hargreaves-Samani equation to estimate potential evapotranspiration (PETo) since the variables required by more complex equations are not readily available for the future scenario periods. Further, surface temperatures were adjusted to account for elevation by estimating the lapse rate from historical ground-based observations at multiple locations within the basin. For cases where the hydrogeological model includes groundwater extractions, the pumped water was incorporated as irrigation inputs to the soil balance.

4.2.3 Climate forcing

The primary climate drivers used to force the UppGb model are *Temperature* (used to estimate the PETo) and *Precipitation*. A series of transformations were applied to the mean basin-scale GCM simulations of these variables, first to correct for bias in the GCMs outputs, and second to generate high-resolution spatially distributed rainfall fields via a stochastic rainfall generation process (SRGP) model. For the latter, separate SRGP models were developed for each of 8 different Atmospheric Circulation Patterns (ACPs) and 6 seasons (SSNs) during the year, as discussed briefly below; see ***Sapriza et al. (2013a)*** for more details. This allows us to track the non-stationarity of the rainfall generation process through the year, and as the patterns of atmospheric circulation change in response to variations in climate.

4.2.3.1 Classification of Seasonal Atmospheric Circulation Patterns

A discrete classification of 8 ACPs (Table 4-1) over the Iberian Peninsula was determined by using an automated version of the Lamb Weather classification scheme (***Jenkinson and Collinson, 1977***; ***Jones et al., 1993***), in accordance with the recommendations of ***Goodess and Palutikof (1998)***. The Lamb classification scheme is based on the direction and vorticity of surface wind in geostrophic units. To obtain '*observed*' ACP values for each day we used gridded values, at 16 points covering the Iberian Peninsula, of historical mean sea level pressure provided by the NCEP-NCAR re-analysis data set (***Kalnay et al., 1996***). To obtain the GCM simulated ACPs (for historical and future projection) we used the sea level pressure estimated by the model, without correction, at the same 16 points. ACP was then analyzed by seasons *SSN = {JanFebMa, AprMay, Jun, JulAug, Sep, OctNovDec}* to properly track the climatology of the study area, as discussed in ***Sapriza et al. (2013a)***. This resulted in 8x6=48 ACP-SSN types and hence 48 different stochastic models for the generation of high-resolution spatially distributed rainfall fields.

ACP Type	Description
C	Cyclonic
HYC	Hybrid cyclonic
UC	Unclassified/light flow cyclonic
A/HYA	Anticyclonic/ hybrid-anticyclonic
UA	Unclassified/light flow-anticyclonic
W/NW/SW/N	Westerly/ northwesterly /southwesterly/northerly directional types
E/NE	Easterly/northeasterly directional types
S/SE	Southerly/southeasterly directional types

Table 4-1 Atmospheric Circulation Pattern classification.

4.2.3.2 Selection of GCMs and Projected Future Scenario

The quality of the climate simulations provided by different GCMs can be highly variable particularly when evaluated at the local (study region) scale (***Brekke et al., 2008; Pierce et al., 2009; Dominguez et al., 2010***). Therefore, to maximize confidence in our results, we selected a subset of 5 GCMs (Table 4-2) from a set of 20 models participating in Phase 5 of the Coupled Model Intercomparison Project (CMIP5 http://cmip-pcmdi.llnl.gov/cmip5/) (***Taylor et al., 2011***). The methodology and criteria for this selection are reported by ***Gupta et al. (2013)***; briefly, these 5 were the only ones (of the 20 examined) found to provide reasonable reproduction of historical annual frequency of ACPs over the Iberian Peninsula, and of the overall climatology and ACP-climatology (climatology by ACP type) of key hydrometeorological variables over the UppGB.

ID	GCM	Historical	RCP8.5
gcm1	CanESM2	✓	✓
gcm2	CsiroMk36	✓	✓
gcm3	GissE2R	✓	×
gcm4	MPI-ESM-LR	✓	✓
gcm5	MPI-ESM-MR	✓	✓

Table 4-2 List of good GCM selected.

For this analysis we considered two 40 year periods: (1) a historical period from 1960 to 1999; and (2) a future scenario period from 2060 to 2099. For the future period we selected the RCP85 scenario, which is the most severe of the 4 '*Representative Concentration Pathway*' greenhouse gas (GHG) emission projections developed for the 5th IPCC Assessment Report (***Moss et al., 2010***). Briefly, RCP85 is characterized by GHG emissions that cause an increase in radiative forcing to 8.5 W/m^2 by the end of the century. This scenario was selected so as to obtain a plausible upper bound on the hydrometeorological impacts that might be expected due to climate change, so as to provide sufficient contrast with the historical response of the basin.

4.2.3.3 Bias Correction of GCM Outputs

The GCM evaluation performed by ***Gupta et al. (2013)*** shows that the 5 selected GCMs do an excellent job of simulating the annual and seasonal frequencies of atmospheric circulation patterns over the Iberian Peninsula. Further, these models also provided good simulations of the climatology of basin-scale temperatures (min, max and average), although with a small positive additive bias. Similarly, the models are able to track the climatological

patterns of precipitation intensity and frequency of rainy days, but with severe (largely positive) biases in mean wet-day precipitation amount.

Based on these findings and assuming that the impact of climate will be associated to the cumulative effects of increases in Temperature, changes in annual and climatological ACP frequency, changes in PoR (significant reductions), and changes in WDA (minor reductions) as reported by ***Gupta et al. (2013***), we applied the following bias corrections (BC) to the daily data provided by each of the 5 selected GCMs. In each case, for each of the 48 ACP-SSNs, the mean daily wet day amount (WDA) of precipitation, probability of rain (PoR), and temperature were adjusted as indicated below. Interestingly, we found that simply adjusting the means also caused the corresponding entire distributions to conform; in the case of precipitation wet day amounts this is because the daily data are approximately lognormal. Accordingly, a primary assumption of this approach is that the GCMs are able to provide relatively good simulations of the daily time-step time-evolution of the ACPs over the Iberian Peninsula, and how these can be expected to change into the future.

First we discuss bias-correction for the historical period. For each ACP-SSN, the PoR represents the fraction of corresponding days that can be expected to be rainy (having non-zero precipitation). In some cases the GCM's have a tendency to rain more often (less often), in which case the PoR is too high (too low). We therefore adjusted the PoR for each model for each ACP-SSN as follows:

a) Compute $RH\_PoR^{k}_{i,j} = \mu ObsHistPoR_{i,j}/\mu GcmHistPoR^{k}_{i,j}$ for the i^{th} season, j^{th} ACP and k^{th} GCM, where $\mu ObsHistPoR$ represents the historically observed PoR (1960-1999) and $\mu GcmHistPoR_{i,j}$ represents the GCM-based PoR over the same period.

b) If RH_PoR < 1 the number of rainy days produced by the GCMs for that ACP-SSN needs to be reduced. For each corresponding rainy day, generate a random value Z from a uniform distribution Z=U[0,1]. If Z >*RH_PoR* set the day to be non-rainy and wet-day amount to zero.

c) If *RH_PoR*>1 the number of rainy days produced by the GCM for that ACP-SSN needs to be increased. For each corresponding non-rainy day, generate a uniform random variable Z=U[0,1]. If Z< *RH_PoR*-1 set the day is set to be rainy, and randomly generate a spatial-mean wet-day amount from a Gamma distribution, where the scale and shape parameters have previously been estimated for that ACP-SSN from the observed data (see ***Sapriza et al., 2013a***).

Having corrected the PoR, we next bias-correct the GCM simulated WDA by applying a simple *multiplicative* correction to the daily GCM-based WDA for each ACP-SSN. The correction coefficient was computed as follows: $BCWDA^{k}_{i,j} = \mu ObsHistWDA_{i,j}/\mu GcmHistWDA^{k}_{i,j}$ where $\mu ObsHistWDA$ is the corresponding historically observed mean WDA and $\mu GcmHistWDA$ is the GCM-based mean WDA.

Finally, the GCM simulated temperature was adjusted by applying a monthly *additive* correction defined as $\Delta TH^{p} = \mu ObsHistTemp^{p} - \mu GcmHistTemp^{p}$, for $p=\{Jan,Feb,\ldots,Dec\}$, where $\mu ObsHistTemp$ is the historical mean observed temperature, and $\mu GcmHistTemp$ is the corresponding GCM-based value.

Of course, for the future period we have no available observations. Therefore, lacking any rational basis for thinking otherwise, and as is common in bias-correction strategies, we assume that the nature of the biases in PoR, WDA and temperature remain the same (stationary) for each GCM. We therefore apply the same bias correction factors to the future period as discussed above. This amounts to an assumption that each GCM is able to provide internally consistent simulations of the hydrometeorological changes we can expect under the presumed scenario conditions. Of course, it is quite possible that these corrections would need to be different, but this seems a reasonable way to proceed. Note however, that any changes in annual and climatological frequency of the regional ACP's due to global GHG induced warming, as projected by the GCM's, <u>will</u> act to change the hydrometeorological response over the basin in a non-stationary manner.

4.2.4 *Stochastic Generation of High-Resolution Spatially-Distributed Rainfall Fields*

Sapriza et al. (2013b) have reported on the importance of rainfall spatial variability (RSV) to both the overall and spatially distributed water balance response of the UppGb hydrogeological system. In that work, we showed that spatial variability in the amount of rainfall significantly affects the amount of groundwater recharge, and thereby the overall response of the system. Here, we adopt the same Stochastic Rainfall Generation Process (SRGP) model developed by ***Sapriza et al. (2013a,b)*** for spatially downscaling the GCM-based bias-corrected simulations of daily catchment-mean wet day precipitation amount. The main difference from the aforementioned work, where the SRGP simulations were explicitly conditioned on historical observations from several rain gauges throughout the watershed, is that these stochastic simulations cannot be directly conditioned on gauge data; they do

however reflect information regarding spatial covariance structures and elevation-based drift obtained from the historical gauge record. Therefore, the SRGP does approximately account for two major non-stationarities; a) changes in the frequencies of different precipitation generating mechanisms (frontal and convective), and b) spatial non-stationarities caused by interactions of meso-scale atmospheric patterns with topography (primarily orographic effects).

In summary, our approach uses 48 separate SRGP models (one for each ACP-SSN) to spatially downscale bias-corrected basin-scale mean wet day precipitation amounts simulated by each GCM. In doing so, we take as given the daily sequence of ACPs specified by each GCM, the daily sequence of rainy / non-rainy days (bias-corrected as indicated above), and the corresponding spatial mean wet day amount for that day (bias-corrected as indicated above). Since ***Gupta et al (2013)*** conclude that the GCM's do a remarkably good job of representing the annual and climatological frequencies of ACP arrivals over the Iberian Peninsula, we assume that the time evolution sequence of ACPs provided by the GCMs can be trusted and used without any correction. As shown further in ***Gupta et al (2013)*** these annual and climatological frequencies do change under scenario RCP85 projections, lending support to our approach for climate impact analysis.

4.3 Evaluation Strategy

4.3.1 Testing for Stochastic Equivalence

For the purposes of hydrological modeling in support of Water Resources Management (WRM), it seems reasonable to assume that knowledge of the exact daily sequences of precipitation and temperature is not critical, but that what is required is accurate reproduction of monthly values, longer-term trends, and associated stochastic (distributional) properties. This assumption (if valid) permits us to conduct catchment impact analysis using (properly) bias-corrected GCM simulations (from properly selected models). Hence, validity is established assessing that, for the historical period, the GCM-based simulation strategy produces stochastically equivalent catchment hydrological responses to those actually observed, or to those generated by the Catchment Model by using actually observed forcing data. We note that such tests are not commonly performed (exceptions include ***Wood et al., 2004***).

In this work we examine the assumption of stochastic equivalence for the 40-year historical period 1960-1999 between the hydrogeological responses simulated by the spatially distributed hydrogeological catchment model when driven by a) observed (SRGP models conditioned by catchment gage data; case OBS) precipitation and temperature data, and b) corresponding GCM-based bias-corrected and downscaled data (SRGP models driven by GCMs; case GCMH). In both cases, we simulate the daily catchment response for the historical 1960-1999 period under naturalized conditions (without groundwater pumping), and initialized using average initial conditions from previous naturalized case runs. Note that since we are examining the 'naturalized' situation, comparisons to observations are not possible. However, since this comparison eliminates the confounding effects of model structural and parameter estimation errors, it allows us to isolate the effects of differences due to the source of the climatic forcing used. In each case, we generate 50 realizations of the rainfall fields for each day and use these in conjunction with temperature based estimates of PETo to drive the UppGb model. As explained above, for the GCMH case, the sequence of ACP provided by each GCM was not corrected.

4.3.2 Evaluation of GCM-based Projections of Climate Impacts under Naturalized Conditions

To evaluate the potential effects of projected Climate Change under RCP85, we first examined the differences in catchment responses between the 40-year historical period 1960-1999 and the 40-year future period 2060-2099 under naturalized conditions (no groundwater pumping). These impacts can therefore be assumed to be the accumulated effects of increases in Temperature, changes in annual and climatological ACP frequency, changes in PoR, and changes in WDA as reported by ***Gupta et al. (2013***).

One small difference from the procedure used for the evaluating stochastic equivalence was that daily RCP85 simulations for one of the 5 selected GCMs (the GISS model) were not available. Therefore our assessment is based on the 4 remaining models. As discussed before, we assumed stationarity in the bias-corrections for daily PoR, WDA and temperature for each ACP-SSN, and used the GCM specified ACP sequences to generate spatially distributed rainfall fields via the SRGP stochastic downscaling approach.

4.3.3 Examining the Additional Effects of Groundwater Pumping

Having examined projected changes in the UppGb under naturalized conditions, we next explored the potential additional impacts that might be expected due to groundwater pumping. For this, we assumed that the future space-time pumping pattern will follow that of 2006 (Figure 4-2), selected as a representative year from the historical pumping record. We applied the same seasonal pattern for each year, for both the historical and future periods. Therefore, the cyclical pattern of pumping is assumed to be the same. However, for the future period we applied a small increase (from 549 hm^3/year to 553 hm^3/year) in pumping to correspond to the changes in estimated demand associated with agriculture assessed in the Hydrological Plan for the Guadiana Basin (HPGB) for the UppGb. These assumptions about predicted demand are consistent with the fact that the HPGB predicts almost no increase in agricultural demand for water (provided almost entirely by groundwater pumping) over the next 20 years.

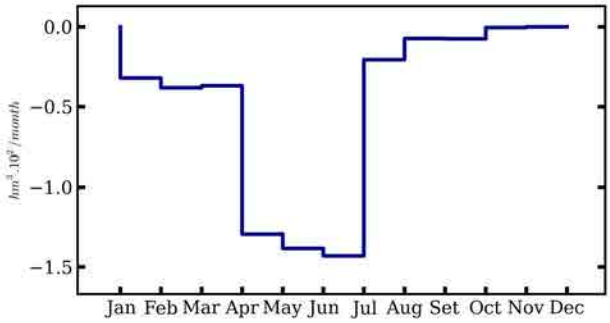

Figure 4-2 Groundwater Pumping for the year 2006 used to generate the space-time series of pumping for the historical and future period.

To investigate the additional effect of groundwater pumping, three cases were examined. In the first (called Historical), we look at the differences during the historical period under naturalized (GCMH) and assumed pumping conditions (GCMH+PMP). In the second (called Future), we look at the differences during the future period under naturalized (GCM-RCP85) and assumed pumping conditions (GCM-RCP8.5+PMP). Finally in the third (called Change), we look at the change from historical assumed pumped conditions (GCM-RCP85) to future assumed pumped conditions (GCM-RCP85+PMP). In all three cases the UppGb model was initialized to identical conditions as mentioned earlier. However, for purposes of response analysis, we discarded the first 5 years of each simulation to minimize potential impacts of the initialization assumption.

4.3.4 Overall Evaluation Strategy

In each of the study cases described in Section 3, we followed a general evaluation strategy of comparing the envelopes of the ensemble of hydrogeological responses provided by the UppGb model for the 50 stochastically generated realizations. In each case, the stochastic uncertainty was expressed as 5-95 % confident interval limits. To account for future uncertainty due to GCM model differences, the GCM-based ensembles were obtained by grouping together all of the individual GCM-based realizations.

The UppGb hydrological responses examined in this analysis are Soil Moisture (SM), Actual Evapotranspiration (AET), fractional area covered by Wetlands (WFA), Spatial Runoff Generation (QESC), Groundwater Recharge (RCH), Groundwater Surface water exchange (eGSW), River Runoff discharge (QRV) at the outlet of the basin, and Net Groundwater Storage aquifer (STG). Note that the WFA is defined as the number of soil cells that are at saturated state (SM=1) divided by the total number of cell of the upper layer in the UppGb model. The STG is computed as the sum of all the inputs and outputs fluxes to the aquifers.

4.4 Results

4.4.1 Stochastic Equivalence

A comparison of the catchment scale drivers is shown in Figure 4-3. The OBS and GCMH simulations of PETo (Figure 4-3c) agree very well in climatological pattern and amount. Precipitation volume (Figure 4-3a) indicates a very good agreement from April to November including February. However for January, March and December GCMH tends to provide larger amounts. Since general good agreement in historical ACP frequency has been observed (***Gupta et al., 2013***), and the PoR and WDA have been bias-corrected, these differences are due to differences in the number of ACPs (which differ between the observations and the GCMs). These variations are caused by the directional ACP W/NW/SW/N for winter, which is one of the wettest ACP for that season. For this ACP, all the GCM produce larger number of ACPs. This results in the differences in numbers of rainy days seen in Figure 4-3b.

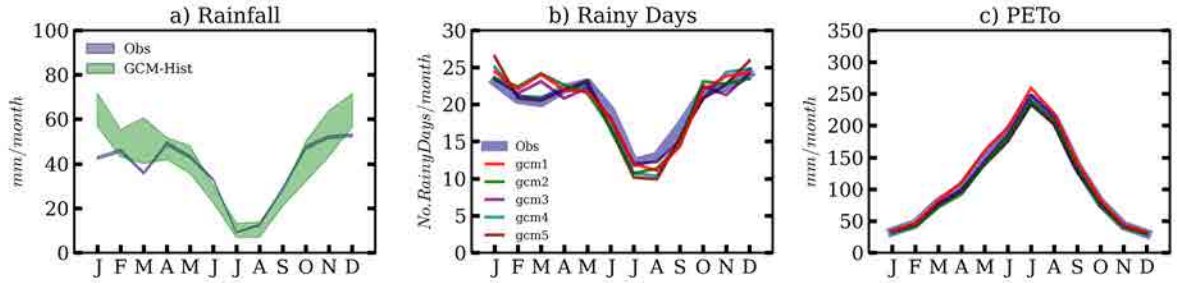

Figure 4-3 Climatologic climate driving forcing for the stochastic equivalence evaluation. They are compared the Observed and the GCM historical for the same period of time (1960-1999). Panel a) shows the wet day amount precipitation simulated on both cases with the SRGP model with the 5-95% percentile over the ensembles. Panel b) shows the number of rainy days per month for the observation (blue line) and the bias corrected probability of rain for the 5 GCMs. Panel c) shows the potential evapotranspiration comparing the observed with the estimated with the bias corrected GCM temperatures.

Next, the climatology of the mean areal basin scale hydrogeological response is compared in Figure 4-4. Overall, the match is very good, and differs primarily due to the propagation through the hydrogeological system of the difference reported in precipitation for the winter months. Note that while SM (Figure 4-4a) and AET (Figure 4-4b) show remarkably good agreement, the difference for the winter months in the precipitation leads to larger amounts of runoff generation and streamflow (Figure 4-4 c and g), recharge (Figure 4-4d), WFA (Figure 4-4e), and groundwater recharge (Figure 4-4h), and smaller amounts of groundwater-surface water exchange, particularly during the wettest and coldest winter months. These results highlight the strong sensitive of the hydrological system to the rainfall input variable. It is also interesting to note that the reduced uncertainty in precipitation during the summer months translates into quite narrow uncertainty intervals for the hydrogeological responses.

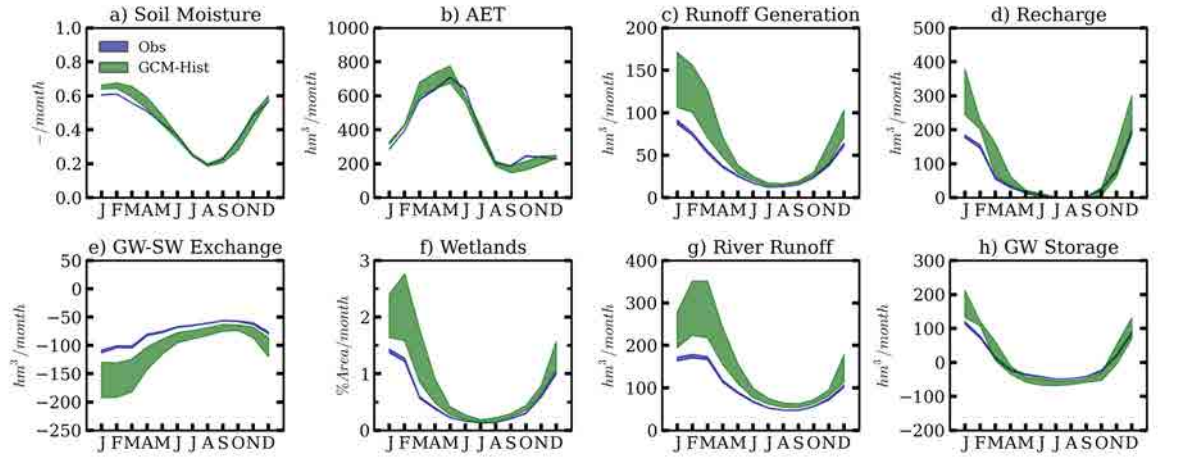

Figure 4-4 Climatologic hydrogeological response for the stochastic equivalence evaluation. They are compared the Observed (Blue)and the GCM historical (Green) Hydrological response for the same period of time (1960-1999)under naturalized conditions (no groundwater pumping) In each case is showed the 5-95% percentile over the ensembles.

4.4.2 GCM Projection of Climate Impacts under Naturalized Conditions

Figure 4-5 presents the climatological comparison of climate forcing between the historical (GCMH) and future (GCM-RCP85) periods. Note, that projected future PETo increases in a predictable fashion by a 20 %, especially during the summer months (April to September) with a peak in July (30 %) in response to increases in temperature. Meanwhile, the projected number of rainy days and overall rainfall amount are reduced by an annual average decrease of 14% and 25% respectively. In each case the width of the uncertainty bounds increases as should be expected due to GCM differences. Note however, that while the increase in rainfall uncertainty is greater for the cold and wet winter months, the large increase in summer uncertainty of number of rainy days (i.e. probability of rain) indicates greater unpredictability in regards to expected weather during the summer.

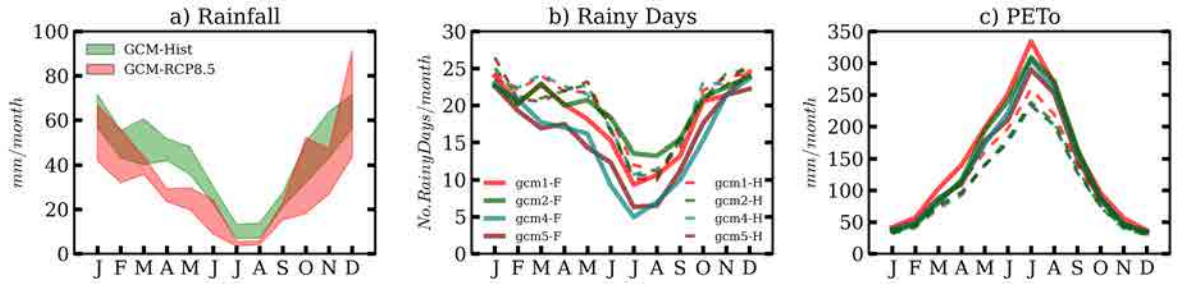

Figure 4-5 Climatologic climate driving forcing for the GCM Projections of Climate Impacts. They are compared the GCM historical (1960-1999) and the GCM-RCP8.5 (2060-2099).Panel a) shows the wet day amount precipitation simulated on both cases with the SRGP model with the 5-95% percentile over the ensembles. In panel (b) and (c) bold line are the GCM-RCP8.5 and the dotted lines the GCM-Historical. Panel b) shows the number of rainy days per month for the bias corrected probability of rain for the 4 GCMs on both periods. Panel c) shows the potential evapotranspiration bias corrected GCM temperatures.

The corresponding naturalized condition hydrogeological responses (Figure 4-6) show that a clear reduction can be expected in the quick responses of the system, represented by SM and AET (Figure 4-6 a and b), due to these climatological changes. In both cases the reductions are more significant from May to September, with a quite similar 20% percentage change (Figure 4-7 a and b). Meanwhile the results indicate an increase in the number of months having very low recharge (Figure 4-6d), resulting in an extended dry season from April to September. This corresponds to an annual decrease of ~40% (Figure 4-7d). The other variables (Qesc, eGSW, WFA and QRV; Figure 4-6 c,e,f,g and Figure 4-7c,e,f,g) show approximately the same patterns of change. Further, there are large increases in uncertainty, particularly from December to April. Interestingly the simulations indicate no significant change in groundwater storage (Figure 4-6h); however the percent difference plots (Figure 4-7h) indicate lower general inputs of water (reflecting the reduction in recharge) from

November to January and from May to October, and a reduction in the output of water (eGSW) from the aquifer.

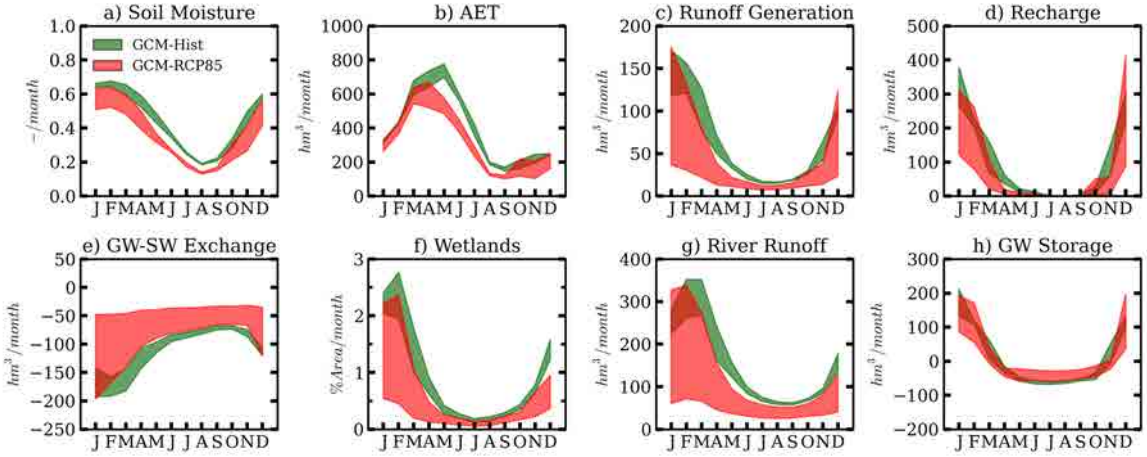

Figure 4-6 Climatologic hydrogeological response for the GCM Projections of Climate Impacts. They are compared the GCM historical (Green) and GCM-RCP85 (Red) Hydrological response for the periods 1960-1999 to 2060-2099 under naturalized conditions (no groundwater pumping). In each case is showed the 5-95% percentile over the ensembles.

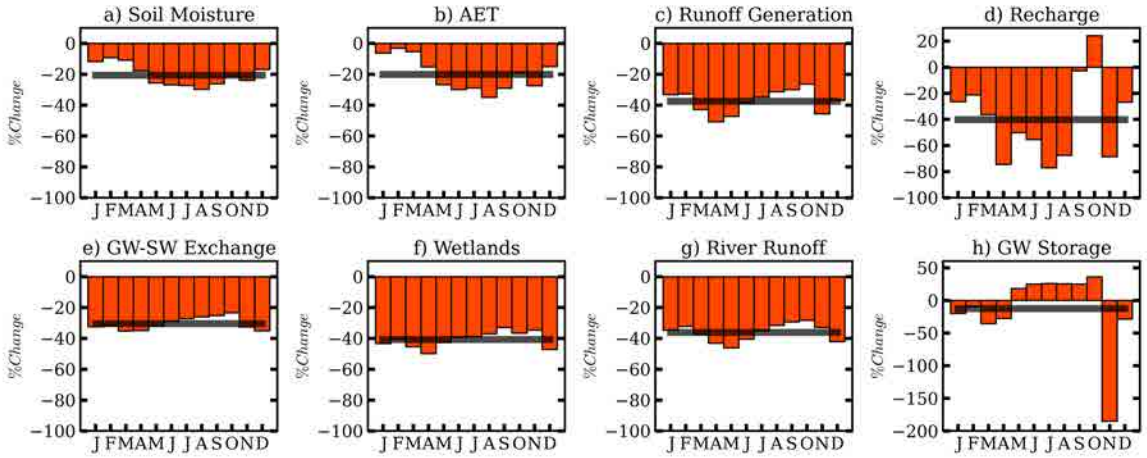

Figure 4-7 Relative Changes of the mean difference between the mean climatologic hydrogeological responses for the GCM Projections of Climate Impacts. The shadow black line represents the annual mean relative change.

4.4.3 Additional Effects of Groundwater Pumping

4.4.3.1 Historical

First we examine the additional impacts of pumping on naturalized conditions during the historical period (Figure 4-8). The SM and AET responses (Figure 4-8 a and b) show only small increases from May to September due to pumping, caused by the fact that the pumped water is incorporated as irrigation inputs to the soil balance. As a consequence, recharge is largely unaffected (Figure 4-8d); although on a percentage basis there appear to be large increases during the summer months (Figure 4-8d), these correspond to periods where

recharge is almost zero. Meanwhile, the other variables (Qesc, eGSW, WFA and QRV; Figure 4-8 c,e,f,g) generally decrease by ~50% during throughout the year. In terms of absolute values, the differences are more notable from December to March while the relative changes (Figure 4-9 c,e,f,g) are bigger during June to October. Pumping appears to have little impact of the climatological uncertainty. Note however that pumping has a clear and profound impact on the groundwater storage (Figure 4-8h) with significant decreases from May to August, and an interesting and non-negligible increase from September to April. These changes are in response to the reductions in eGWS (Figure 4-8e and Figure 4-9e), the constancy of recharge, and the reduced levels of pumping during the latter months.

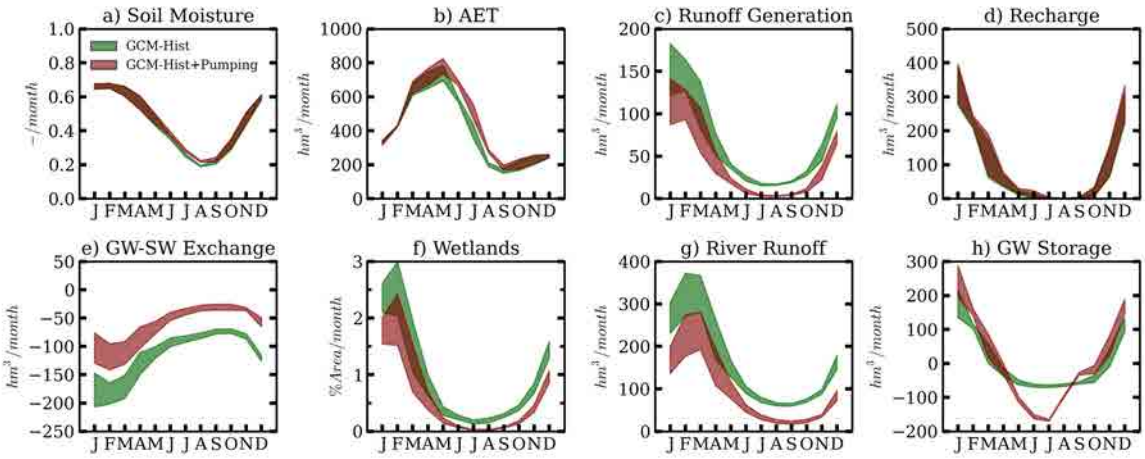

Figure 4-8 Effects of groundwater pumping in the Climatologic hydrogeological responses for the GCM Historical case (1960-1999). They are compared the GCM historical (Green) and GCM-historical+Pumping (Maroon). In each case is showed the 5-95% percentile over the ensembles.

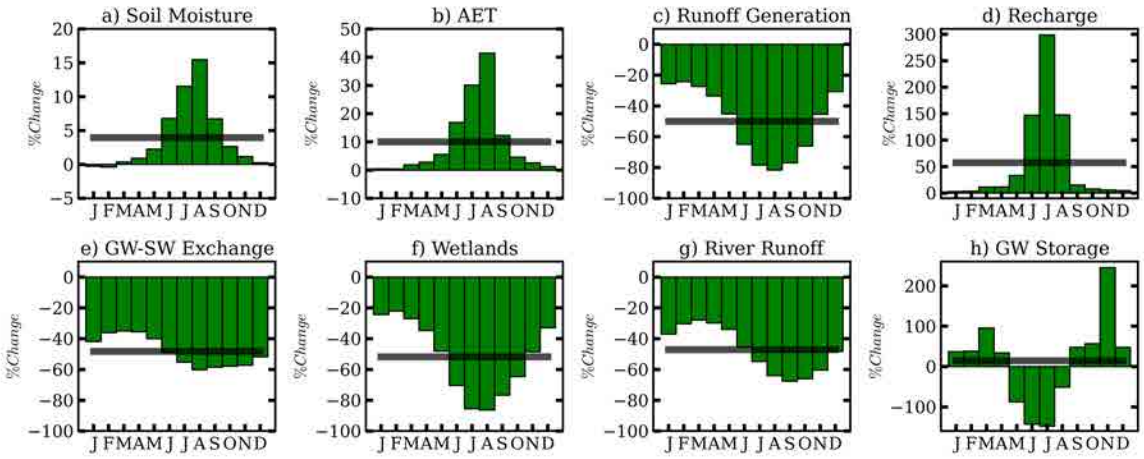

Figure 4-9 Relative Changes of the mean difference between the mean climatologic hydrogeological responses for the effect of groundwater pumping for GCM Historical cases. The shadow black line represents the annual mean relative change.

4.4.3.2 Future under Scenario RCP8.5

Next we examine the impacts of pumping on projected future response (Figure 4-10 and Figure 4-11). In general the absolute impacts of pumping are seen to be quite similar to those observed during the historical case (Figure 4-10). However, due to the combined and cumulative effects of both climate change and pumping, some of the responses (Qesc, eGSW, WFA and QRV) approach zero levels during some of the months, even resulting in an *inversion* of the groundwater-surface water exchange, absence of river flow, and drying up of the wetlands areas during some of the months. On a relative basis, the decreases approach ~70% (Figure 4-11) in comparison to ~50 % during the historical case. Overall, there is a significant increase in the uncertainty bounds when compared with the historical period.

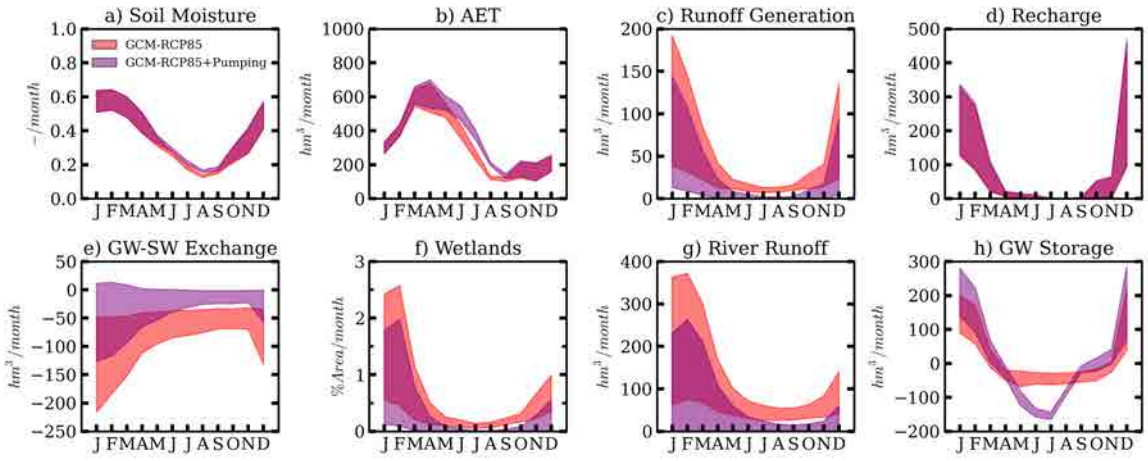

Figure 4-10 Effects of groundwater pumping in the Climatologic hydrogeological responses for the GCM future projection RCP8.5 case (2060-2099). They are compared the GCM RCP8.5 (Red) and GCM-RCP8.5+Pumping (Purple). In each case is showed the 5-95% percentile over the ensembles.

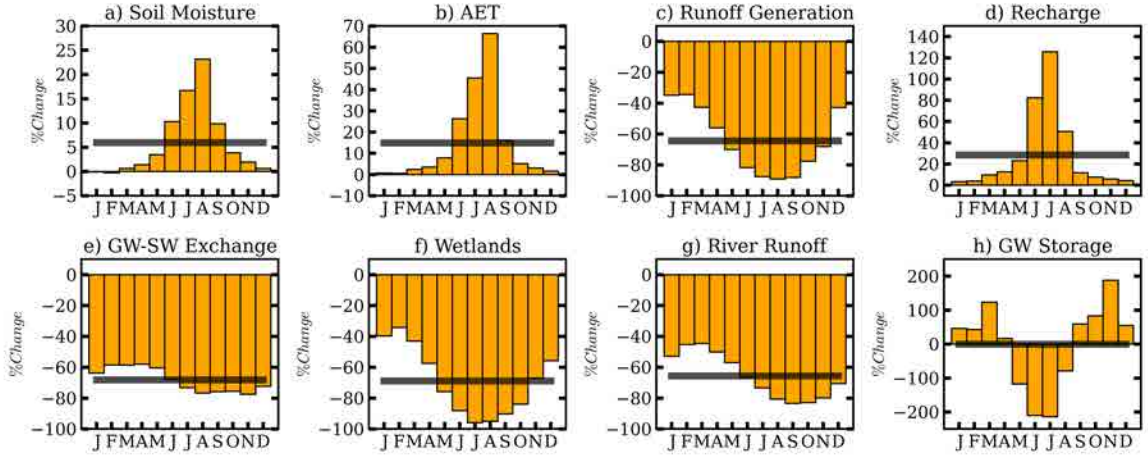

Figure 4-11 Relative Changes of the mean difference between the mean climatologic hydrogeological responses for the effect of groundwater pumping for GCM RCP8.5 cases. The shadow black line represents the annual mean relative change.

4.4.3.3 Changes from Historical-Pumped to Future-Pumped under RCP8.5

Finally, we examine the projected changes on pumped response under RCP85 (Figure 4-12). This represents changes due to the cumulative effects of groundwater pumping and projected climate change. The most obvious result of this comparison is to highlight the overall and significant increases in uncertainty. In general, SM and AET show annual average reductions of about -20% (Figure 4-13), and recharge (Figure 4-12d) shows an increase of number of months with very low recharge and relative decreases of ~45% (Figure 4-13d). However, the variables more directly affected by pumping (Qesc, eGWS, WFA, QRV;Figure 4-12 c,e,f,g) show a higher contrast indicating that the combined effects will have a strong effect on the dynamics of the system (reductions of ~60%; Figure 4-13 c,e,f,g). Meanwhile, there is relatively little effect on the overall climatology of groundwater storage (Figure 4-12h and Figure 4-13h), although relative changes can be seen for specific months.

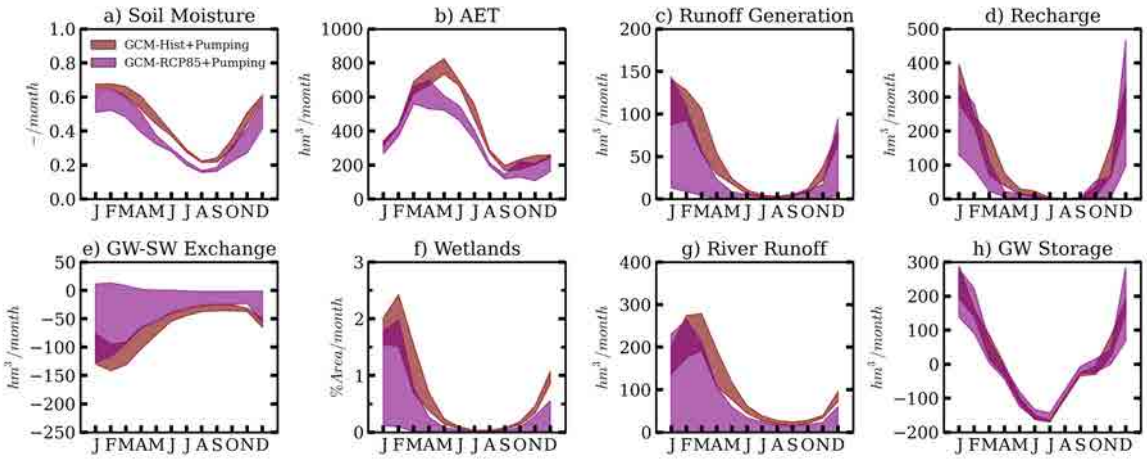

Figure 4-12 Cumulative effects of climate change and groundwater pumping comparing through the climatologic hydrogeological. They are compared the GCM Historical+Pumping (1960-1999) (Maroon) and GCM-RCP8.5+Pumping (2060-2099)(Purple). In each case is showed the 5-95% percentile over the ensembles.

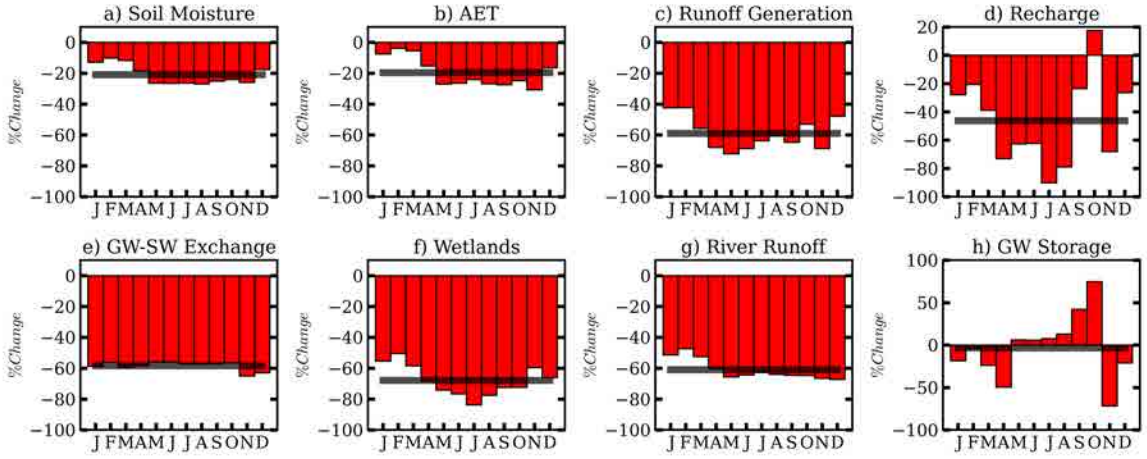

Figure 4-13 Relative Changes of the mean difference between the mean climatologic hydrogeological responses for cumulative effect of climate change and groundwater pumping. They are compared the

GCM Historical+Pumping (1960-1999and GCM-RCP8.5+Pumping (2060-2099) The shadow black line represents the annual mean relative change.

4.5 Discussion and conclusions

In this study we assumed that the catchment scale climate variables necessary to evaluate the hydrogeological responses of a basin could be obtained by interpreting the bias corrected downscaled and GCMs outputs as realizations from a hypothetical non-stationary stochastic process with an underlying physical process represented by the (physics-based) GCM itself. We hypothesized that the stochastic climate variable realizations generated by this process could be used to produce hydrogeological responses that are stochastically equivalent to those provided when the system is forced using observations. Under these assumptions, any non-stationary in the response is interpreted as arising from the ability of the GCMs to produce plausible future projections. Provided that these assumptions can be demonstrated to be acceptable, we could conclude that reliance upon GCMs outputs is both possible and meaningful, thereby demonstrating the viability and benefit of such studies for evaluating the potential impacts of climate change on the water resources of a basin.

The purpose of testing for Stochastic Equivalence is to lend support to the aforementioned hypothesis in the case of the UppGb. However, our results indicate that an exactly equivalent stochastic response is not achievable for all the response in all the months for this basin using the methods developed for this study. The main differences are attributable to differences in the number of ACP between the observed and GCM-simulated data. In particular, the wettest directional ACP (W/NW/SW/N) for winter explained such differences. These differences result in larger volumes of rainfall during the winter months, thereby producing correspondingly greater amounts of recharge that are dynamically propagated and amplify the difference in the response through the hydrogeological system. Despite these differences, we found that the GCMH methodology provides reasonable patterns of hydrogeological response, thereby providing an uncommon, albeit necessary evaluation steps before proceeding with Climate Change impacts studies. It is clear that further investigation is needed to come up with ways to compensate for the biases not completely resolved by our approach.

Bearing in mind that the results and differences in hydrogeological response between the GCM-based historical and future simulations cases can be compared on an equal basis, our results are useful to decision makers seeking to understand what changes in water resources management might be necessary. By evaluating the isolated effects of climate

change we see that reductions in the probability of rain expressed by drop of 14% in number of rainy days can be expected, albeit with a wide range of variation among the selected GCMs. This, together with reductions in wet day amount by a 25%, results in less water entering the system, and the increases in temperature result in increased potential evapotranspiration by 20%, primarily from April to September. These changes cascade through the hydrogeological system, causing a general relative reduction of 20% in soil moisture and AET, and a 40 % reduction in other responses. The net effect is an increase of 3 months in the length of the dry season (from June-September to April-October).

As might be expected, the additional effects of groundwater pumping are primarily on variables most closely related to aquifer response (Qesc, eGWS, WFA, and QRV). We see a slight increase in AET and, to a lesser extent, in soil moisture and recharge due to the pumped water being used for irrigation. Similarly, pumping has a larger impact in the future scenario than in the historical case. System responses to pumping results show annual average relative changes of approximately -50% and -70%, for the historical and future periods respectively for the aquifer related responses.

Finally, the combined effects of pumping and climate change result in reductions for all of the variables, with soil moisture and AET reduced by 20% and recharge by 50%. Meanwhile, the aquifer related responses show annual average reductions of approximately 60%.

Overall, our results indicate that the combined effects of climate change and groundwater overexploitation can be expected to affects the system response through significant decreases in availability of water throughout the year, but most notably during an extended hotter and drier summer season. Under naturalized conditions the effects of climate change are to reduce the input (less precipitation) and increasing the output (higher PETo) – no surprise there. However, these effects propagate through the hydrogeological system and, when combined with groundwater pumping, accelerate the process of drying considerably by directly affecting groundwater levels and thereby the exchanges with surface water.

From a scientific point of view, future studies should be also performed to evaluate and better understand the individual and cumulative effects of change in each of the driving factors (the ACP sequencing, PoR, WDA and temperatures) that affect climatological conditions over the basin. This will help us to better understand which factors are dominant, and which factors combine in synergistic ways.

5 General Conclusions

The main aim of this thesis is to evaluate the combined impact of climate change and groundwater overexploitation on the availability of water resources in the UppGb. To this end, the methods and evaluation procedures were adopted to analyze the human impact on water resources in a non-stationary framework, with an appropriate uncertainty assessment.

The main contributions of the thesis are:

- The development of a Stochastic Rainfall Generating Process (SRGP) for simulating/downscaling daily rainfall fields with enough spatial resolution for use in spatially distributed hydrological modeling. The approach incorporates several sources of information, and simulates major non-stationarity features of rainfall fields. By exploiting the GCMs information on the sequence of ACPs it is possible to obtain time stationary sequences of SRGPs. In essence, the method assumes that for each ACP and season the spatial rainfall distribution remains stationary. It is assumed therefore that non-stationarity in rainfall is represented as the evolution of rainy days and the sequence of ACPs, which can be derived from GCM. The approach may be employed to develop multiple stochastic ensembles of downscaled rainfall fields for use in climate change impact study assessments (including uncertainty analysis) as discussed in Chapter 4. Furthermore, the approach can also generate rainfall fields conditioned to the rain gauge data as shown in Chapter 3, where the effect of RSV was tested.
- SRGP was tested in the UppGb showing that provides an accurate reproduction of the major spatio-temporal features of rainfall needed for hydrological modeling and water resource evaluations. The incorporation of spatial drift related to orographic precipitation significantly improved the results. The incorporation of seasons enabled the reproduction of the observed climatology of spatial averaged rainfall. ACP clustering improved the reproduction of the inter-annual climatological variability

- Spatial variability of rainfall exerts a significant influence on the hydrogeological response of the Upper Guadiana basin. RSV was analyzed through the application of multiple realizations of stochastic rainfall fields with different spatial resolutions as meteorological driving hydrologic variables. RSV affected the response of the hydrogeological system in two ways: (1) the soil moisture and the actual evapotranspiration are practically insensitive to the overall hydrological response; and (2) the overall response is significantly higher with greater variability in the rainfall fields for groundwater recharge and the spatial runoff generation processes. Larger recharges result in greater groundwater head levels and therefore produce larger groundwater-surface water exchanges and river runoff discharge. Consequently, the system is less affected by groundwater withdrawals. These findings reinforce the need to implement high resolution rainfall fields for water resource and climate change impact assessments.

- The Stochastic Equivalence concept was introduced to evaluate the validity of the outputs of a number of GCM for use in hydrological modeling. This concept evaluates how properly bias corrected downscaled climate variables derived from GCM outputs can yield hydrogeological responses that are indistinguishable from those obtained from actual observations. The results indicate that an identical equivalent stochastic response cannot be totally achieved in the UppGb for all the responses. The main differences are attributable to differences in the number of ACP between the observed and GCM-simulated data. In particular, the wettest directional ACP (W/NW/SW/N) for winter accounted for these differences. These variations result in larger volumes of rainfall during the winter months, producing correspondingly greater amounts of recharge that are dynamically propagated through the hydrogeological system. Despite these differences, the hydrogeological response patterns obtained are reasonable. The stochastic equivalence provides an uncommon albeit necessary evaluation step before undertaking Climate Change impact studies. In view of the above results, the hydrogeological response between the GCM-based historical and future simulation cases is comparable.

- The combined impact of climate change and groundwater overexploitation on the availability of water resources in the UppGb may be greater than the effect of the individual variable. The effect of climate change without groundwater pumping was estimated as the cumulative effect of increases in temperature, changes in ACP frequency, and in the reduction of probability/volume of rainfall. These changes led to reductions of 14% and 25% in the number of rainy days and volume of rainfall, respectively, and to an increase of 20% in potential evapotranspiration. As a result of the propagation of these changes through hydrogeological system, all the variables were reduced; soil moisture and actual evapotranspiration were reduced by 20%, and groundwater recharge spatial runoff generation, groundwater-surface water exchange and river runoff discharge were reduced by 40 %. The incorporation of pumping to the natural simulation case yields the same percentage for soil moisture and actual evapotranspiration and 50% for recharge. Likewise, the aquifer related responses show annual average reductions of approximately 60%. The net effect is an increase of 3 months in the length of the dry season (from June-September to April-October). The general evaluation procedure indicates that the combined effects of climate change and groundwater overexploitation are expected to affect the system response through significant decreases in availability of water throughout the year, especially during an extended hotter and drier summer season. Under natural conditions, climate change leads to a reduction in the aquifer recharge (less precipitation) and increases water loss owing to a higher potential evapotranspiration. Consequently, head water levels in the aquifer fall and the interaction between groundwater and surface water decreases. Moreover, the effect of a massive pumping scheme on the hydrogeological system considerably accelerates the impact on the groundwater levels, and hence the groundwater and surface water relationship.

6 References

Bader D.C., C. C., & Zhang, M. (2008). *CCSP:Climate Models: An Assessment of Strengths and Limitations.* Tech. rep., U.S. Climate Change Science Program and the Subcommittee on Global Change Research Department of Energy, Office of Biological and Environmental Research, Washington, D.C., USA, 124 pp.

Barancourt, C., Creutin, J. D., & Rivoirard, J. (1992). A method for delineating and estimating rainfall fields. *Water Resour. Res., 28*(4), 1133-1144. doi:10.1029/91WR02896

Bardossy, A., & Plate, E. J. (1992). Space-time model for daily rainfall using atmospheric circulation patterns. *Water Resour. Res., 28*(5), 1247-1259. doi:10.1029/91WR02589

Barros, A. P., & Lettenmaier, D. P. (1994). Dynamic modeling of orographically induced precipitation. *Rev. Geophys., 32*(3), 265-284. doi:10.1029/94RG00625

Bell, T. L. (1987). A Space-Time Stochastic Model of Rainfall for Satellite Remote-Sensing Studies. *J. Geophys. Res., 92*(D8), 9631-9643. doi:10.1029/JD092iD08p09631

Bell, V. A. and Moore, R. J.(2000) The sensitivity of catchment runoff models to rainfall data at different spatial scales. *Hydrol. Earth Syst. Sci.*, 4, 653-667, doi:10.5194/hess-4-653-2000.

Bellone, E., Hughes, J. P., & Guttorp, P. (2000). A hidden Markov model for downscaling synoptic atmospheric patterns to precipitation amounts. *Clim Res, 15*(1), 1-12. doi:10.3354/cr015001

Besbes, M., & Marsily, G. D. (1984). From infiltration to recharge: use of a parametric transfer function . *J. Hydrol. , 74*(3-4), 271-293. doi:10.1016/0022-1694(84)90019-2

Beven, K. (2011). I believe in climate change but how precautionary do we need to be in planning for the future? *Hydrol. Process., 25*(9), 1517-1520. doi:10.1002/hyp.7939

Brath, A., and A. Montanari (2003), Sensitivity of the peak flows to the spatial variability of the soil infiltration capacity for different climatic scenarios, *Phys. Chem. Earth*, 28, 247– 254.

Brekke, L., Dettinger, M., Maurer, E., & Anderson, M. (2008). Significance of model credibility in estimating climate projection distributions for regional hydroclimatological risk assessments. *Climatic Change, 89*(3-4), 371-394. doi:10.1007/s10584-007-9388-3

Buishand, T. A., & Brandsma, T. (2001). Multisite simulation of daily precipitation and temperature in the Rhine Basin by nearest-neighbor resampling. *Water Resour. Res., 37*(11), 2761-2776. doi:10.1029/2001WR000291

Burton, A., Fowler, H. J., Kilsby, C. G., & O'Connell, P. E. (2010). A stochastic model for the spatial-temporal simulation of nonhomogeneous rainfall occurrence and amounts. *Water Resour. Res., 46*(11), W11501. doi:10.1029/2009WR008884

Chandler, R. E., & Wheater, H. S. (2002). Analysis of rainfall variability using generalized linear models: A case study from the west of Ireland. *Water Resour. Res., 38*(10), 1192. doi:10.1029/2001WR000906

Chiew, F. H., Teng, J., Vaze, J., Post, D. A., Perraud, J. M., Kirono, D. G., et al.,. (2009). Estimating climate change impact on runoff across southeast Australia: Method, results, and implications of the modeling method. *Water Resour. Res., 45*(10), W10414. doi:10.1029/2008WR007338

Cho, H.-K., Bowman, K. P., & North, G. R. (2004). A Comparison of Gamma and Lognormal Distributions for Characterizing Satellite Rain Rates from the Tropical Rainfall Measuring Mission. *J. Appl. Meteor., 43*(11), 1586-1597. doi:10.1175/JAM2165.1

Corte-Real, J., Xu, H., & Qian, B. (1999). A weather generator for obtaining daily precipitation scenarios based on circulation patterns. *Clim Res, 13*(1), 61-75. doi:10.3354/cr013061

Cowpertwait, P. S. (1995). A Generalized Spatial-Temporal Model of Rainfall Based on a Clustered Point Process. *Proceedings: Mathematical and Physical Sciences, 450*(1938), 163-175.

Cowpertwait, P. S. (2010). A spatial-temporal point process model with a continuous distribution of storm types. *Water Resour. Res., 46*(12), W12507. doi:10.1029/2010WR009728

Custodio, E. (2002). Aquifer overexploitation: what does it mean? *Hydrogeol. J, 10*, 254-277. doi:10.1007/s10040-002-0188-6

Dai, A. (2006). Precipitation Characteristics in Eighteen Coupled Climate Models. *J. Climate, 19*(18), 4605-4630. doi:10.1175/JCLI3884.1

De Oliveira V (2004) A simple model for spatial rainfall fields. *Stoch Environ Res Risk Assess* 18:131–140. doi:10.1007/s00477-003-0146-4

Deutsch, C., & Journel, A. (1997). *GSLIB: Geostatistical Software Library and User's Guide*. Oxford University Press, USA.

Dominguez, F., Cañon, J., & Valdes, J. (2010). IPCC-AR4 climate simulations for the Southwestern US: the importance of future ENSO projections. *Climatic Change, 99*(3-4), 499-514. doi:10.1007/s10584-009-9672-5

Doneaud, A. A., Ionescu-Niscov, S., Priegnitz, D. L., & Smith, P. L. (1984). The Area-Time Integral as an Indicator for Convective Rain Volumes. *J. Climate Appl. Meteor., 23*(4), 555-561. doi:10.1175/1520-0450(1984)023<0555:TATIAA>2.0.CO;2

Ebtehaj, M., & Foufoula-Georgiou, E. (2010). Orographic signature on multiscale statistics of extreme rainfall: A storm-scale study. *J. Geophys. Res., 115*(D23), D23112. doi:10.1029/2010JD014093

Ehret, U., Zehe, E., Wulfmeyer, V., Warrach-Sagi, K., & Liebert, J. (2012). HESS Opinions "Should we apply bias correction to global and regional climate model data?". *Hydrol. Earth Syst. Scis, 16*(9), 3391-3404. doi:10.5194/hess-16-3391-2012

Eltahir, E. A., & Bras, R. L. (1993). Estimation of the Fractional Coverage of Rainfall in Climate Models. *J. Climate, 6*(4), 639-644. doi:10.1175/1520-0442(1993)006<0639:EOTFCO>2.0.CO;2

Fowler, H. J., Blenkinsop, S., & Tebaldi, C. (2007). Linking climate change modelling to impacts studies: recent advances in downscaling techniques for hydrological modelling. *Int. J. Climatol., 27*(12), 1547-1578. doi:10.1002/joc.1556

Fowler, H., Kilsby, C., O'Connell, P., & Burton, A. (2005). A weather-type conditioned multi-site stochastic rainfall model for the generation of scenarios of climatic variability and change. *J. Hydrol., 308*(1-4), 50-66. doi:10.1016/j.jhydrol.2004.10.021

Fowler HJ, Kilsby CG, O'Connell PE (2000) A stochastic rainfall model for the assessment of regional water resource systems under changed climatic condition. *Hydrol Earth Syst Sci* 4(2):263–281.doi:10.5194/hess-4-263-2000

Frost, A. J., Charles, S. P., Timbal, B., Chiew, F. H., Mehrotra, R., Nguyen, K. C., et al.,. (2011). A comparison of multi-site daily rainfall downscaling techniques under Australian conditions. *J. Hydrol., 408*(1-2), 1-18. doi:10.1016/j.jhydrol.2011.06.021

Furrer, E. M., & Katz, R. W. (2008). Improving the simulation of extreme precipitation events by stochastic weather generators. *Water Resour. Res., 44*(12), W12439. doi:10.1029/2008WR007316

Gabellani, I., G. Boni, L. Ferraris, J. von Hardenberg, and A. Provenzale (2007), Propagation of uncertainty from rainfall to runoff: A case study with a stochastic rainfall generator, *Adv. Water Resour.*, 30, 2061– 2071, doi:10.1016/j.advwatres.2006.11.015.

Girard, G. M. (1972). Modèle précipitations-débits à discrétisation spatiale. *Cahiers ORSTOM, serie Hydrologie, 9(4)*, 35-52.

Gleckler, P. J., Taylor, K. E., & Doutriaux, C. (2008). Performance metrics for climate models. *J. Geophys. Res., 113*(D6), D06104. doi:10.1029/2007JD008972

Gómez-Hernández, J. J., & Srivastava, R. M. (1990). ISIM3D: An ANSI-C three-dimensional multiple indicator conditional simulation program. *Comput. Geosci., 16*(4), 395-440. doi:10.1016/0098-3004(90)90010-Q

Gómez-Hernández, J., & Cassiraga, E. (1994). *Theory and practice of sequential simulation. Geostatistical Simulations.* (M. ;. Armstrong, Ed.) Springer.

Goodess, C. M., & Palutikof, J. P. (1998). Development of daily rainfall scenarios for southeast Spain using a circulation-type approach to downscaling. *Int. J. Climatol., 18*(10), 1051-1083. doi:10.1002/(SICI)1097-0088(199808)18:10<1051::AID-JOC304>3.0.CO;2-1

Goovaerts, P. (1997). *Geostatistics for Natural Resources Evaluation.* Oxford University Press, USA.

Guillot, G. (1999). Approximation of Sahelian rainfall fields with meta-Gaussian random functions. *Stoch. Env. Res. Risk A., 13*, 100-112. doi:10.1007/s004770050034

Gupta, V. K., & Waymire, E. C. (1993). A Statistical Analysis of Mesoscale Rainfall as a Random Cascade. *J. Appl. Meteorol., 32*(2), 251-267. doi:10.1175/1520-0450(1993)032<0251:ASAOMR>2.0.CO;2

Gupta, H. V., Sapriza, G., Jodar-Bermudez, J. and Carrera-Ramirez, J. (2013). Circulation pattern-based assessment of projected climate change for a catchment in Spain. *To be submitted*

Hay, L. E., McCabe, G. J., Wolock, D. M., & Ayers, M. A. (1991). Simulation of precipitation by weather type analysis. *Water Resour. Res., 27*(4), 493-501. doi:10.1029/90WR02650

Hundecha, Y., & Bardossy, A. (2008). Statistical downscaling of extremes of daily precipitation and temperature and construction of their future scenarios. *Int. J. Climatol., 28*(5), 589-610. doi:10.1002/joc.1563

IPCC, 2013: Climate Change 2013: The Physical Science Basis. Contribution of Working Group I to the Five Assessment Report of the Intergovernmental Panel on Climate Change

IPCC, 2007: Climate Change 2007: The Physical Science Basis. Contribution of Working Group I to the Fourth Assessment Report of the Intergovernmental Panel on Climate Change [Solomon, S., D. Qin, M. Manning, Z. Chen, M. Marquis, K.B. Averyt, M.Tignor and H.L. Miller (eds.)]. Cambridge University Press, Cambridge, United Kingdom and New York, NY, USA.

Jenkinson, A., & Collison, F. (1977). An initial climatology of gales over the North Sea. *Synoptic Climatology Branch Memorandum, 62*.

Jódar, J., Carrera, J., & Cruz, A. (2010). Irrigation enhances precipitation at the mountains downwind. *Hydrol. Earth Syst. Scis, 14*(10), 2003-2010. doi:10.5194/hess-14-2003-2010

Johnson, F., & Sharma, A. (2011). Accounting for interannual variability: A comparison of options for water resources climate change impact assessments. *Water Resour. Res., 47*(4). doi:10.1029/2010WR009272

Johnson F, Sharma A (2012) A nesting model for bias correction of variability at multiple time scales in general circulation model precipitation simulations. *Water Resour Res* 48(W01504):16. doi:10.1029/2011WR010464

Jones, P. D., Hulme, M., & Briffa, K. R. (1993). A comparison of Lamb circulation types with an objective classification scheme. *Int. J. Climatol., 13*(6), 655-663. doi:10.1002/joc.3370130606

Jothityangkoon, C., Sivapalan, M., & Viney, N. R. (2000). Tests of a space-time model of daily rainfall in southwestern Australia based on nonhomogeneous random cascades. *Water Resour. Res., 36*(1), 267-284. doi:10.1029/1999WR900253

Kalnay, E., Kanamitsu, M., Kistler, R., Collins, W., Deaven, D., Gandin, L., et al.,. (1996). The NCEP/NCAR 40-Year Reanalysis Project. *Bull. Amer. Meteor. Soc., 77*(3), 437-471. doi:10.1175/1520-0477(1996)077<0437:TNYRP>2.0.CO;2

Kang, B., & Ramirez, J. A. (2010). A coupled stochastic space-time intermittent random cascade model for rainfall downscaling. *Water Resour. Res., 46*(10), W10534. doi:10.1029/2008WR007692

Kedem, B., & Chiu, L. S. (1987). On the lognormality of rain rate. *Proceedings of the National Academy of Sciences, 84*(4), 901-905.

Kedem, B., & Pavlopoulos, H. (1991). On the Threshold Method for Rainfall Estimation: Choosing the Optimal Threshold Level. *J. Am. Stat. Assoc., 86*(415), 626-633.

Kleiber, W., Katz, R. W., & Rajagopalan, B. (2012). Daily spatiotemporal precipitation simulation using latent and transformed Gaussian processes. *Water Resour. Res., 48*(1), W01523. doi:10.1029/2011WR011105

Korkmaz, S., Ledoux, E., & Onder, H. (2009). Application of the coupled model to the Somme river basin. *J. Hydrol., 366*(1-4), 21-34. doi:10.1016/j.jhydrol.2008.12.008

Krajewski, W. F., Lakshmi, V., Georgakakos, K. P., & Jain, S. C. (1991). A Monte Carlo Study of rainfall sampling effect on a distributed catchment model. *Water Resour. Res., 27*(1), 119-128. doi:10.1029/90WR01977

Kundu, P. K., & Siddani, R. K. (2007). A new class of probability distributions for describing the spatial statistics of area-averaged rainfall. *J. Geophys. Res., 112*(D18), D18113. doi:10.1029/2006JD008042

Kursinski, A. L., & Zeng, X. (2006). Areal estimation of intensity and frequency of summertime precipitation over a midlatitude region. *Geophys. Res. Lett., 33*(22), L22401. doi:10.1029/2006GL027393

Kyriakidis, P., & Journel, A. (1999). Geostatistical Space–Time Models: A Review. *Math. Geol., 31*, 651-684. doi:10.1023/A:1007528426688

Kyriakidis P, Miller N, Kim J (2004) A spatial time series framework for simulating daily recipitation at regional scales. *J Hydrol* 297(1–4):236–255. doi:10.1016/j.jhydrol.2004.04.022

Lanza, L. G. (2000). A conditional simulation model of intermittent rain fields. *Hydrol. Earth Syst. Scis, 4*(1), 173-183. doi:10.5194/hess-4-173-2000

Llamas, M. and Martínez-Santos, P. (2005). "Intensive Groundwater Use: Silent Revolution and Potential Source of Social Conflicts." J. Water Resour. Plann. Manage., 131(5), 337–341. doi: 10.1061/(ASCE)0733-9496(2005)131:5(337)

Maraun, D., Wetterhall, F., Ireson, A. M., Chandler, R. E., Kendon, E. J., Widmann, M., et al.,. (2010). Precipitation downscaling under climate change: Recent developments to bridge the gap between dynamical models and the end user. *Rev. Geophys., 48*(3), RG3003. doi:10.1029/2009RG000314

Martínez-Cortina, L. (2000). *Estimación de la recarga en grandes cuencas sedimentarias mediante modelos numéricos de flujosubterráneo. Aplicación a la cuenca alta del Guadiana [Recharge estimation in large sedimentary basins using groundwaterflow numerical models. Application to the Upper Guadiana Basin.* Ph.D. dissertation, University of Cantabria, Spain.

Mehrotra R, Sharma A (2007) A semi-parametric model for stochastic generation of multisite daily rainfall exhibiting low-frequency variability. *J Hydrol* 335(1–2):180–193.doi:10.1016/j.jhydrol.2006.11.011.

Mehrotra, R., & Sharma, A. (2009). Evaluating spatio-temporal representations in daily rainfall sequences from three stochastic multi-site weather generation approaches. *Adv. Water Resour., 32*(6), 948-962. doi:10.1016/j.advwatres.2009.03.005

Mehrotra R, Sharma A (2010) Development and application of a multisite rainfall stochastic downscaling framework for climate change impact assessment. *Water Resour Res* 46. doi:10.1029/2009WR008423

Mejía, J. M., & Rodríguez-Iturbe, I. (1974). On the synthesis of random field sampling from the spectrum: An application to the generation of hydrologic spatial processes. *Water Resour. Res., 10*(4), 705-711. doi:10.1029/WR010i004p00705

Milly, P. C., Betancourt, J., Falkenmark, M., Hirsch, R. M., Kundzewicz, Z. W., Lettenmaier, D. P., et al.,. (2008). Stationarity Is Dead: Whither Water Management? *Science, 319*(5863), 573-574. doi:10.1126/science.1151915

Moss, R. H., Edmonds, J. A., Hibbard, K. A., Manning, M. R., Rose, S. K., van Vuuren, D. P., et al.,. (2010). The next generation of scenarios for climate change research and assessment. *Nature, 463*(7282), 747-756. doi:10.1038/nature08823

Nicótina, L., Alessi Celegon, E., Rinaldo, A., & Marani, M. (2008). On the impact of rainfall patterns on the hydrologic response. *Water Resour. Res., 44*(12), W12401.

Northrop, P. (1998). A Clustered Spatial-Temporal Model of Rainfall. *Proceedings: Mathematical, Physical and Engineering Sciences, 454*(1975), 1875-1888.

Obled, C., Wendling, J., & Beven, K. (1994). The sensitivity of hydrological models to spatial rainfall patterns: an evaluation using observed data. *J. Hydrol., 159*(1-4), 305-333. doi:10.1016/0022-1694(94)90263-1

Onibon, H., Lebel, T., Afouda, A., & Guillot, G. (2004). Gibbs sampling for conditional spatial disaggregation of rain fields. *Water Resour. Res., 40*(8), W08401. doi:10.1029/WR010i004p00705

Perica, S., & Foufoula-Georgiou, E. (1996). Model for multiscale disaggregation of spatial rainfall based on coupling meteorological and scaling descriptions. *J. Geophys. Res., 101*(D21), 26347-26361. doi:10.1029/96JD01870

Piani, C., Weedon, G., Best, M., Gomes, S., Viterbo, P., Hagemann, S., et al.,. (2010). Statistical bias correction of global simulated daily precipitation and temperature for the application of hydrological models. *J. Hydrol., 395*(3-4), 199-215. doi:10.1016/j.jhydrol.2010.10.024

Pierce, D. W., Barnett, T. P., Santer, B. D., & Gleckler, P. J. (2009). Selecting global climate models for regional climate change studies. *Proceedings of the National Academy of Sciences, 106*(21), 8441-8446. doi:10.1073/pnas.0900094106

Randall, D. R., & Taylor, K. (2007). *Cilmate Models and Their Evaluation. Climate Change 2007: The Physical Science Basis. Contribution of Working Group I to the Fourth Assessment Report of the Intergovernmental Panel on Climate Change [Solomon, S., D. Qin, M. Manning, Z. Chen, M. Marquis, K.B. Averyt, M.Tignor and H.L. Miller (eds.)]*. (C. U. Cambridge University Press, & N. U. New York, Edits.) Cambridge University Press, Cambridge, United Kingdom and New York, NY, USA.

Rodríguez-Iturbe, I., Cox, D. R., & Eagleson, P. S. (1986). Spatial Modelling of Total Storm Rainfall. *P Roy. Sso. Lond. A Mat., 403*(1824), 27-50.

Sapriza Azuri, G., Jódar, J., Carrera, J., & Gupta, H. (2013a). Stochastic Simulation of Nonstationary Rainfall Fields, Accounting for Seasonality and Atmospheric Circulation Pattern Evolution. *Math. Geosci., 45*(5), 621-645. doi:10.1007/s11004-013-9467-0

Sapriza Azuri, G., Jodar, J., Carrera, J., and Gupta, H. (2013b). Impacts of rainfall spatial variability on hydrogeological response . *Submited.*

Schertzer, D., & Lovejoy, S. (1987). Physical Modeling and Analysis of Rain and Clouds by Anisotropic Scaling Multiplicative Processes. *J. Geophys. Res., 92*(D8), 9693-9714. doi:10.1029/JD092iD08p09693

Schuurmans, J. M., & Bierkens, M. F. (2007). Effect of spatial distribution of daily rainfall on interior catchment response of a distributed hydrological model. *Hydrol. Earth Syst. Scis, 11*(2), 677-693. doi:10.5194/hess-11-677-2007

Shah, S., O'Connell, P., & Hosking, J. (1996). Modelling the effects of spatial variability in rainfall on catchment response. 1. Formulation and calibration of a stochastic rainfall field model. *J. Hydrol., 175*(1-4), 67-88. doi:10.1016/S0022-1694(96)80006-0

Sharma, A., & Mehrotra, R. (2010). Rainfall generation. En *Geophys. Monogr. Ser.* (Vol. 191, págs. 215-246). Washington, DC: AGU. doi:10.1029/2010GM000973

Sherman, M. (2011). *Spatial Statistics and Spatio-Temporal Data: Covariance Functions and Directional Properties*. John Wiley \& Sons.

Slooten, L. J. (2009). *An Object Oriented approach to groundwater optimization and simulation problems.* Ph.D. dissertation, Universitat Politecnica de Catalunya.

Smith, J. A., Baeck, M. L., Meierdiercks, K. L., Nelson, P. A., Miller, A. J., & Holland, E. J. (2005). Field studies of the storm event hydrologic response in an urbanizing watershed. *Water Resour. Res., 41*(10). doi:10.1029/2004WR003712

Solari, S., & Losada, M. A. (2012). A unified statistical model for hydrological variables including the selection of threshold for the peak over threshold method. *Water Resour. Res., 48*(10), W10541. doi:10.1029/2011WR011475

Srikanthan, R., & McMahon, T. A. (2001). Stochastic generation of annual, monthly and daily climate data: A review. *Hydrol. Earth Syst. Scis, 5*(4), 653-670. doi:10.5194/hess-5-653-2001

Stern, R. D., & Coe, R. (1984). A Model Fitting Analysis of Daily Rainfall Data. *Journal of the Royal Statistical Society. Series A (General), 147*(1), 1-34.

Taylor, K. E., Stouffer, R. J., & Meehl, G. A. (2011). An Overview of CMIP5 and the Experiment Design. *Bull. Amer. Meteor. Soc., 93*(4), 485-498. doi:10.1175/BAMS-D-11-00094.1

Teo, C.-K., & Grimes, D. I. (2007). Stochastic modelling of rainfall from satellite data. *J. Hydrol., 346*(1-2), 33-50. doi:10.1016/j.jhydrol.2007.08.014

Trenberth, K. (2011). Changes in precipitation with climate change. *Clim Res, 47*(1-2), 123-138. doi:10.3354/cr00953

Trenberth, K. E., Dai, A., Rasmussen, R. M., & Parsons, D. B. (2003). The Changing Character of Precipitation. *Bull. Amer. Meteor. Soc., 84*(9), 1205-1217. doi:10.1175/BAMS-84-9-1205

Vrac, M., & Naveau, P. (2007). Stochastic downscaling of precipitation: From dry events to heavy rainfalls. *Water Resour. Res., 43*(7), W07402. doi:10.1029/2006WR005308

Vrac, M., Stein, M. L., Hayhoe, K., & Liang, X.-Z. (2007). A general method for validating statistical downscaling methods under future climate change. *Geophys. Res. Lett., 34*(18), L18701. doi:10.1029/2007GL030295

Waymire, E., Gupta, V. K., & Rodriguez-Iturbe, I. (1984). A Spectral Theory of Rainfall Intensity at the Meso-beta Scale. *Water Resour. Res., 20*(10), 1453-1465. doi:10.1029/WR020i010p01453

Weedon, G. P., Gomes, S., Viterbo, P., Shuttleworth, W. J., Blyth, E., Osterle, H., et al.,. (2011). Creation of the WATCH Forcing Data and Its Use to Assess Global and Regional Reference Crop Evaporation over Land during the Twentieth Century. *J. Hydrometeor, 12*(5), 823-848. doi:10.1175/2011JHM1369.1

Wheater, H., Chandler, R., Onof, C., Isham, V., Bellone, E., Yang, C., et al.,. (2005). Spatial-temporal rainfall modelling for flood risk estimation. *Stoch. Env. Res. Risk A., 19*, 403-416. doi:10.1007/s00477-005-0011-8

Wilby, R. L., Charles, S. P., Zorita, E., Timbal, B., Whetton, P., & Mearns, L. O. (2004). Guidelines for use of climate scenarios developed from statistical downscaling methods.

Wilks, D. S. (1998). Multisite generalization of a daily stochastic precipitation generation model. *J. Hydrol., 210*(1-4), 178-191. doi:10.1016/S0022-1694(98)00186-3

Wilson, C. B., Valdes, J. B., & Rodriguez-Iturbe, I. (1979). On the influence of the spatial distribution of rainfall on storm runoff. *Water Resour. Res., 15*(2), 321-328. doi:10.1029/WR015i002p00321

Wood, E. F., Sivapalan, M., Beven, K., & Band, L., (1988). Effects of spatial variability and scale with implications to hydrologic modeling. *J. Hydrol.,*, 102(1), 29-47.

Wood, A. W., Leung, L. R., Sridhar, V., & Lettenmaier, D. P. (2004). Hydrologic Implications of Dynamical and Statistical Approaches to Downscaling Climate Model Outputs. *Climatic Change, 62*, 189-216. doi:10.1023/B:CLIM.0000013685.99609.9e

Yang, C., Chandler, R. E., Isham, V. S., & Wheater, H. S. (2005). Spatial-temporal rainfall simulation using generalized linear models. *Water Resour. Res., 41*(11), W11415. doi:10.1029/2004WR003739

Yang, W., Bardossy, A., & Caspary, H.-J. (2010). Downscaling daily precipitation time series using a combined circulation- and regression-based approach. *Theor. Appl. Climatol., 102*, 439-454. doi:10.1007/s00704-010-0272-0

Younger, P. M., Freer, J. E., & Beven, K. J. (2009). Detecting the effects of spatial variability of rainfall on hydrological modelling within an uncertainty analysis framework. *Hydrol. Process., 23*(14), 1988-2003. doi:10.1002/hyp.7341

Zhang, Z., & Switzer, P. (2007). Stochastic space-time regional rainfall modeling adapted to historical rain gauge data. *Water Resour. Res., 43*(3), W03441. doi:10.1029/2005WR004654